T-2892

WAVE PROPAGATION FROM AN EXPLOSIVE SOURCE

by

Farrokh Jalinoos

ProQuest LLC.
789 East Eisenhower Parkway
P.O. Box 1346
Ann Arbor, MI 48106 – 1346

T-2892

A thesis submitted to the Faculty and the Board of Trustees of the Colorado School of Mines in partial fulfillment of the requirements for the degree of Master of Science (Geophysics).

Golden, Colorado

Date 17 SEPT 1984

Signed: Farrokh Jalinoos
Farrokh Jalinoos

Approved: J. E. White
Dr. J.E. White
Thesis Advisor

Golden, Colorado

Date 17 Sep 84

P R Romig
Dr. P.R. Romig,
Head of Department
of Geophysics

ABSTRACT

A model is proposed to more physically describe the primary seismic pulse from an explosive source than those accounted for in the literature. The existing models, generally known as "Sharpe's theory", describe wave propagation from a spherical cavity in an infinitely extended elastic medium, but none, with the exception of Peet (1960), includes an account of the rock fracturing that occurs around the explosive source. Here in this study, we have assumed the deformed or "shattered" region to behave as a viscous liquid of visco-elastic rheology. The method of Fourier synthesis is used in solving the problem in the frequency domain. The theoretical results were then compared to field data in three sedimentary environments of shale, sandstone and a marl formation to test for effectiveness of the model.

Various rock mechanics applications including expressions for normal components of radial and tangential stress are evaluated at the deformed boundary. A value for the theoretical tensile stress as well as a presumed dynamical failure criterion is also discussed. Results, as recent laboratory findings, indicate that the theoretical dynamical tensile stress of rocks is not constant, contrary

to that required by the laws of similitude or scaling theory. Some seismic scaling relationships are derived, including charge size as a function of observed "amplitude".

TABLE OF CONTENTS

LIST OF FIGURES

LIST OF TABLES

ACKNOWLEDGEMENTS

I wish to thank Dr. J.E. White who as my advisor provided countless hours of helpful comments and discussions with regard of this thesis which otherwise would not have developed to this stage. I would also like to sincerely thank Drs. Hadsell and Schneider who served on my committee. Special thanks goes to M. Bahavar and I. Shiao for providing me with the plotting programs used in plotting the transient waveforms.

I am deeply indepted to the Integrated Geophysical Project (IGP) for carrying my financial support during my masters studies at Colorado School of Mines.

Finally, I like to thank both my parents who always gave the strongest moral support.

INTRODUCTION

I.1 Historical Background

Seismic exploration has its origins in obtaining reflection or refraction records resulting from the detonation of buried charges as the source of energy. Since the employment of dynamite as the primary source of transmission of mechanical energy into ground, numerous theoretical investigations have been undertaken in the geophysical literature in search of suitable mathematical-physical models which can properly describe the initiation process of the seismic pulse. As yet, however, no model has been proposed that can be regarded as satisfactory in fully predicting all aspects of the resulting ground motion. This is despite of the great theoretical advances that have occurred in understanding all other aspects of wave motion, namely propagation, dispersion, refraction and reflection of the initial pulse from the geological boundaries.

Parallel to the exploration geophysicist's interest in dynamite as an exploration tool, many other applications

of explosives have been found in the mining and the military activities, though the attention here is more confined to the explosive's ability in blasting type operations. In the mining field in particular, a knowledge of the degree and extent of fragmentation of a given explosive detonated at a known depth and geological environment can enhance the practicing engineer's ability in designing effective production procedures in the practice of blasting. Interest in the military fields, on the other hand, is more limited to the degree of micro-structure damage that can occur by generally much stronger types of explosives such as TNT.

In seismic prospecting though, the greatest utility of dynamite comes about in its ability in converting available chemical energy to useful downgoing energy of motion. In a study conducted on eight commonly used land seismic sources in Eastern Colorado, Janak (1982) concluded that in Pierre shale at least, a 5 lb dynamite charge was the most efficient source at converting available energy into downgoing compressional wave radiation. This same charge, moreover, produced the largest amount of compressional energy, probably due to the great coupling that is obtained between borehole explosives and the earth.

While perhaps the first "explosive" used by mankind was black powder, it was not until 1881 that the detonation

process was descovered by Alfred B. Nobel when he accidentally spilled a shipment of his "Blasting oil" into its packed Kieselguhr. This, in effect, marked the begining of high or detonating explosives. Today, most dynamites consist of a mixture of an energy and gas producing product such as ammonium nitrate with a sensitizing compound such as nitroglycerin in proper proportions.

Although "straight" dynamite can be obtained with nitroglycerin as its sole ingredient, due to its sensitivity to shock and high costs it is rarely being used. Oftentimes nitrocotton is dissolved in nitroglycerin in forming a thick viscous jelly used as the base for gelatin dynamites. If a portion of nitroglycerin is replaced by the ammonium nitrate the resulting mix is termed ammonium gelatin dynamite.

Based on composition, an explosive energy source, as described by Clark (1968), can roughly be classified as "black powder, dynamite, ammonium nitrate blasting agents, slurries, metalized explosives, military explosives (TNT, etc.), and nuclear explosives". The total reaction time for the chemical reactions in detonation ranges from a micro-second, for most fine grained and pure liquid high explosive, to nearly 100 microseconds for coarse uncrushed ANFO. For a deflagrating explosive such as black powder, however, chemical reaction times are generally longer than a

millisecond.

Even though the chemical reactions in detonation are thus some 100 to 10,000 times faster than deflagrating explosives, exact thermodynamics and hydrodynamic analysis can only be used in predicting explosive performance parameters for the former case. This includes calculations of detonation pressures, velocities and other physical chemical properties of detonation.

I.2 Important Factors in Rock Fragmentation.

The usefulness of dynamite comes about in the almost instantaneous transfer of energy that occurs after detonation to a portion of the rock body. The mechanics of this energy transfer is complicated and the resulting rock breakage and seismic wave motion is likewise dependant on many factors. Before making many simplifying assumptions with regard to suitable mathematical models that can describe the detonation process, it is desirable to take a closer look at all the physical parameters which can directly influence the propagation of the downgoing seismic wavelet. Atchison (1968) identified three factors of explosive, charge loading and rock parameters as being important in the resulting fragmentation and wave propagation process which we here proceed to briefly outline below

I.2.A Explosive parameters. As was mentioned previously, the explosive parameters differ considerably depending on the chemical content and portion mix of the explosives being used. It is, for example, observed that larger amplitudes are obtained in exploding a high-speed explosive, such as dynamite, rather than a low speed one

like black powder even though the detonation pressure are made to be equal(Nash and Martin, 1936). A particular type of high speed dynamite can moreover yield different amplitudes of motion depending on its chemical mix. Three explosive properties of detonation pressure, rate of energy release and pressure-time history are particularly relevant to our analysis. The dynamite's detonation pressure P_0 in Kilobars (Kbar) is defined as

$$P_0=KdV^2 \qquad (1\text{-}1)$$

where

K=proportionality constant=$2.5\text{x}10^{-6}$

d=density in gr/cm^3

V=detonation velocity in m/sec

As an example, for a typical Tovex S charge as was used by Janak (1982), a density of 1.25 gr/cm^3 and detonation velocity of 4630 m/sec is realized giving rise to a detonation presure of about 67 kbar or 10^6 pounds per square inch (psi). Although this value is for the ideal confinement, under borehole environment it can be expected to be considerably reduced in magnitude. Another very important explosive property needed for the theoretical modeling of the problem is the pressure-time history of the gases produced. This is very difficult to measure

experimentally and will be discussed in more detail in a later part of this chapter.

I.2.B Charge loading parameters are factors that relate to both explosive and the rock. They include charge geometry, diameter, type and point of initiation and degree of confinement of the charge. Often times they play a more important role than the explosive parameters in the resulting amplitudes of ground motion. Gaskell (1956), for example, found explosion of charges in larger water-filled holes results in three or four times greater seismic amplitudes than narrow ones. This was the case for holes larger than the cavity that the charge makes for itself in the process of detonation. Where the hole size was less than the cavity size, no variation in seismic amplitude was observed. So the practice of "springing" of a hole with an initial smaller charge was concluded to result in no appreciable increase in seismic amplitude from a later larger charge. The size of the hole along with the degree of confinement of the charge are also expected to control the detonation pressure of the same type of explosive.

Finally, charge geometry, defined as the ratio of length to the diameter of the charge, as well as point of initiation of the charge are important factors particularly

for cylindrical charges. Variations in the above parameters have been shown by Duvall et al. (1965) to produce larger differences in peak strains in the rock than using a different type of explosive.

I.2.C Rock parameters are important chemical and physical properties of the rocks that are needed to be considered. They include the bulk and rigidity moduli, energy absorption, elastic strain limit to deformation, threshold pressures for plastic and shock wave propagation, porosity and rock structures including bedding, joints etc. In addition to rock structures, rocks generally exhibit gross variabilities and are neither homogeneous nor isotropic. This obviously influences the wave motion in them. The compressive and tensile strength of the rocks govern the extent of rock breakage and will be more fully analyzed in chapter 4. Of interest is a very large ratio of compressive to tensile strength, or blastability coefficient, indicating that rocks are far less resistant to tension than to compression in failure.

I.3 Processes In Rock Fragmentation

In this section we proceed to describe the physical processes that are generally observed in the rocks surrounding the shothole after the detonation of an explosive source. The charge is considered to be buried in an infinitely extended solid medium so that the effects of free boundaries are not examined. Figure 1.1 illustrates the different regions being produced as a results of the detonation. Roughly speaking, three zones of interest have been identified. These include the source zone where the processes are essentially hydrodynamic, followed by a transitional or "shattered" zone which includes crushing and radial cracking of the surrounding rocks and a seismic zone where the pulse travels essentially as an elastic wave, neglecting the attenuation losses.

The source zone is concerned with the origin of the energy loading which may include variety of sources such as high explosives, nuclear explosives, high velocity-mechanical impacts and so forth. For a high explosive, following the detonation the explosive cavity is initially thought to be filled with gaseous detonation products at high pressures and temperatures in orders of 1000

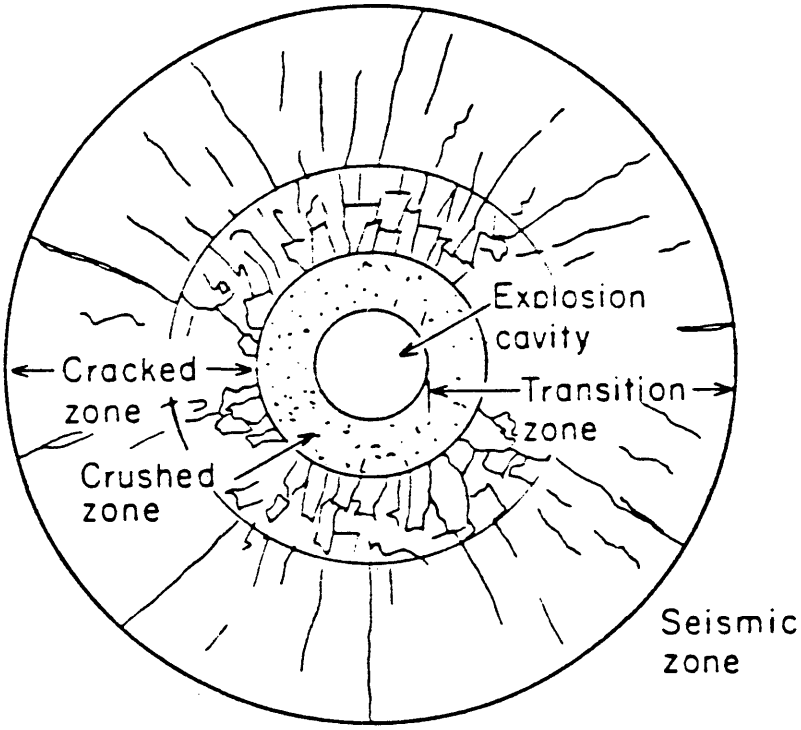

Figure 1-1 Observed zones of deformation after the detonation of a chemical explosive.

megapascals (MPa) (or about 1.45×10^5 psi) and 3000° K respectively. This high pressure pulse generally requires times of the order of few milliseconds in order to fall appreciably as compared to tens of micro-seconds in reaction time required for the chemical reactions in detonation to take place. In a chemical explosives, very high kinetic energy is produced in the resulting gaseous molecules, atoms and ions, which if the explosive completely fills the hole, is immedialtely applied to the surrounding undisturbed rocks.

Important to any theoretical investigation is a good knowledge of the pressure-time history of the gases produced as a result of detonation. Although experimentally this is a formidable task, many strain measurements have been made by the U.S. Bureau of mines in the seismic zone near the explosion (see for example Duvall and Atchison, 1957, and their extensive bibliography). Generally speaking, their measurements involved radial strain measurements from gages that were placed in drill holes at various distances along a linear array from the shotholes. Measurements were generally taken in a wide variety of rock environments using both concentrated and long cylindrical charges and different loading methods. A typical record is shown in Figure 1.2. For most charges in the sedimentary environments of interest

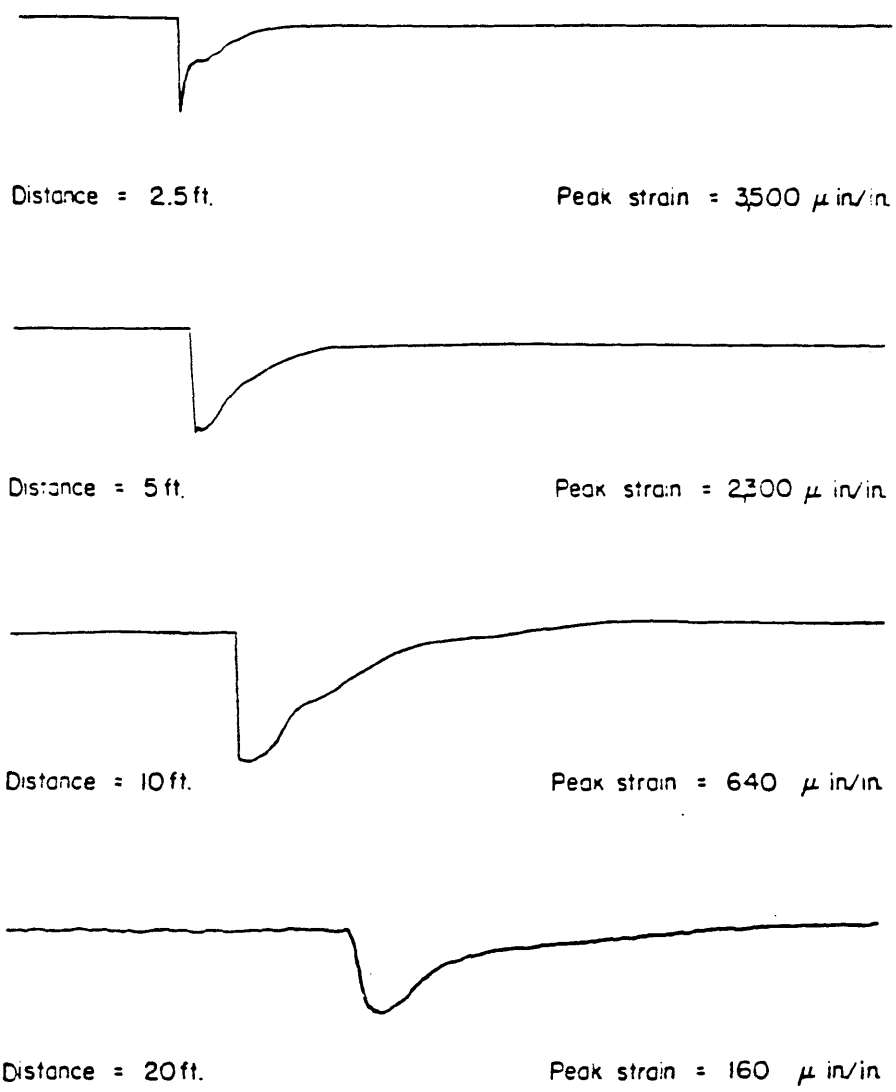

Figure 1-2 Strain measurements in a sandstone formation. (after Duvall, and Atchison, 1957)

to exploration geophysics and at close distances from the source, the strain pulse consisted of a strong compressive phase which fell to zero in 1-3 milliseconds. At larger distances, however, the strain becomes more oscillatory with a tensile phase also becoming more evident resembling a damped sinusoid.

Although one can extrapolate this type of strain measuremets from close-in gages for obtaining the p-t history of the gases produced at the cavity, this method is not fully satisfactory due to the many complicated processes that occur in the transitional boundary. An implication of the method, none-the-less, is that the pressure wave can be modelled as an exponentially decaying step function in time.

Recently, however, pressure measurements have been made for various size charges at the source cavity (Otuonye, et al.). These measurements are shown in Figure 1.3. Although some questions have been raised with regard to the degree of the reliance of the experimental technique being used, the results indicate the decay rate and the peak observed pressure to increase with increasing charge sizes. For a 20-gram size charge, for example, the pressure has decayed appreciably after 2 milliseconds time duration.

In our physical modelling of the problem we have assumed the p-t curve to drop appreciably in one model in

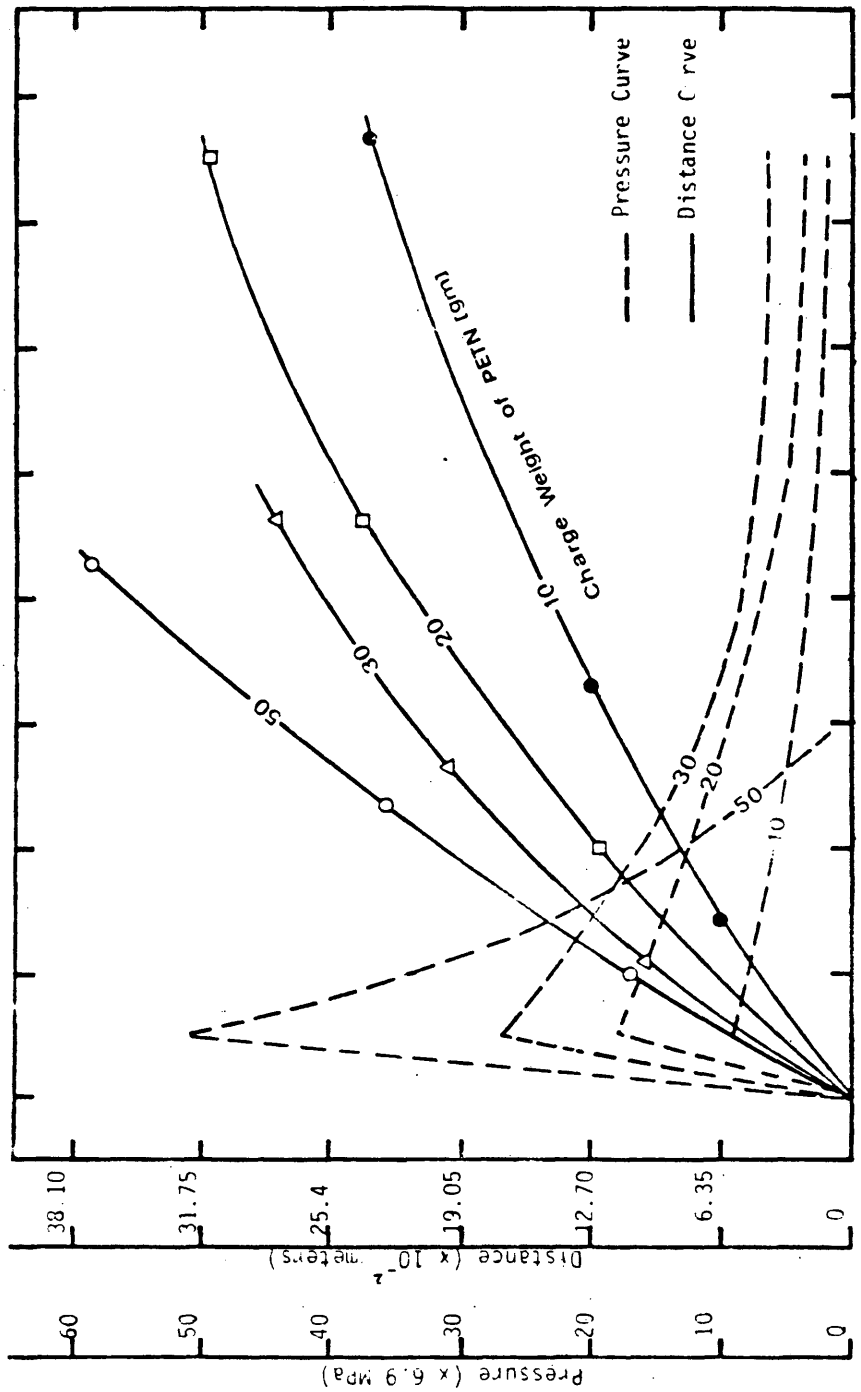

Figure 1-3 Pressure-time measurements for dynamite sources at the cavity wall. (after Otuonye et al., 1983)

about 0.83 milliseconds and 0.2 seconds in the other so that the 1/e points in the exponential decay of the theoretical pressure functions corresponded to 1.66 msec and 0.1 seconds respectively. In effect then, the latter case can be considered like a step response as compared to the former.

Due to the very high pressures exerted by the detonation wave, the rock immediately surrounding the source zone is considered to fail in a complicated manner. This zone where non-elastic and possibly non-linear permanent deformations are known to occur is generally regarded as the transitional (after Atchison and Duvall) or the "shattered" zone by some authors. For a chemical explosive this region generally consists of a small crushed zone followed by a larger cracked zone due the radial cracking of the rocks from the expanding gases in detonation. Although no appreciable vaporization or melting which is characteristic of a nuclear type source is observed, rocks in the shattered boundary are severely crushed and caused to flow plastically as the result of the explosion. To date no satisfactory theory is proposed to successfully describe the various phenomena at hand nor the size of the transitional zone from the source and rock properties. Due to the many experimental complications, very few data are available in the rock mechanics literature on this region.

Historically, this zone was thought to have been formed as a result of shock waves generated at the cavity boundary. A shock wave is known to be developed by successive pressure pulses of ever-increasing velocities which by overrunning those in front, are developed to a sharp discontinuous step wave front. Although the behavior of shock waves in fluids are relatively well known (for example Cole, 1948) little information is available in the literature concerning the mechanics of formation and propagation of shock waves in solids. The basic criterion for the existance of the shock waves requres $d\sigma/d\varepsilon>K$ for stress σ and strain ε and K bulk modulus, in addition to the Von Neumann criterion that the shock velocity V to be greater than sonic velocity for the development of stable shock waves. Based on the Von Neumann's second criterion, a threshold pressure for shock wave propagation in various materials can be calculated. Cook (1974) surveyed the literature for threshold pressures for various rock types and metals and found the value to range from 30 kb for lead to 210 kb for Solenhofen limestone, 310 kb for a marble and to 315 kb for Westerly granite. Considering the very high threshold pressures involved, shock propagation is not considered to take place in normal blasting unless very high porosities are involved. This was confirmed by Duvall and

Atchison (1962) where they studied the phenomenon in many rock types including chalk, sandstone (density 2.2 gr/cm^3 and porosity 20%), marlstone (density 2.1 gr/cm^3) and a granite (density of 2.63 gr/cm^3). From the observed data, the shock wave phenomenon was only hinted at in the porous sandstone formation with only one of the basic criteria for the existance of shock waves being observed. Further examination of the data along with the consideration of the high threshold pressures needed for the existance of shock waves led the authors to conclude that plastic waves were essentially involved in all four rock types. In the crushed zone, however, both crushing and plastic expansion is known to be taking place.

Despite the general lack of an acceptable theory describing the transitional zone, a number of measurements have been taken by various authors in the literature. Atchison et al (1964) measured the radius of crushed zone to be twice and the transitional zone some 12 times the charge radius. Short (1961) examined the same phenomenon for a 1000-lb charge of TNT in Winnfield salt and observed plastic deformation with no evidence for crushing. Radial cracks, however, extended up to 12 times the charge radius. Duvall and Atchison (1957) also measured the extent of the transitional zone and concluded that for charges less than

100 lb, this boundary is not likely to be larger than 10 ft for the four rock types of granite, marlstone, sandstone and chalk. Measurements near a 1.5 kiloton nuclear explosive in Nevada likewise indicated the shattered zone to be relatively small, terminating at only 275 ft from the source (Latter et al., 1959). The extent of the transitional zone is thus very small, of the order of 7-12 times the charge radii for the charges and the sedimentary environments of interest to exploration geophysics.

Outside the transitional boundary, normally a strong compressive stress pulse is transmitted with its shape governed more by the rock than source properties. The seismic zone has, of course, been subject to extensive research in the geophysical literature.

I.4 Survey of Some Proposed Physical Models

Most of the literature concerning the problem of dynamite behavior in a rock body describes the application of an appropiate source function to a spherical or cylindrical boundary in an infinitely extended medium. Some of the mathematical-physical models which have been considered describe wave behavior in rock masses of ideally elastic, elastic solid-friction and several attenuating models including visco-elastic Voigt and Maxwell rheologies.

For the spherical wave equation, several authors investigated the application of a pressure pulse to an empty spherical boundary in an elastic surrounding medium. Sharpe (1942) and Blake (1952) solved this boundary problem for several source functions including an exponentially decaying one by means of a Fourier integral. Clark (1952) used the method of Laplace transform to solve the problem for a unit step function while Duvall (1953) used a double exponential decay source of the form

$$P(t)=P_0(e^{-\alpha t}-e^{-\beta t}) \qquad (1\text{-}2)$$

to account for some of the waveform variations of the input source function.

Typical solutions for a unit step source as obtained from Sharpe's calculations indicate the radial displacement to start at zero and execute a damped sinusoidal behavior. The waveform shape roughly resembled the observed field data for the dynamite pulses. For a typical cavity size of 10 cm, however, the pulse duration is reduced by a factor of 10 or so from what is normally observed. Only if the size of the cavity is increased to a few meters in radius can the pulse duration be extended to the right order of magnitude. Some authors (Sharpe, 1942; Gaskell, 1956) have, therefore, proposed an "equivalent radiator" hypothesis which requires large empty spherical sources with their outer boundary defining the limiting elastic behaviour of the surrounding rocks. As discussed earlier, most of the rock fracturing around the source occurs at a much smaller radius than that suggested by this hypothesis, so one can conclude that the "equivalent cavity" hypothesis does not correspond to any physical surface and is only a means of increasing the time duration of the signal.

Following Sharpe's model for a spherical cavity in an elastic medium, Heelan (1953) obtained far-field solutions due to a transient pressure pulse applied to a

short length of an infinitely extended cylindrical hole in terms of two displacement potentials. He investigated the stress acting radially as well as circumferentially and axially on the cylinder wall. For the latter two cases, he found the radiated displacements to be proportional to displacements due to a simple source consisting of two couples with moment and a point force, respectively.

Recognizing the non-elastic attenuation properties of the earth, some authors analyzed the same problem in a lossy earth material. For a linear visco-elastic Voigt solid, Collins (1960) solved the plane wave equation with a unit impulsive type source by means of Laplace transform and Ricker (1951) by Fourier transform. Ricker (1951) derived expressions for plane wave particle velocity and compared them with a series of VSP type field data obtained from various size charges. He concluded the earth material to behave essentially as a visco-elastic solid. This implies the attenuation coefficient to vary as the square of the frequency. Later work by Mcdonal et al. (1958), however, obtained a more linear attenuation frequency relationship for most sedimentary earth materials.

Some authors considered the solution for the spherical wave equation for the Voigt solid. Lee (1964) obtained the steady state solution for both sinusoidal and

exponentially decaying pressure functions applied to a modified Voigt solid. In his Fourier integral expressions, however, he introduced a "constant Q" assumption which implied attenuation coefficient to vary linearly with frequency. This assumption introduced some mathematical difficulties and his expressions were inverted into the real time plane by the residue method.

Another model which assumes attenuation to vary as frequency to the first power is the solid friction model as discussed by Knopoff (1956). Clark (1966) investigated the solution in the solid friction model due to an exponentially decaying source and concluded the digitally computed particle displacement values to be similar to the constant loss factor results obtained by Lee (1964). Both of these models indicate a non-zero value for displacement at the delayed time value equal to zero and are thus non-causal.

Although most of these models treat wave motion resulting from the application of various forms of forcing functions to the surface boundaries of spherical or cylindrical cavities in a variety of earth models, none has taken the transitional shattered zone into consideration. This can perhaps explain some of discrepancies that exist between observed field data and the theoretical calculations. Only Peet (1960) included some account of the

deformation zone that occurs around the explosive zone. Following the analysis of Cole for underwater explosives, Peet (1960) assumed shock waves to be propagated in the shattered zone. Assuming that most dynamite shots were detonated in porous water-saturated rocks, he reasoned water to govern the transmission of the high-stress waves. He thus concluded an exponentially decaying source to retain its form with only its amplitude being reduced to a value characteristics of a limiting yield stress value of the surrounding rocks. The model therefore, implies application of the assumed pressure function to a large fictitious equivalent cavity.

Although as discussed earlier, shock waves are not generally observed in the shattered zone, Peet's calculations constituted an attempt to include the rock deformational phenomenon in the modeling of the problem. By making use of Cole's similarity conditions, Peet also found the radius of the shattered zone to vary as a third power of the charge size. He did not, however, attempt to calculate a typical size of the shattered zone due to unknown values of proportionality constants in his relationships.

The nature and size of the shattered zone has been of some importance particularly for the mining industries in predicting the extent of the "craters" (see for example

Atchison, 1968) that are formed as a result of relatively shallow shots. Since the theories are of little use to the practicing engineer in the field, most of the crater scaling information has been obtained from the data collected in the field, most notably by the U.S. Bureau of Mines. Only Cherry (1967) described a computer scheme which could predict some of the crater dimensions being formed from mostly high explosives and nuclear sources.

Work done by the U.S. Bureau of Mines has attempted to find the correlation between crater size and the measured peak compressive strains in rocks. These measured strain waves in various rock formations have been useful in comparing differing explosives, but again not yet employed in production purposes despite of the vast number of measurements being made.

In the transitional zone around the cavity, it is well known that a great amount of energy is absorbed by the complicated processes of crushing and cracking that occur as a result of explosion. Also due to intense micro- and macro-fracturing, the rocks around the shothole can not be expected to retain the integrity of their bulk structure and can be assumed to behave as a plastic fluid of a very high viscosity. Although the region of shattered zone can be formed by more than one process, in our model we have

assumed it to solely behave as a highly viscous liquid of linear Voigt type visco-elastic rheology. Other mathematical models can equally be applied to describe this zone like the low loss or near-elastic model (White, 1983) where here the loss of energy can be introduced by a small frequency independant phase angle term that strain lags behind stress. In this work, however, only a visco-elastic type of liquid is considered. A sharp transition is further assumed between the shattered viscous boundary and the surrounding elastic zone. So here we proceed with a formal statement of the problem:

> Given a spherical cavity of radius A first within a visco-elastic liquid of radius B and then surrounded by an ideally homogeneous, isotropic and infinitely extended elastic medium, to find the solution to the wave equation by Fourier transform as a result of application of a pressure pulse to the interior of the cavity.

In our physical modeling of the problem as well as most of the published papers in the literature, we have assumed a spherical type charge with a known and constant p-t history for all size charges to completely fill a shothole cavity. A graphical representation of the model along with notations used for elastic rock properties are shown in Figure 1.4.

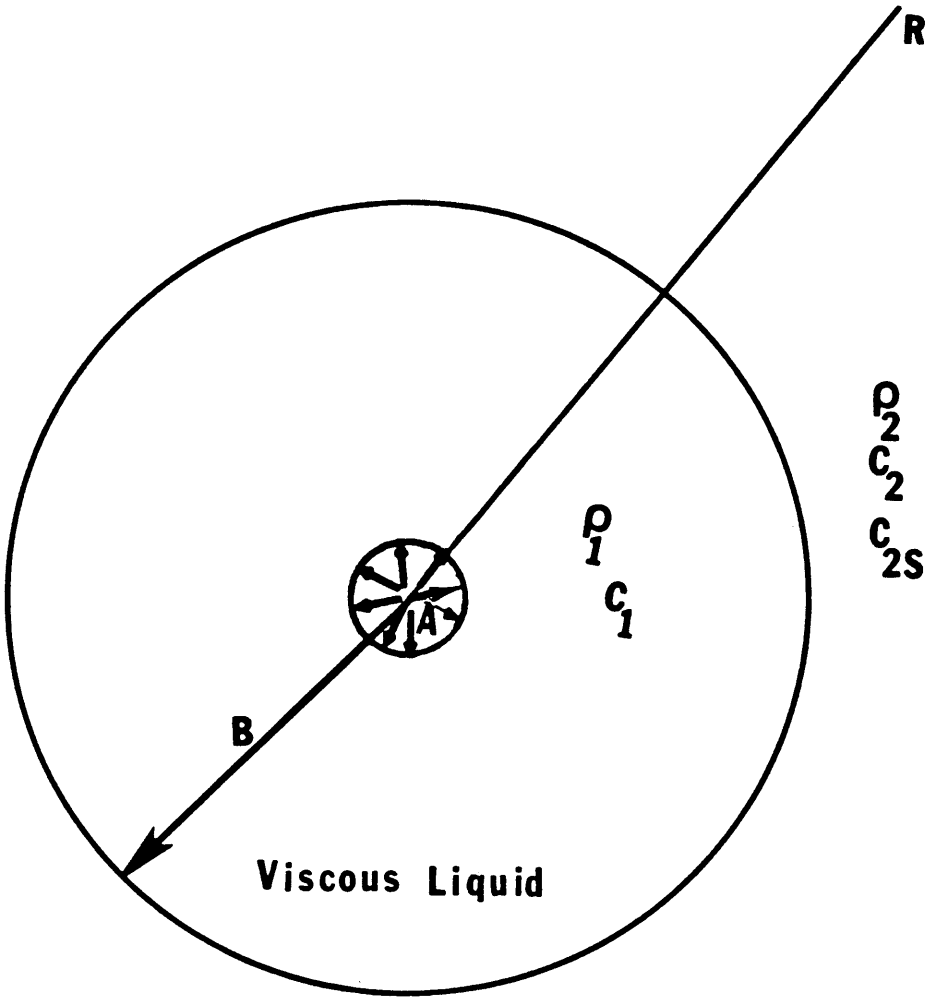

Figure 1-4 The assumed model.

II. MATHEMATICAL FORMULATION AND THE DEVELOPMENT OF THE THEORY

II.1 Method of Approach

The purpose of this chapter is to trace the theoretical development required in solving our problem using a digital computer. Solutions to the wave equation are to be considered in both visco-elastic and elastic regions subject to the appropiate boundary conditions. These include the continuity of radial stress at the two boundaries r=a and r=b and continuity of radial displacement at r=b as defined in our model (Figure 1.4). The computed expressions for particle velocity $V(r,\omega)$ are then to be inverse Fourier transformed to obtain the time expressions $v(r,t)$ as the final output to be displayed. This chapter also develops the theoretical considerations in the analysis and Fourier transformation of one-dimensional digitized data.

Throughout this discussion a subscript "1" specifies the visco-elastic liquid and subscript "2" indicates our reference to the surrounding infinitely extended elastic medium. The upper case functions, in addition, are used to denote complex frequency amplitudes.

II.2 Development of Solution in terms of Displacement Potential in the Elastic Medium.

Let us first consider wave propagation in the surrounding elastic medium. For the wave equation given by

$$\nabla^2\phi_2 = \frac{1}{c^2}\,\frac{\partial^2\phi_2}{\partial t^2} \qquad (2\text{-}1)$$

we seek a solution in terms of displacement potentials ϕ_2, where the radial component of displacement is given by $u_r = \frac{\partial\phi_2}{\partial r}$. Due to the geometry involved, we recognize the spherical coordinate system as natural in solving the boundary problem. Since we assume a uniform pressure to be applied to the interior of cavity, all the particle motions are considered to be radial and irrotational and therefore independent of the angular variables so that

$$\nabla^2\phi_2 = \frac{1}{r^2}\,\frac{\partial}{\partial r}\left(r^2\,\frac{\partial\phi_2}{\partial r}\right) \qquad (2\text{-}2)$$

The solution in 2-1 can now be separated out into a

time and space dependent factors, as

$$\phi_2(r,t) = R(r)\ T(t) \tag{2-3}$$

The time dependence in 2-3 is assumed to be exponential and we set it equal to $e^{i\omega t}$. A possible solution to the wave Equation 2-1 representing a wave going in an outward direction in the elastic medium assumes the form

$$\phi_2(r,t) = \frac{1}{2\pi} \int_{-\infty}^{\infty} \frac{C(\omega)}{r}\ e^{-i\omega r/c_2}\ e^{i\omega t}\ d\omega \tag{2-4}$$

$$= \frac{1}{2\pi} \int_{-\infty}^{\infty} \frac{C(\omega)}{r}\ e^{-k_2 r}\ e^{i\omega t}\ d\omega \tag{2-5}$$

where c_2 is the compressional wave velocity and k_2 is the wave number which we define as $i\omega/c_2$. Displacement is then given by

$$u_2 = \frac{\partial \phi_2}{\partial r} \tag{2-6}$$

and $C(\omega)$ is an arbitary complex coefficient to be determined from the boundary conditions.

II.3 Displacement Potential Solution in the Visco-Elastic Liquid

As mentioned previously the "shattered" zone around the spherical hole is modelled as a visco-elastic liquid. Most of the mathematical relationships describing a visco-elastic or Voigt solid are described in Appendix A.

It is shown that the classical scalar wave equation for displacement potentials is modified to

$$\nabla^2[\phi_1 + \frac{1}{\omega_0} \frac{\partial \phi_1}{\partial t}] = \frac{1}{c_1^2} \frac{\partial^2 \phi_1}{\partial t^2} \tag{2-7}$$

for a Voigt solid, where

$$\omega_0 = \frac{\lambda_1 + 2\mu_1}{\lambda_1' + 2\mu_1'} = \frac{M_1}{M_1'} \tag{2-8}$$

$$c_1^2 = \frac{\lambda_1 + 2\mu_1}{2\rho} \tag{2-9}$$

and M_1 is the plane wave modulus. For a liquid with no rigidity, we have $\mu=0$ and furthermore we take the following simplifying assumption as $\lambda'=0$ (see Appendix A), so the wave equation 2-7 for visco-elastic liquid becomes

$$[\lambda_1 + 2\eta \frac{\partial}{\partial t}] \nabla^2(\phi_1) = \rho \frac{\partial^2(\phi_1)}{\partial t^2} \tag{2-10}$$

where η is the viscosity of the liquid.

A possible solution to the modified wave equation 2-10 represents a propagating outgoing spherical wave from the surface of the spherical cavity (r=a) and a reflected wave from the elastic/inelastic boundary (r=b) as

$$\phi_1(r,t) = \frac{1}{2\pi}\left\{\int_{-\infty}^{\infty} \frac{A(\omega)}{r} \exp\left[-a_1 r + i\omega\left(t - \frac{r}{c_1}\right)\right] + \right.$$
$$\left. + \frac{B(\omega)}{r} \exp\left[a_1 r + i\omega\left(t + \frac{r}{c_1}\right)\right]\right\} d\omega \qquad (2\text{-}11)$$

Writing

$$\phi_1(r,t) = \frac{1}{2\pi} \int_{-\infty}^{\infty} \Phi_1(r,\omega)\, e^{i\omega t}\, d\omega \qquad (2\text{-}12)$$

we obtain from equation 2-11

$$\Phi_1(r,\omega) = \frac{A(\omega)}{r} e^{-k_1 r} + \frac{B(\omega)}{r} e^{k_1 r} \qquad (2\text{-}13)$$

where k_1 is the attenuated wave number defined as

$$k_1 = a_1 + \frac{i\omega}{c_1} \qquad (2\text{-}14)$$

and a_1 is the attenuation coefficient, (White, 1983)

$$a_1 = \frac{\omega_0(\omega^2/\omega_0^2)}{[2(M/\rho)(1+\omega^2/\omega_0^2)(\sqrt{1+\omega^2/\omega_0^2}+1)]^{\frac{1}{2}}} \tag{2-15}$$

$$c_1 = \left[\frac{2(M/\rho)(1+\omega^2/\omega_0^2)}{\sqrt{1+\omega^2/\omega_0^2}+1}\right]^{\frac{1}{2}} \tag{2-16}$$

Note that Eqs. 2-15 and 2-16 which are derived for the case of plane waves are valid, in our problem, for spherical waves as well . $A(\omega)$ and $B(\omega)$ are again complex values to be determined from the boundary conditions in the problem. Since the condition of $\omega^2 >> \omega_0^2$ is satisfied, in our computations we can use the low frequency approximation forms to the equations above

$$a_1 = [\omega_0/2(M/\rho)^{\frac{1}{2}}]\ (\omega^2/\omega_0^2)$$

$$c_1 = (M/\rho)^{\frac{1}{2}} \tag{2-17}$$

II.4 Boundary Conditions

For the three complex constants $A(\omega)$, $B(\omega)$ and $C(\omega)$ we have 3 boundary conditions which are as follows:

1- The continuity of the radial stress P_{rr} in the visco-elastic liquid with the pressure applied to the interior surface of the cavity p(t) at r=a or

$$P(\omega)=-P_{rr1}(a,\omega)$$

2- The continuity of radial stress across the r=b boundary

$$P_{rr1}(b,\omega)=P_{rr2}(b,\omega)$$

3- The continuity of the radial component of displacements at r=b or

$$U_{rr1}(b,\omega)=U_{rr2}(b,\omega)$$

Boundary condition #1 requires the continuity of the pressure applied to the spherical cavity p(t) with the radial stress in the visco-elastic medium. If we take p(t) to be Fourier transformable, we may write

$$p(t) = \frac{1}{2\pi} \int_{-\infty}^{\infty} P(\omega)\, e^{i\omega t}\, d\omega \qquad (2\text{-}18)$$

or $p(t) \longleftrightarrow P(\omega)$

Observe that upon cancellation of the time

dependence from the boundary conditions one can solve the problem in the frequency domain and transform into time domain using a Fourier synthesis approach.

The modified expression for radial stress in a visco-elastic liquid (η=0, λ_1'=0) is taken from Lee (1964) as

$$p_{rr1} = -\{[\lambda + 2\mu' \frac{\partial}{\partial t}] \frac{\partial u_1}{\partial r} + 2(\lambda) \frac{u_1}{r}\} \tag{2-19}$$

Recognizing

$$u_1(r) = \frac{\partial \phi_1}{\partial r} \tag{2-20}$$

and

$$\frac{\partial}{\partial t} u_1(r) \longleftrightarrow i\omega U_1(r) \tag{2-21}$$

We substitude 2-13 in 2-19 so that

$$\begin{aligned} P(\omega) = \{A(\omega)\, e^{-k_1 r} [&\frac{\lambda_1 k_1^2}{r} + \frac{4\mu_1' i\omega}{r^3} + \frac{4\mu_1' i\omega k_1}{r^2} + \frac{2\mu' i\omega k_1^2}{r}] + \\ &+ B(\omega)\, e^{k_1 r} [\frac{\lambda_1 k_1^2}{r} + \frac{4\mu_1' i\omega}{r^3} - \frac{4\mu_1' i\omega k_1}{r^2} + \\ &+ \frac{2\mu' i\omega k_1^2}{r}]\}\Big|_a \end{aligned} \tag{2-22}$$

In order to simplify the equation 2-22 above, we use the

following definitions

$$k_1 = a_1 + i\omega/c_1$$

$$\gamma = \mu_1' \, i\omega \tag{2-23}$$

$$\beta = \lambda_1 + 2\mu_1' \, i\omega$$

Multipying both sides of 2-22 by a^3 we obtain our first expression of the boundary problem

$$A(\omega)\,[4\gamma + 4a\gamma k_1 + \beta a^2 k_1^2]\, e^{-k_1 a} + \tag{2-24}$$

$$B(\omega)\,[4\gamma - 4a\gamma k_1 + \beta a^2 k_1^2]\, e^{k_1 a} = -\,P(\omega)\, a^3$$

Boundary condition #2 expresses the continuity of the radial stress at r=b, the inelastic/elastic boundary. The expression for radial stress in an elastic medium is given by

$$-p_{rr2}(r,t) = (\lambda_2 + 2\mu_2)\,\frac{\partial^2 \phi_2}{\partial r^2} + \frac{2\lambda_2}{r}\,\frac{\partial \phi_2}{\partial r} \tag{2-25}$$

Substituting the expression for ϕ_2 (equation 2-5) into 2-25, $P_{rr2}(r,\omega)$ becomes

$$-P_{rr2} = \left[\frac{C(\omega)}{r}\,\lambda_2\, k_2^2\, e^{-k_2 r} + 2\mu C(\omega)\left[\frac{2}{r^3} + \frac{2k_2}{r^2} + \frac{k_2^2}{r}\right] e^{-k_2 r}\right. \tag{2-26}$$

Equation 2-26 and 2-22 are equal at r=b and using definitions in 2-23 and M_2 below for the plane wave modulus,

$$M_2 = \lambda_2 + 2\mu_2 \tag{2-27}$$

we obtain at the expression for the second boundary condition

$$\begin{aligned} &A(\omega)[4\gamma + 4\gamma k_1 b + k_1^2 b^2 \beta]\, e^{-k_1 b} + \\ &+ B(\omega)\,[4\gamma - 4\gamma k_1 b + k_1^2 b^2 \beta]\, e^{k_1 b} + \\ &- C(\omega)\,[4\mu_2 + 4\mu_2 b k_2 + b^2 k_2^2 M]\, e^{-k_2 b} = 0 \end{aligned} \tag{2-28}$$

Boundary condition #3 requires the continuity of radial displacement at r=b. We note that for r=b

$$\frac{\partial \phi_1}{\partial r} = \frac{\partial \phi_2}{\partial r} \tag{2-29}$$

Setting the equality above, we write

$$\begin{aligned} &-A(\omega)[1 + k_1 b]\, e^{-k_1 b} + B(\omega)[-1 - k_1 b]\, e^{k_1 b} + \\ &C(\omega)[1 + k_2 b]\, e^{-k_2 b} = 0 \end{aligned} \tag{2-30}$$

II.5 Solving the Problem with the Aid of a Digital Computer

Our goal is to solve for the radial component of velocity $V_2(r,\omega)$ for each value of frequency in the computer and then transform into the time domain using a suitable Fast Fourier Transform subroutine (FFT). Expression for radial displacement is given by

$$U_2(r,\omega) = - C(\omega)[\frac{1}{r^2} + \frac{k_2}{r}] e^{-k_2 r} \tag{2-31}$$

We recognize that $V_2(r,\omega) = i\omega U_2(r,\omega)$

$$v_2(r,t) = \text{FFT } [V_2(r,\omega)] \tag{2-32}$$

The complex coefficient $C(\omega)$ in 2-31 is found by solving the boundary problem.

Computer program CONSTANT in Appendix (B) was written to digitally calculate $C(\omega)$ and perform the Fourier transformation. This program uses the following simplified definitions:

$$\begin{aligned} \Omega &= [4\gamma + 4\gamma a k_1 + k_1^2 a^2 \beta]\ e^{-k_1 a} \\ \Omega' &= [4\gamma - 4\gamma a k_1 + a^2 k_1^2 \beta]\ e^{k_1 a} \end{aligned} \tag{2-33}$$

$$\Gamma = [4\gamma + 4\gamma k_1 b + k_1^2 b^2 \beta]\, e^{-k_1 b}$$

$$\Gamma' = [4\gamma - 4\gamma k_1 b + k_1^2 b^2 \beta]\, e^{k_1 b}$$

$$\Gamma'' = [4\mu_2 + 4\mu_2 k_2 b + k_2^2 M b^2]\, e^{-k_2 b} \qquad (2\text{-}34)$$

$$\psi = -[1 + k_1 b]\, e^{-k_1 b}$$

$$\psi' = [-1 + k_1 b]\, e^{-k_1 b}$$

$$\psi'' = [1 + k_2 b]\, e^{-k_2 b}$$

The expression for boundary conditions simplify to

$$A\Omega + B\Omega' = -P(\omega)\, a^3$$

$$A\Gamma + B\Gamma' - \Gamma'' C = 0 \qquad (2\text{-}35)$$

$$A\psi + B\psi' + C\psi'' = 0$$

where the complex constant $C(\omega)$ is then found by solving the simultaneous equations above:

$$C(\omega) = \frac{P(\omega)\, a^3 (\Gamma\psi' - \psi\Gamma')}{(-\Omega\psi''\Gamma' + \Omega'\Gamma\psi'' + \psi\Omega'\Gamma'' - \Gamma''\Omega\psi')} \qquad (2\text{-}36)$$

The variable names in the computer program CONSTANT are defined on the same basis as the text to avoid confusion. The value of $C(\omega)$ is thus calculated for each value of

frequency in this program. In the final process of calculating the complex constant $C(\omega)$ values for a source function $P(\omega)$ and a suitable pre-conditioning window have to be calculated.

II.6 Digital Developments Leading to FFT

As mentioned before, a Fourier Synthesis approach is adopted to solve our problem in the frequency domain. Our sampled frequency waveform has to be inverse Fourier transformed into the time domain for analysis. In order to use the computer-efficient procedure of a Fast Fourier Transform (FFT) algorithm, it is required to adopt a dualistic approach (e.g., Hadsell, 1980, p. 3-90) in that neither time nor frequency domains are taken to be basic for digital analysis. An implication of this approach is that both time and the transformed frequency functions are represented by a periodic distribution of equally-spaced spikes with equal number of samples in both domains. This procedure, however, calls for special care in the choice of the parameters being used.

Since the problem is posed in the frequency domain, we take our frequency function $G(r,\omega)$ to be Fourier transformable in that

$$g(r,t) = \frac{1}{2\pi} \int_{-\infty}^{\infty} G(r,\omega)\ e^{i\omega t}\ d\omega \qquad (2\text{-}37)$$

Before discussing the digital analysis of $G(r,\omega)$ let us look at its components individually, namely, our source function, which gets multiplied by a "transmission coefficient" as in Eqs. 2-36 and 2-31 and the truncating window.

II.6.A Source function

Since the pressure applied to the surface of the empty cavity in our model is due to that of a dynamite charge, our source function can be thought to have a rapid rise at the origin, followed by an exponential decrease of amplitude as a function of time. A particularly convenient model can thus be written as

$$\begin{aligned} p(t) &= P_0\ e^{-t/t_0}\ U(t) \\ &= P_0\ e^{-\alpha t}\ U(t) \end{aligned} \qquad (2\text{-}38)$$

where $\alpha(=1/t_0)$ is the damping factor, $U(t)$ is the unit step function and $p(t)$ has a Fourier transform given by

$$P(\omega) = P_0\ \frac{1}{\alpha + i\omega} = |P(\omega)|\ e^{i\theta} \qquad (2\text{-}39)$$

The real and imaginary components as well as the amplitude and phase are given

$$\begin{aligned} \mathrm{Re} &= \frac{P_0\alpha}{\alpha^2 + \omega^2} \\ \mathrm{Im} &= \frac{-P_0\omega}{\alpha^2 + \omega^2} \\ |P(\omega)| &= \frac{P_0}{(\alpha^2 + \omega^2)^{\frac{1}{2}}} \\ \theta(\omega) &= \tan^{-1}\left(\frac{-\omega}{\alpha}\right) \end{aligned} \qquad (2\text{-}40)$$

These relations are plotted in Figure 2.1-A in time and in Fig. 2.1-B as a function of linear frequency f. Here we choose one of our sampling parameters, namely, the time period T as 0.2 seconds long. The time constant t_0 in 2-38 is then taken as 0.1 seconds so that the amplitude of the forcing function is reduced sufficiently after the 0.2 second time interval. Note also that after 0.1 seconds, the amplitude is reduced to the 1/e value. A second choice in the time rate of decay of our source function was afforded by choosing the damping factor α, to equal 600 sec^{-1} instead of the previous 10. So our new forcing function can be considered to decay at a much faster rate than the former case. In effect then, the source with α=10 sec^{-1} is like the step response as compared to a more physical case of α=600 sec^{-1}

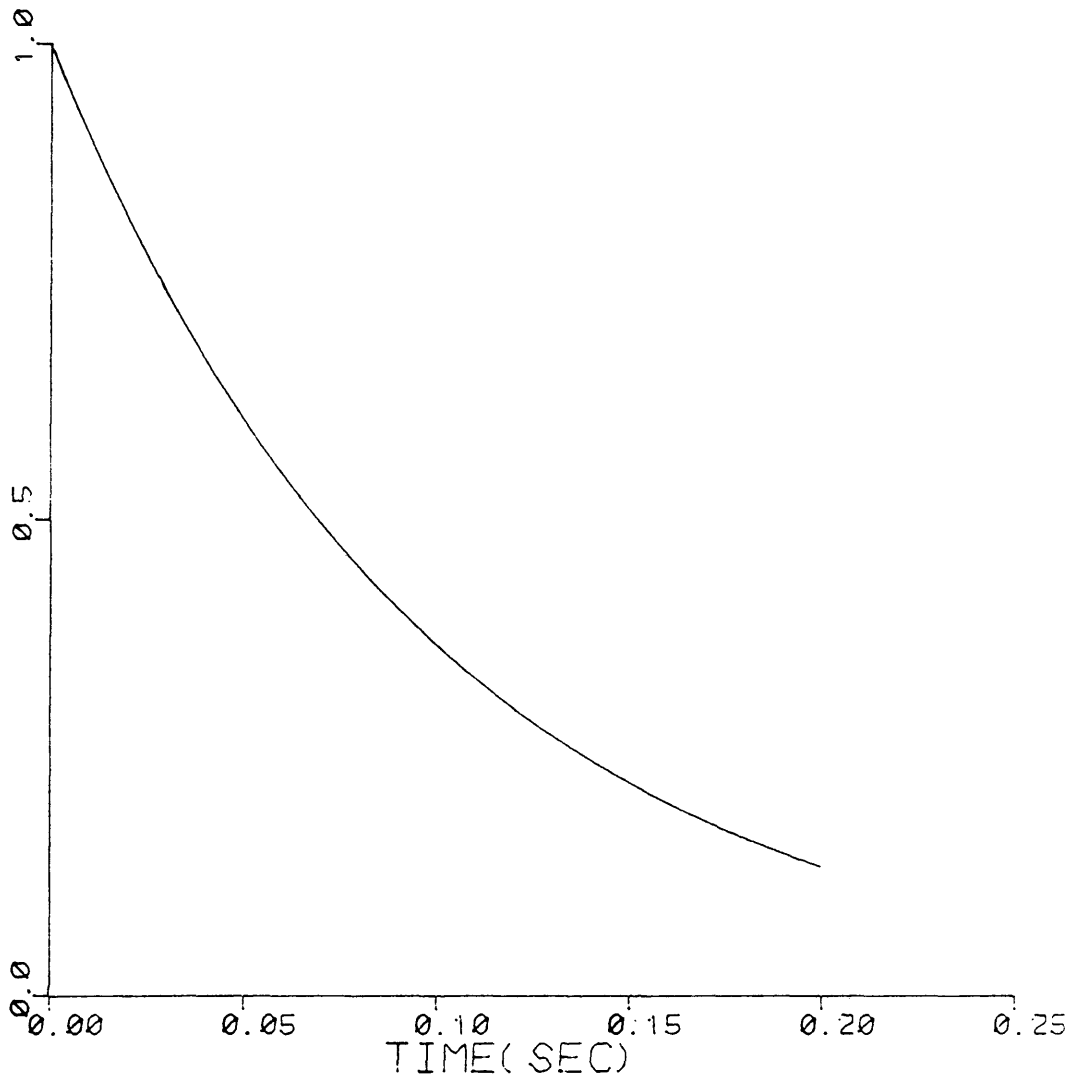

Figure 2-1.A Time domain forcing function.

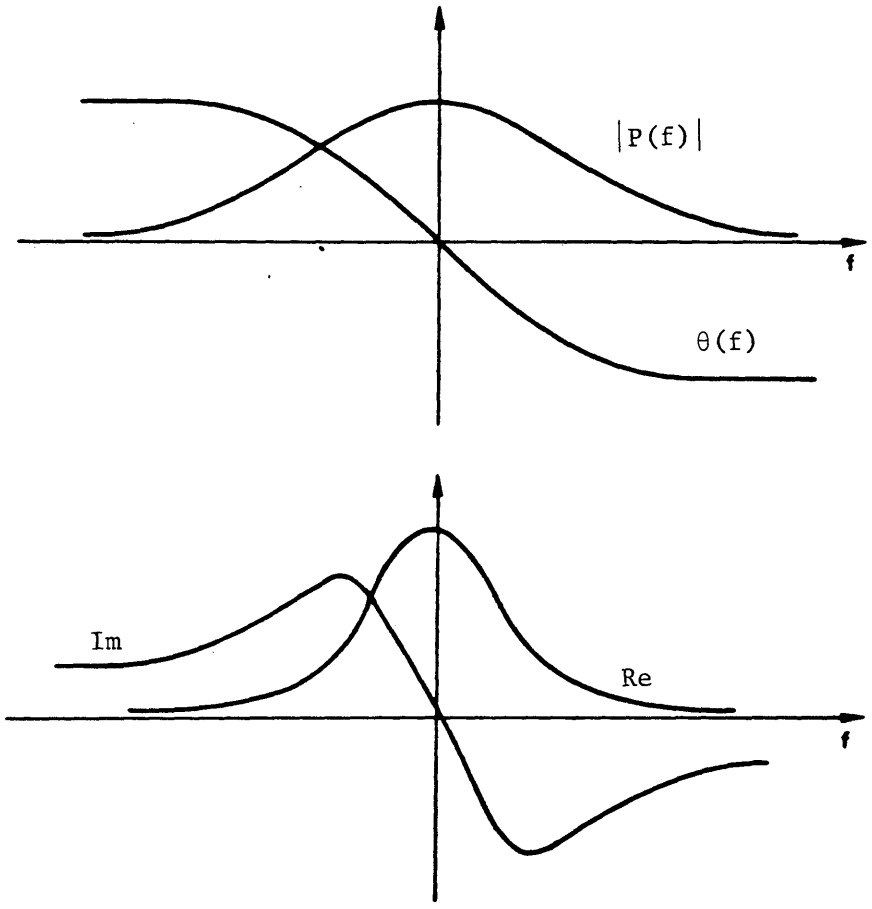

Figure 2-1.B Frequency domain forcing function.

The source function has, however, a zero-frequency component as is evident in Fig. 2.1-B. Since we are to calculate particle velocity, time differentiation of particle displacement results in multiplication by an $i\omega$ factor in the frequency domain (Eq. 2-32). This $i\omega$ factor results in the elimination of the zero-frequency component in the calculations as multiplication of 2-39 with an $i\omega$ gives

$$P'(\omega) = P_0 \frac{i\omega}{\alpha + i\omega} = |P'(\omega)| \, e^{i\theta'} \tag{2-41}$$

with

$$|P'(\omega)| = \frac{P_0 \omega}{(\alpha^2 + \omega^2)^{\frac{1}{2}}} \tag{2-42}$$

and

$$\theta' = \tan^{-1} \left(\frac{\alpha}{\omega}\right) \tag{2-43}$$

So that now we observe that fortunately this "DC" term gets zeroed out from our calculations.

Our forcing function 2-41 is then substituted in the expression for $C(\omega)$ in 2-36 for each value of frequency. But before the FFT procedure, our digitized distribution has to be multiplied by a suitable pre-conditioning window which is described below.

II.6.B Windowing

A simple pre-conditioning filter for the purpose of band limiting of our data is the "Box-car" window $bx(f/2f_c)$ defined as

$$bx(f/2f_c) = 0 \quad \text{if} \quad |f/2f_c| > \tfrac{1}{2}$$
$$= 1 \quad \text{if} \quad |f/2f_c| < \tfrac{1}{2} \tag{2-44}$$

with

$$bx(f/2f_c) \longleftrightarrow 2\, f_c\, \text{sinc}\, (2f_c t) \tag{2-45}$$

where f_c is the cut-off frequency of the window and the sinc function, is defined as

$$\text{sinc}\, (2f_c t) = \frac{\sin\, (2\pi f_c t)}{2\pi\, f_c t} \tag{2-46}$$

Band limiting of our spectrum thus corresponds to the temporal convolution of the original periodic function g(r,t) with a sinc function. If any discontinuities exist in g(r,t), a well-known overshoot (about 9 percent value of the original discontinuity) results on both sides of the discontinuity (Oppenheim and Schafer, 1975; Papoulis, 1962). Increasing the width of window in the frequency only results

in faster oscillations on the overshoot but all at the same amplitude. This is known as the Gibbs' phenomenon and can be reduced somehow through consideration of a less abrupt truncating window.

Many windows have found great utility through smoother descent to zero at both ends. These include Bartlett, Hanning and Hamming windows and so forth, but for the purpose of this thesis we use a half-cycle sinc function as our frequency truncation window W(f) given by

$$W(f) = \frac{\sin(\pi f/f_c)}{nf/f_c} \quad \text{for} \quad |f| < f_c \tag{2-47}$$

$$= 0 \quad \text{for} \quad |f| > f_c$$

Since we have digitized representation $F=2M\Delta f$, where $2M$ is the number of points in frequency, f_c was chosen to be 1400 Hz so that it can be representative of a good wide-band window. Figure 2.2 shows the frequency domain representation of W(f) and Fig. 2.3 corresponds to its Fourier transform.

A much more narrower band DFS-V type windowing was also used on the data which will be described in more detail in the next chapter.

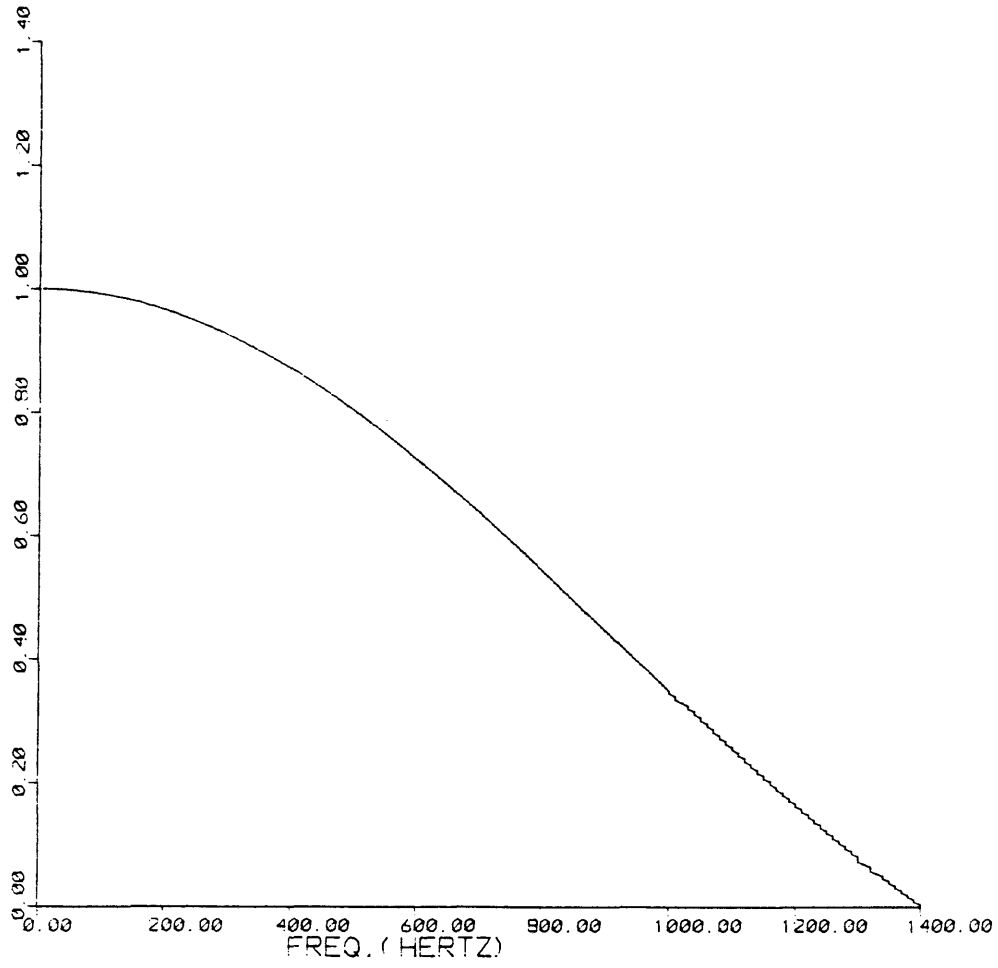

Figure 2-2 Frequency domain window.

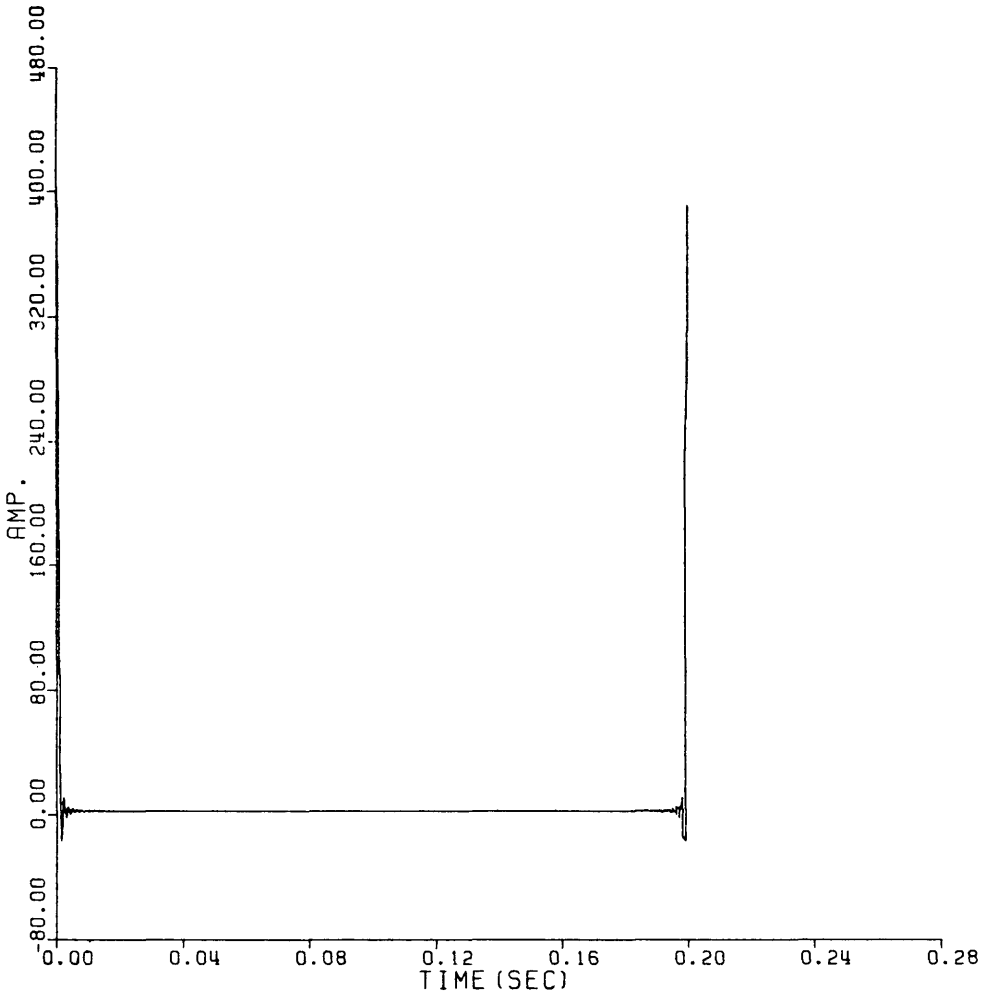

Figure 2-3 Time domain window.

II.6.C Computer analysis

In order for a continuous function G(f) to be suitable for machine computation we first have to digitize it in our calculations. This sampling of G(f) is realized by multiplying it by the "sampling comb" $c_{\Delta f}(f)$

$$C_{\Delta f}(f) = \Delta f \sum_{n=-\infty}^{\infty} \delta(f - n\Delta f) \tag{2-48}$$

so the discrete representation of G(f) is given by the singular distribution

$$G_d(f) = \Delta f \sum_{n=-\infty}^{\infty} G(n\Delta f)\ \delta(f - n\Delta f) \tag{2-49}$$

where $\delta(f)$ is the Dirac's Delta. Since an infinite comb function, or "Dirac's fence", Fourier transforms into another infinite comb, given by

$$2\pi \sum_{n=-\infty}^{\infty} \delta(\omega - n\omega_s) \longleftrightarrow \Delta t \sum_{n=-\infty}^{\infty} \delta(t - n\Delta t) \tag{2-50}$$

for frequency period ω_s, we have temporal convolution of $g_d(t)$ with the right-hand member of 2-50. Because our forcing function is not time-limited, sampling introduces a slight time domain aliasing. To reduce this error we can only choose a smaller Δf, but since the source function's

amplitude is sufficiently reduced after 0.2 second time interval, it is not deemed to be necessary. Note also that $g_d(t)$ becomes periodic as a result of frequency sampling.

Next, we have to truncate the infinity of points represented by 2-49 by means of our window 2-47. Truncation results in again convolution of the aliased g(t) with the Fourier transform of the truncation function. This gives rise to a well-known "rippling" due to the Gibbs' phenomenton. As was mentioned previously, to reduce this rippling we have to increase the width of our window as frequency scaling of the window results in contraction of the w(t) (Fig. 2.3) in the time domain. So now after windowing we have

$$\Delta f \sum_{n=-M}^{M-1} G(n\Delta f)\, \delta(f - n\Delta f)\, W(f) \tag{2-51}$$

Finally, we have to discretize the Fourier transform of 2-51 since this is still a continuous periodic function. This time sampling is equivalent in frequency domain convolution

$$\begin{aligned} \tilde{G}(f) &= \left[\Delta f \sum_{n=-M}^{M-1} G(n\Delta f)\, \delta(f - n\Delta f)\, W(f)\right] * \left[F \sum_{r=-\infty}^{\infty} \delta(f - rF)\right] \\ &= F\Delta f \sum_{r=-\infty}^{\infty} \left[\sum_{n=-M}^{M-1} G(n\Delta f)\, \delta(f - n\Delta f - rF)\right] \end{aligned} \tag{2-52}$$

where here F is the frequency period given by $F=2M\Delta f$. The notation $\tilde{G}(f)$ is to imply that we have an approximate digitized and periodic version of G(f). Now we choose the number of points in the frequency domain 2M (or the time domain) to be 1024 ($=2^{10}$) large enough for our window as will be evident later. Our frequency period F is then

$F=1024x5=5120$ Hz

So now with our choice of Δf and F we have our mathematical relationship in 2-52 complete for 2M = 1024 number of points. $\tilde{G}(f)$ will then have fo be Fourier transformed by the use of computaionally efficient FFT subroutine.

Function $\tilde{G}(f)$ in 2-52 is complex so before FFT is to be performed, we must "fold" the real part of it about the Nyquist frequency to make it an even function (Brigham, 1974, p.135). We therefore, sample the real component up to 512^{th} point and fold it about this point. The imaginary component of $\tilde{G}(f)$, however, has to be odd, which means we have to fold and "flip" it about the 512^{th} point.

Our complex function with even real part and odd imaginary component is to be Fourier transformed into a pure real time function (our transient) with zero imaginary part. Also of interest, observe that a real and even function of

frequency with zero imaginary part will Fourier transform to a real and even function in time. Note that our truncation frequency is 1400 Hz so 280 points are used and the rest of the points are zeroed out up to the 512^{th} point before being folded. It is also evident that since f_c(=1400 hz) < F/2(=2560 Hz), we avoid the aliasing problem.

The subroutine FOURIER in the main computer program CONSTANT is written so as to fill the Fourier coefficients according to the previously-mentioned rule. This subroutine then calls up a modified FFT subroutine adapted from Claerbout (1976). The results are then plotted using a suitable plotting program.

For the purpose of summarizing the steps that have been taken in the computer before resulting in our transient waveform, a convenient guide to this analysis is constructed in Fig. 2.5 in both frequency and time domains similar to Brigham (1974, p.92).

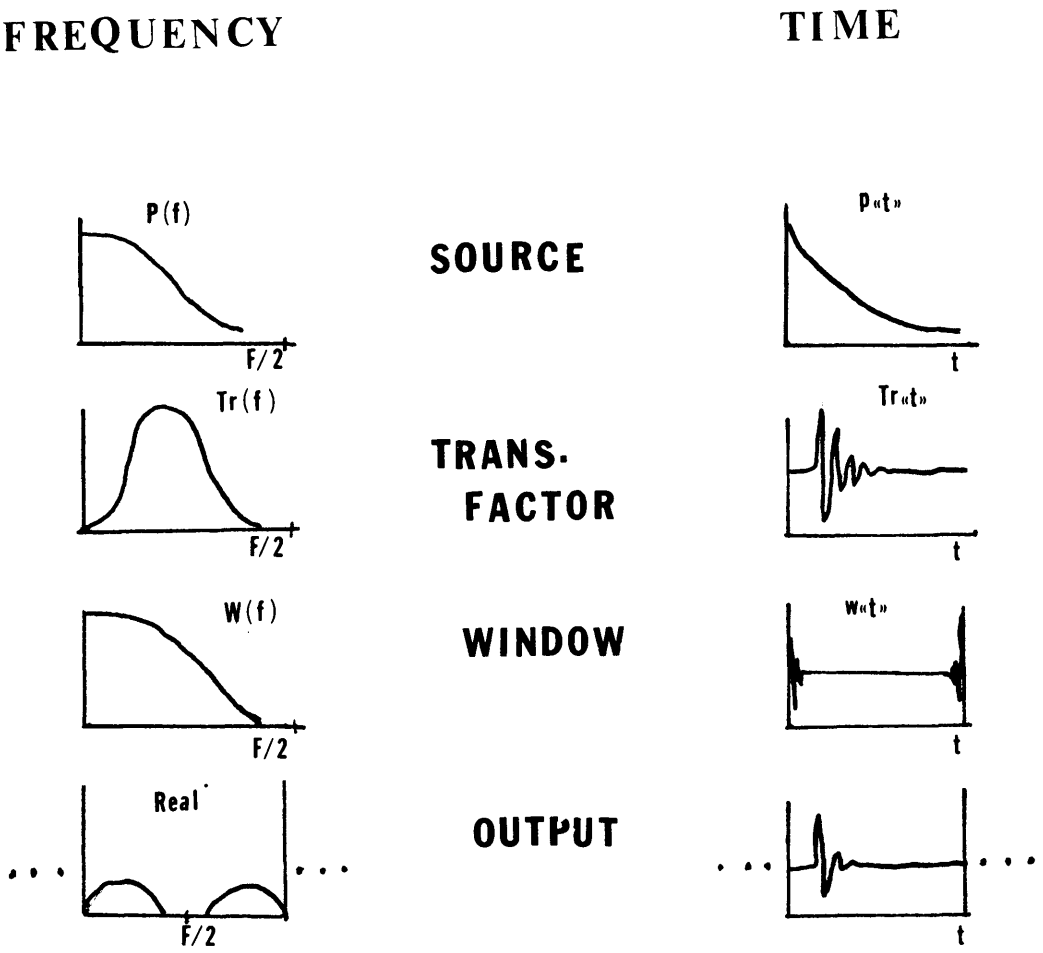

Figure 2-4 Computer computations leading to FFT.

111- DISCUSSION OF THE THEORETICAL RESULTS

Computer program CONSTANT (Appendix D) was written on the Control Data Corporation (CDC) Cyber Computer model 720 (and later changed to also accomodate CSM's Digital Equipment Corporation Dec-10 computer) to apply the theoretical scheme described in chapter II in order to digitally compute various transient outputs of interest. As described in the user manual for the program CONSTANT (Appendix C), this program makes use of an input data file, called Tape 1, for the computer calculations. These are data values that must be specified by the user, in order to obtain a computer output for a specific charge size and medium of interest.

Careful consideration must be taken in choosing numerical values for each of the parameters in Tape 1 which we now proceed to describe in some detail. Variables in the line 4 of Tape 1 ask for number of the sample points up to window's cut-off frequency (KFREQ in the program) and sampling rate (DELTAF) in Hertz, and in line 3 damping coefficient (ALFA) in sec^{-1}, which were all described in the previous chapter. As was shown, we only needed 280 sample

points for a 1400 Hz cut-off frequency window with sampling interval of 5 Hz and a damping coefficient of 10 sec^{-1}.

The physical characteristics of the surrounding rocks are specified in line 2 with the choice of compressional and shear velocities in cm/sec and densities in gr/cm^3. These can ideally be obtained from the borehole logs or any other source of information that is available on the rock formation of interest. The CGS system of units are adopted in all calculations and even if mixed units are specified, as in line 1 of Tape 1 for example, it would automatically be converted into appropiate units in the program.

Finally, in line 1 the size of the dynamite charge Q in pounds and its density in gr/cm^3 are specified so that the physical radius of the assumed spherical charge can be calculated in centimeters. Keeping this charge radius as constant, we then proceeded to compute various transient outputs for different radii of rock deformation by changing B/A ratio in the program.

The dynamite's detonation pressure P_0 is another variable that needs to be specified by the user in line 1 of Tape 1. For a typical dynamite charge this pressure is ideally of order of 10^6 psi or about $7x10^{10}$ dyn/cm^2 in magnitude. This value is, however, considerably reduced in a

borehole environment to a few percent of that above. Its utility comes about in obtaining peak theoretical velocity values mainly for experimental comparisons and a handle in most of the rock mechanical calculations. This will be more fully discussed in the subsequent chapter. Here a value of 2.12×10^9 dyn/cm^2 or about 1/33 of maximum assumed dynamite detonation pressure of 10^6 psi was selected for p_0.

Generally speaking four elastic constants are needed to completely describe an isotropic, homogeneous visco-elastic medium (White, 1983). Two of these constants are the ordinary elastic constants, known as Lame's coefficients λ and μ, which are calculated from velocity and density values given in line 2. From the two corresponding loss parameters, λ' was assumed to be zero (Appendix A) and therefore a knowledge of $\eta=\mu'$ (XMU1P), or ordinary viscosity of the liquid is required. As different ranges of viscosity can give rise to marked variations in the dilatational viscous damping of the outgoing compressional waves (Appendix A), a careful choice of viscosity is required as will be outlined in more detail in the section below.

III.1 Stress Waves in an Infinitely Extended Visco-elastic Liquid

In order to obtain physical insight in the choice of the viscous constants being used, here we consider the problem of radial stress distribution in an infinitely extended viscous liquid. Referring back to Equation 2-19 and again considering an exponential time dependance, we write 2-19 as

$$P_{rr} = \lambda\left[1 + \frac{i2\omega\eta}{\lambda}\right]\frac{\partial U}{\partial r} + 2\lambda\frac{U}{r}$$

$$= \lambda\left(\frac{\partial U}{\partial r} + \frac{2U}{r}\right) + \frac{i2\omega\eta}{\lambda}\frac{\partial U}{\partial r} \qquad (3\text{-}1)$$

where η denotes viscosity ($\mu'=\eta$). If we now consider wave propagation in an infinitely extended Voigt liquid, a solution to the wave Equation 2-10 becomes

$$\Phi(r,\omega) = \frac{D(\omega)}{r}\, e^{-kr}$$

$$k = a + \frac{i\omega}{c} \qquad (3\text{-}2)$$

where: $U = \frac{\partial \Phi}{\partial r}$

and $D(\omega)$ is a complex constant.

Substituting Eq. 3-2 above into 3-1 we obtain

$$P_{rr} = \frac{D(\omega)\ \lambda k^2}{r}\ e^{-kr}\ [1 + \frac{i2\eta\omega}{\lambda}\ (\frac{2}{k^2r^2} + \frac{2}{kr} + 1)] \qquad (3\text{-}3)$$

The coeficient $2\frac{\eta\omega}{\lambda}$ in 3-3 can be thought of as a phase angle θ between stress and strain (Lee 1964, p. 2403) where

$$\tan\theta = \frac{2\eta\omega}{\lambda} \qquad (3\text{-}4)$$

Considering the constants involved in real media, this phase angle is usually much less than unity, which means $\tan\theta \approx \theta$. Equation 3-3 then becomes

$$P_{rr} = \frac{D(\omega)}{r}\ \lambda k^2\ e^{-kr}\ [1 + i\theta(\frac{2}{k^2r^2} + \frac{2}{kr} + 1)] \qquad (3\text{-}5)$$

Let us now proceed with a numerical example to 3-5 above. If we consider a medium with compressional wave velocity (in liquid) of about 1.5×10^5 cm/sec and for frequency of 100 Hz at a distance of 10 cm, we have

$$|K_1| \cong \frac{\omega}{c_1} = \frac{2\ \pi\ 100}{1.5 \times 10^5} \cong 4 \times 10^{-3}\ \text{cm}^{-1}$$

so now

$$\left|\frac{2}{k^2r^2} + \frac{2}{kr} + 1\right| \approx 1300$$

Analogously, for a radius of 100 cm, the term multiplying θ in 3-5 is about 130. So it is evident that this multiplying term can get extremely large at short distances. This effect, however, diminishes at larger r values were we obtain a simple 1/r dependance for radial stress. This behavior of radial stress at smaller distances is also, of course, expected to be dependant on the value of the θ multiplier. As is evident in 3-4 larger viscosities give rise to higher θ values. For the example above, values of viscosity greater than 10^5 result in $\theta > 10^{-3}$ (for 100 Hz) which again severely damps the observed outgoing wave motion at short distances.

This process can physically be thought of as the formation of a small spherical shell of over-pressured rigid liquid around the cavity for larger viscosity values. The resulting dilatational wave motion out of this zone is essentially dominated by the very high frequencies which are probably being cut by our window. This is demonstrated in Figure 3.1 where this effect is pronounced for viscosity values greater than 10^5, so that what we observe is

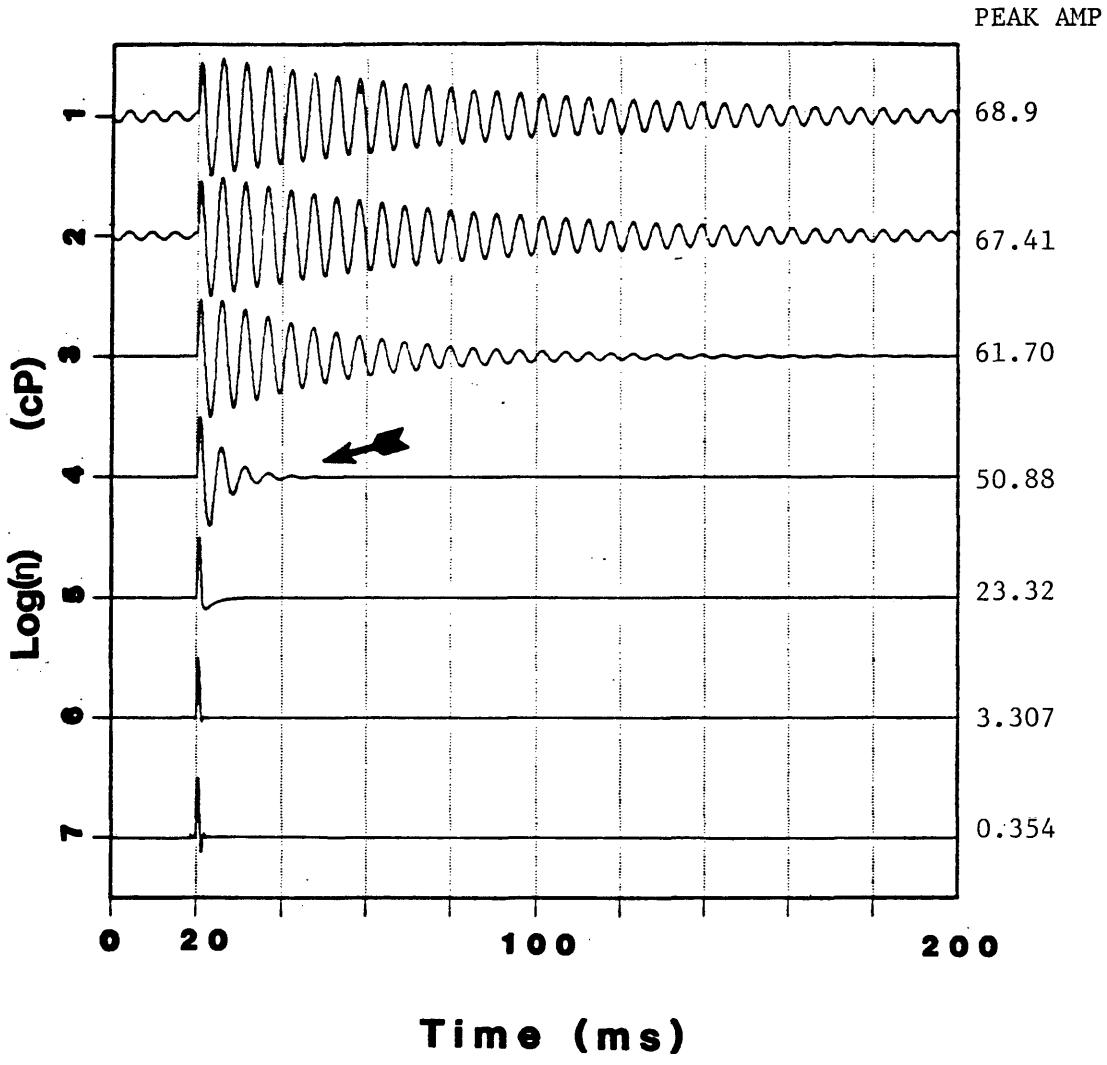

Figure 3-1 Particle velocity as a function of viscosity for a 5 lb charge in Taylor marl. (B/A=7.5, R=50 meters).

essentially the time domain transformation or "time constant" of our window (Peet, 1960). Lower viscosity values (less than 10^3) gives rise to a more "ringy" low frequency-oscillations which is expected.

The indicated "Peak" amplitudes on the right hand margin also reveal that we obtain more than a 100:1 ratio in amplitude in going from 10^7 centipoises (cP) to 10^4 cP in viscosity value. These are maximum peak values reached by a waveform in each transient oscillation and are in units of cm/sec. It is evident, therefore, that considerable amount of damping in amplitude results for these higher viscosities. For lower viscosities, however, we observe far steadier values of amplitude as most of the energy gets through our window. So before any waveform analysis, a careful "viscosity menu" of the form of Fig. 3.1 had to be constructed in order to select the right order of magnitude for viscosity for the medium and windows being used.

It is perhaps justified here to bring a reminder of some of the discussion regarding viscosity (Appendix A). In our model, a change of viscosity η results solely in a change of dilatational viscosity $K'=2/3\eta$ (as tangential stresses are zero), which alters the shape of the resulting compressional wave motion. This viscosity change, then acts as our damping mechanism for the attenuation of the initial

very high frequency content of dynamite in the near deformation zone around the cavity. The assumption of zero dilational viscosity of $\lambda'=-2\eta/3$,as afforded by some authors in the literature like Stokes (1845), should not, in this case, result in any viscous damping of energy and therefore would be analogous to a pure elastic case. The procedure to modify the computer program to output a viscosity rather than a B/A display menu is described in the computer program.

III.2 Effects of Changing the Decay Constant of the Source.

Another important variable which can influence the resulting wave motion is the time decay constant of the source α. As a reminder, we saw in chapter 1 that larger charges gave rise to a faster rate of decay of the initial pressure pulse and thus a larger value of α. However, due to the many experimental complications, no satisfactory knowledge of changes in α for different types or sizes of explosives are known. To demonstrate the changes in waveforms which accompany different values of α, Fig. 3.2 was constructed for a 5/8 lb charge in Pierre shale with a constant B/A ratio and viscosity value but changing α in the y-axis from α=500sec^{-1} (t_0=2 msec) to α=3000 sec^{-1} (t_0=1/3 msec).

As is evident, increasing decay constant α results in a faster oscillation as expected. The shape of each waveform, on the other hand, varies considerably as we observe a more developed second and third peaks in each of the transient oscillations with the second legs becoming more pronounced than the first for larger than 1500 sec^{-1} values. This phenomenon can also be observed in some of the Ricker's (1953) field observations for the smaller size

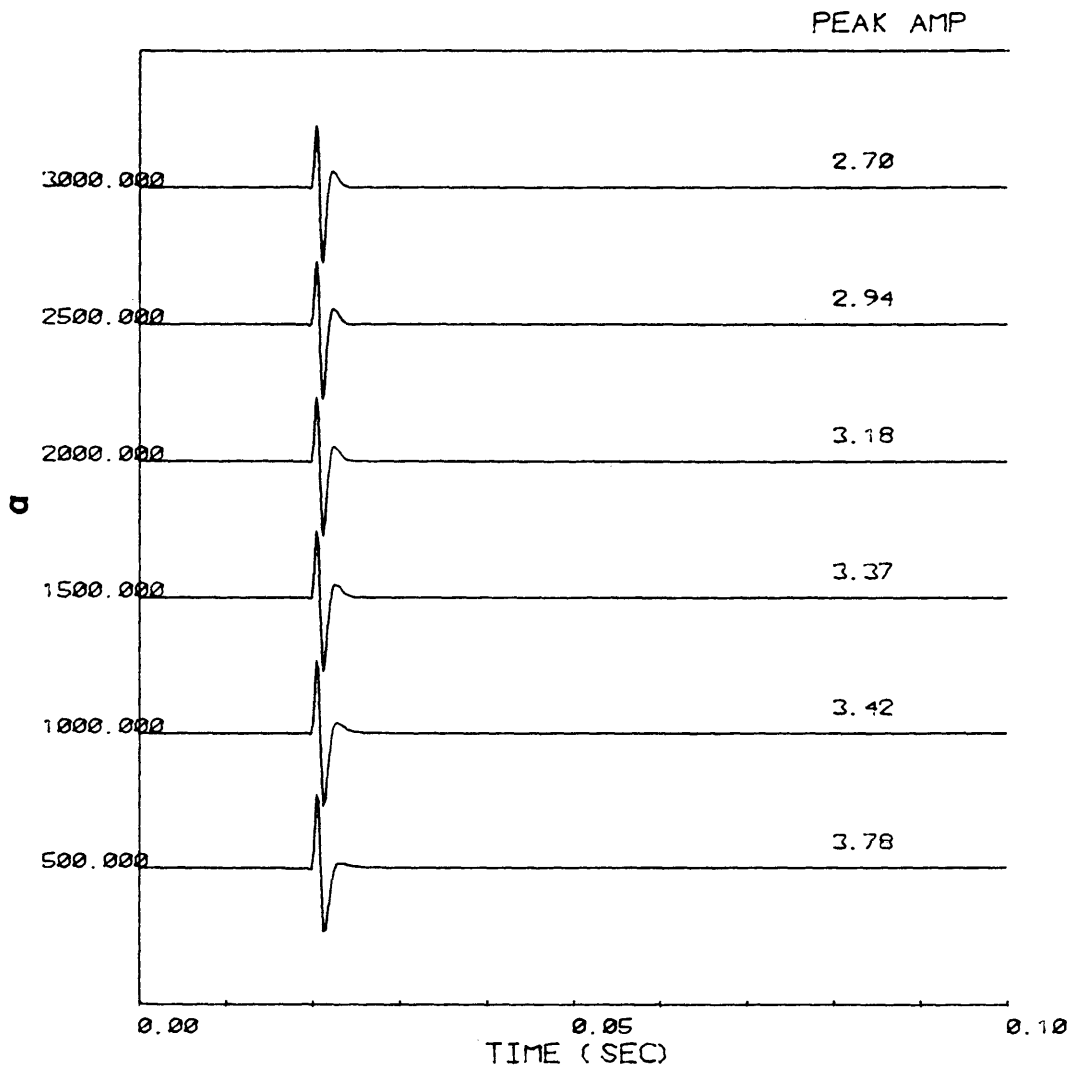

Figure 3-2 Particle velocity as a function of source's damping constant for a 5/8 lb charge in Taylor marl.

charges.

Due to the inherent experimental uncertaintity and computational complications, α, as is the case for almost all theoretical developments, is held constant and independant of charge size in all our calculations. Two values of α were selected with one equal to 600 sec^{-1} corresponding to a moderately fast decaying source and other equal to 10 sec^{-1}. Although the latter is rather small, but it can be thought to represent the step response of the more physically realizable former case.

III.3 Comparisons with the Experimental Data

With the selection of a likely order of magnitude for viscosity , the size of the deformation zone (B/A value) was changed in order to obtain a waveform with a "Period" that would match the field data. For the example cited previously, viscosity was in order of 10^4 cP in value for the variable B/A displays. Keeping the size of the deformation zone as fixed, we then proceeded to again change viscosity but this time at a much finer scale, in order to obtain waveforms with correct "shapes" as judged by the degree of damping, or peak to trough ratios, of individual traces.

Three sets of data are drawn from the literature for the purpose of comparisons with our theoretical results. These include experimental data obtained on the shape of primary seismic wavelet on Taylor marl (Sengbush ,1978); on the Pierre shale (Janak, 1982; Sixta, 1982; McDonal et al., 1958 and Ricker, 1953); and on a London clay formation as reported by O'Brien (1969). For the case of the Taylor marl and Sixta's data on the Pierre shale, calculations are obtained for both faster and slower decaying sources. In

each section, all the computaional procedures leading to the final wavelet selections are outlined for only the slower decaying source. For the faster source function, on the other hand, only final results will be shown.

III.3.A Seismic wavelet in the Taylor marl

Results of pressure measurements for different charge sizes as reported by Sengbush (1978) in the Taylor marl in Kaufman County, Texas are shown in Figure 3.3.A and 3.3.B. These represent various waveforms from two in-line recording holes with 20 ft spacing. One millisecond tic markings are indicated underneath each chart. As is evident, increased values of charge weight gave rise to lower frequency oscillations with the frequency response curves shifting towards lower frequencies.

Let us now refer back to Figure 3.1 which represents plots for our theoretical particle velocities. X-axis represents time which is generally 200 milliseconds (MS) long with 20 MS intervals. Y-axis plots the waveforms for either variable B/A ratio, or viscosity values or charge sizes as specified on each figure. Each display is corrected for geometrical spreading for a shot-receiver distance of 50 meters.

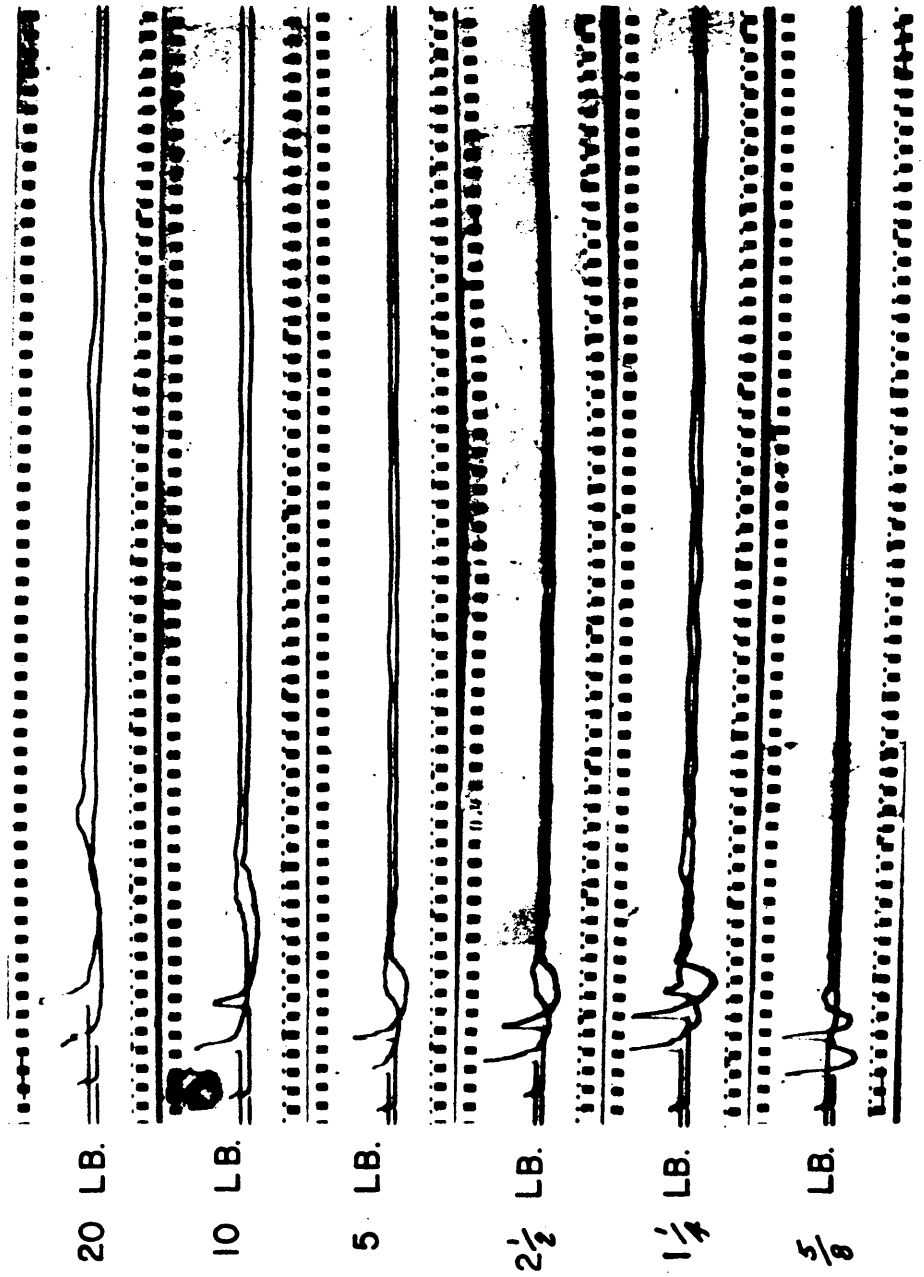

Figure 3-3.A Field waveforms as a function of charge size. (After Sengbush, 1978)

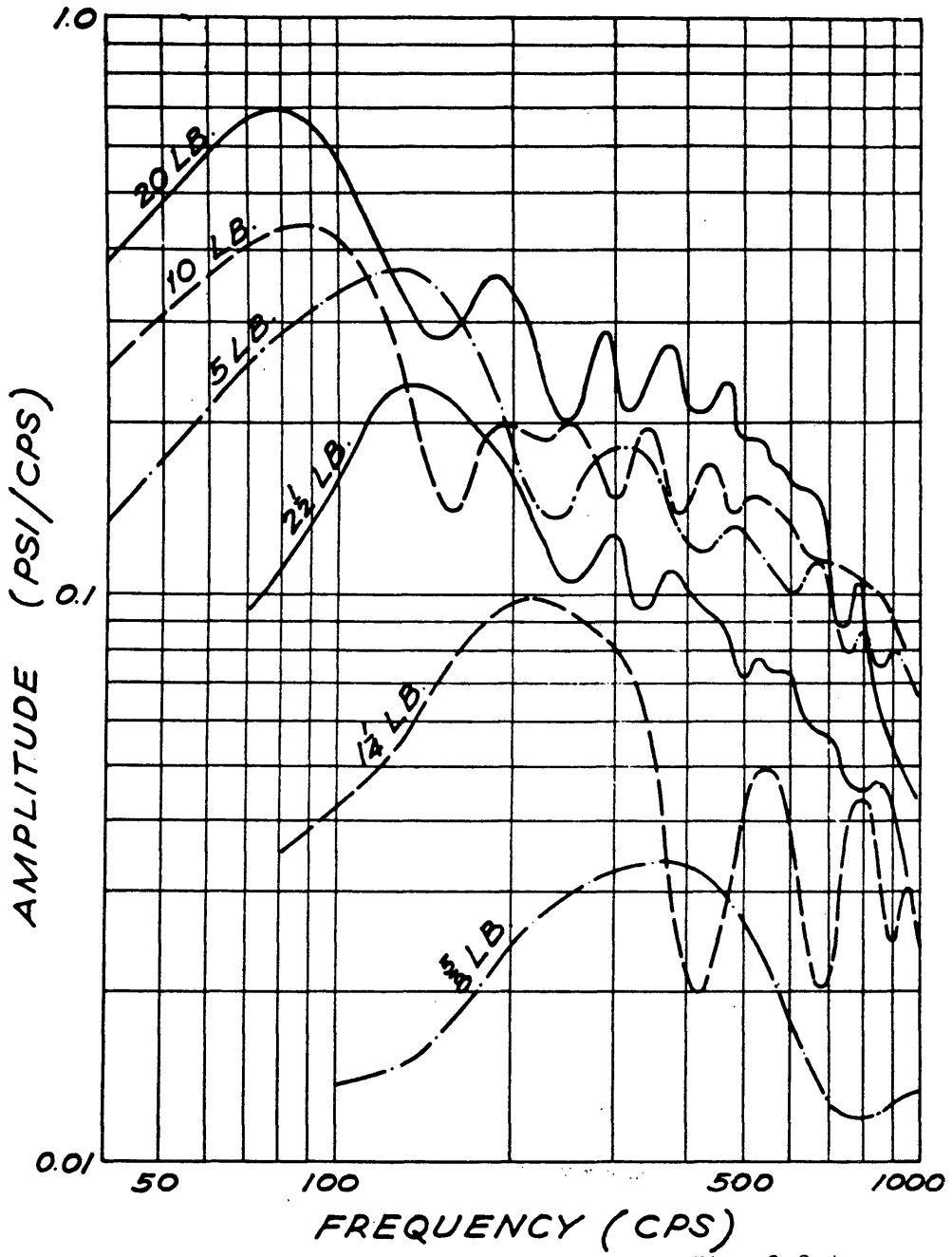

Figure 3-3.B Amplitude spectra of waveforms in Fig. 3-3.A.

As no dependable velocity logs were available, compressionsl wave velocity was calculated directly from the two recording hole data for the 5/8 lb charge and found equal to 2.44 km/sec. A shear-wave velocity of 1.0 km/sec and rock density of 2.16 gr/cm^3 was further estimated as inputs to Tape 1. With no data available on the type or the commercial make of the charges being used, an explosive density of 1.25 gr/cm^3 was also assumed which is a typical value for most dynamite charges employed in exploration. The field data were obtained by a wide-band analog recording system which meant that the half-cycle sinc function, which was described in section II.6.B, was in this case, an appropiate truncating window of our digitized data. The cut-off frequency of this window was assumed equal to 1400 Hz.

Figures 3.4 to 3.9 represent variable B/A plots for all charge sizes. Viscosity was held to be constant and equal to about 10^4 cP as demanded from our viscosity plot of Figure 3.1. For each size charge, a value for B/A was selected as to best fit the "period" in waveforms of Figure 3.3.A. "Period" for each waveform was defined as the length in time from the onset to the second zero crossing of each waveform. Each plot was first displayed on an expanded scale so that an accurate reading for periods can be made. Note that values for B/A in Figures 3.4 to 3.9 may start at

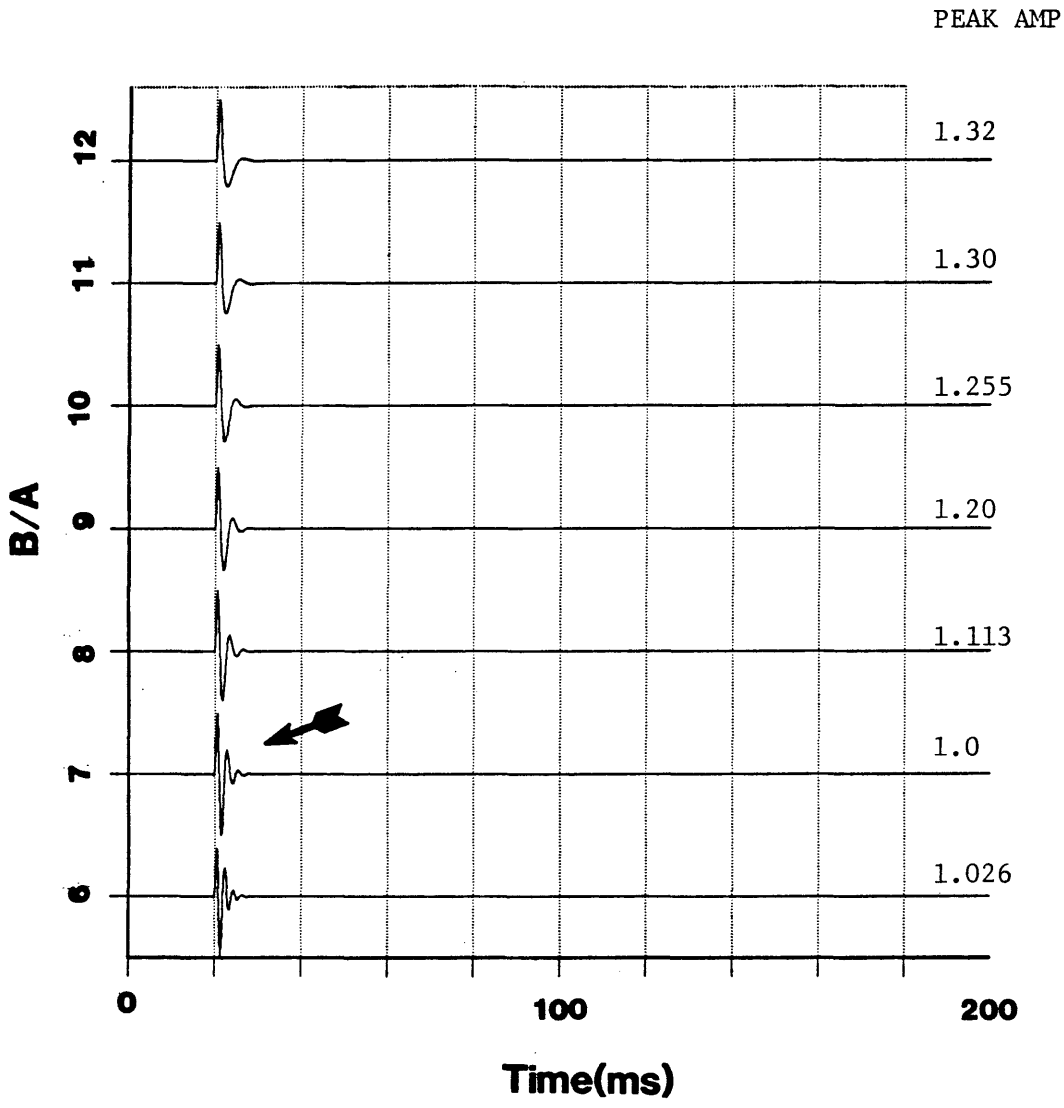

Figure 3-4 Particle velocity as a function of B/A ratio for a 5/8 lb charge in Taylor marl. (Viscosity = 10000 cP).

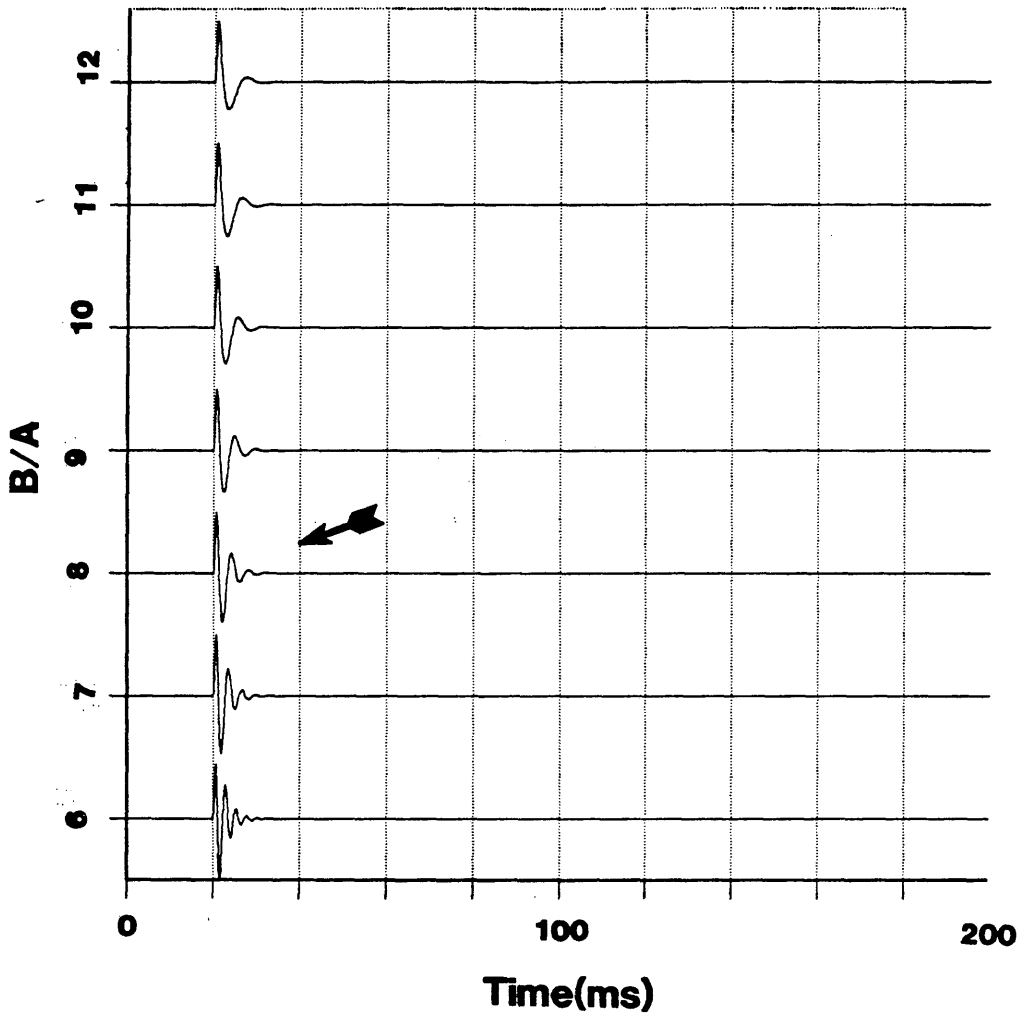

Figure 3-5 Particle velocity as a function of B/A ratio for a 1.25 lb charge in Taylor marl. (Viscosity = 10000 cP).

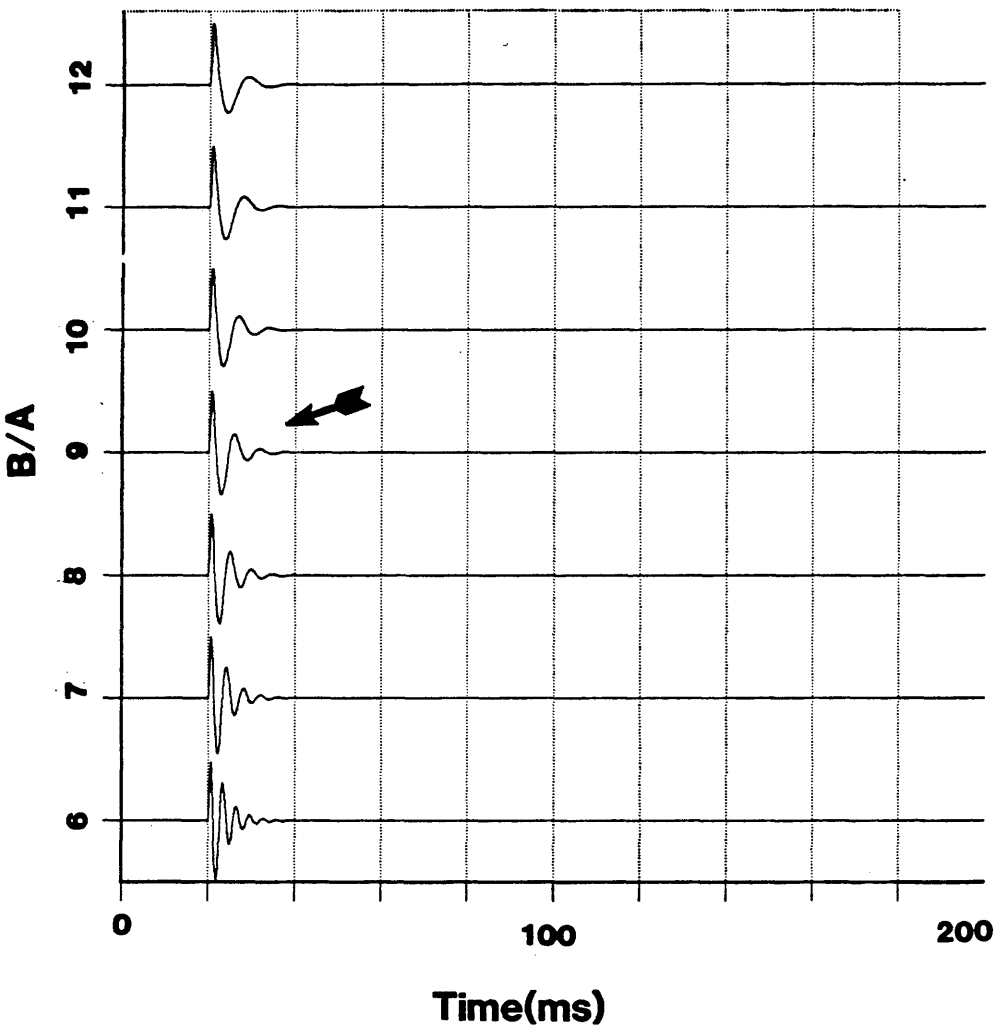

Figure 3-6 Particle velocity as a function of B/A ratio for a 2.5 lb charge in Taylor marl. (Viscosity = 10000 cP).

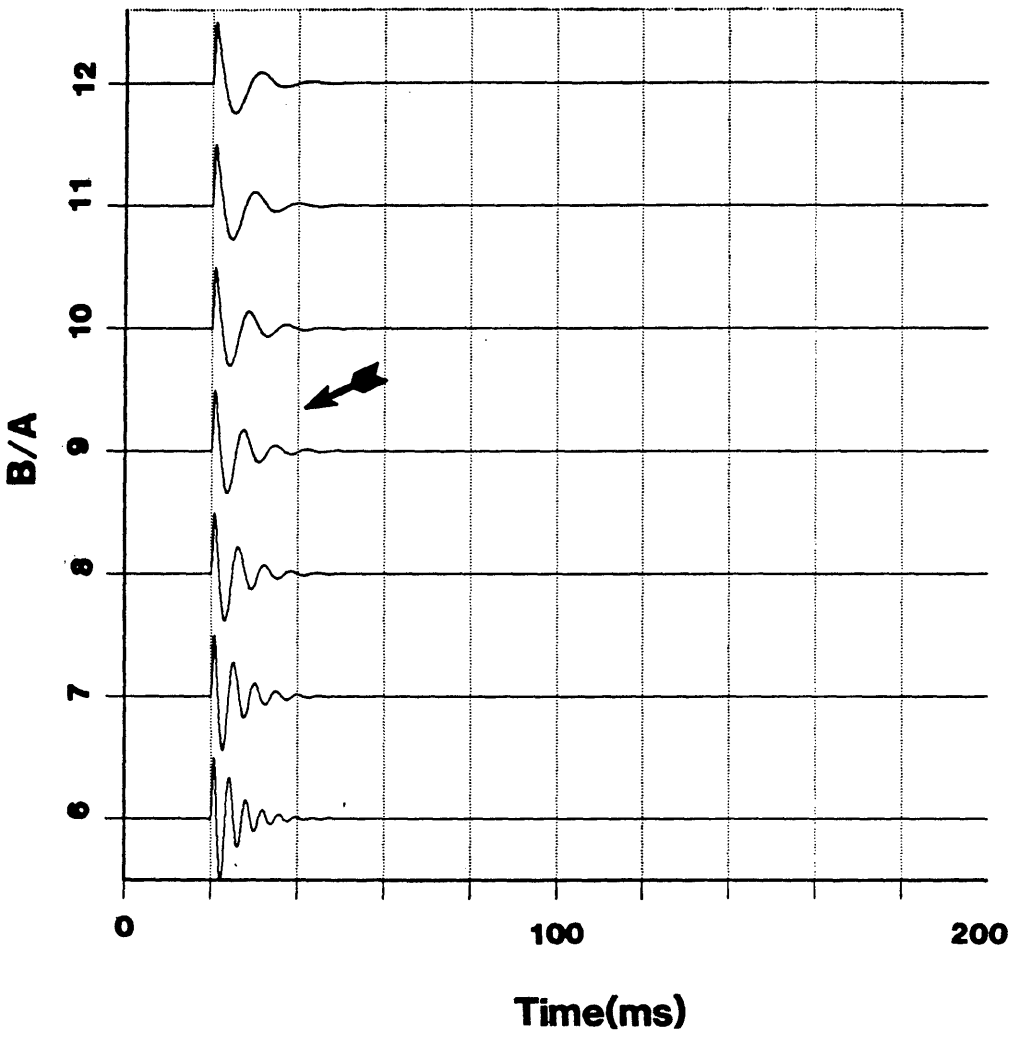

Figure 3-7 Particle velocity as a function of B/A ratio for a 5 lb charge in Taylor marl. (Viscosity = 10000 cP).

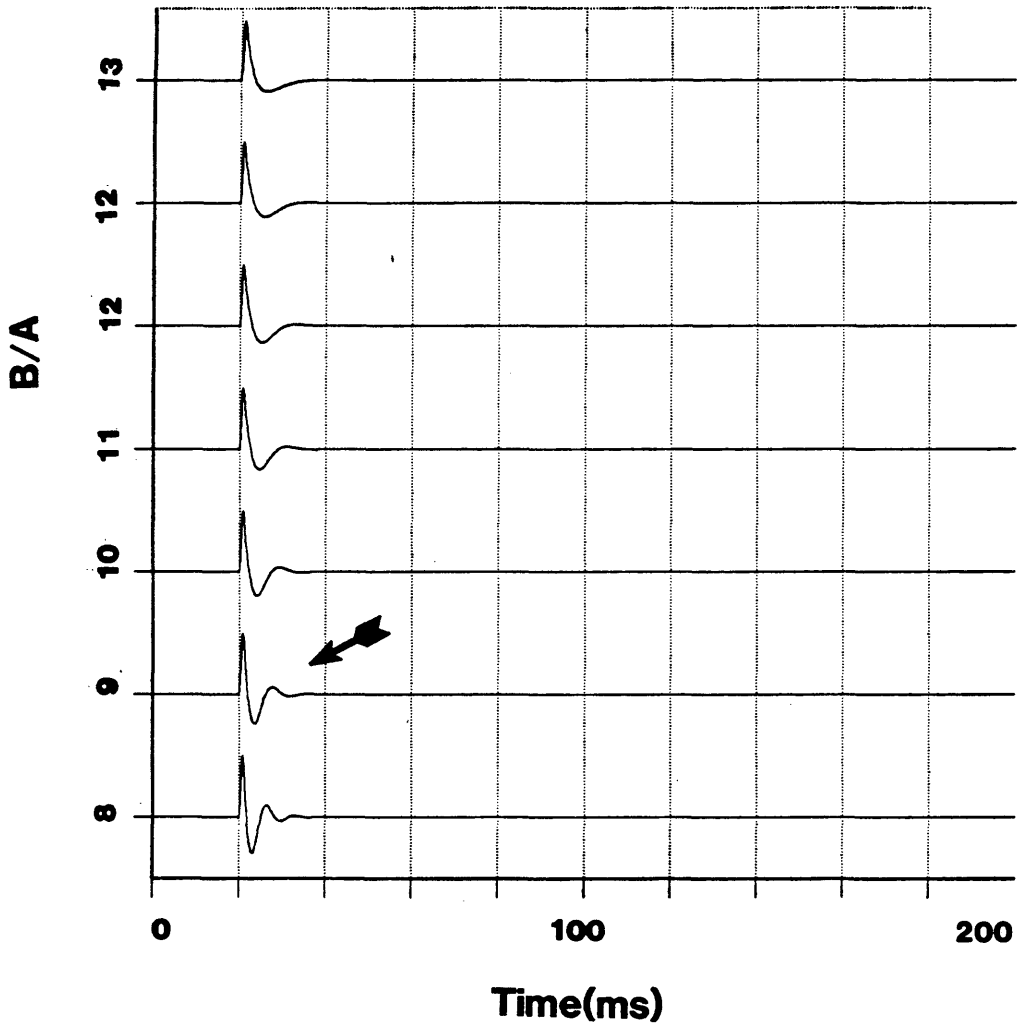

Figure 3-8 Particle velocity as a function of B/A ratio for a 10 lb charge in Taylor marl. (Viscosity = 30000 cP).

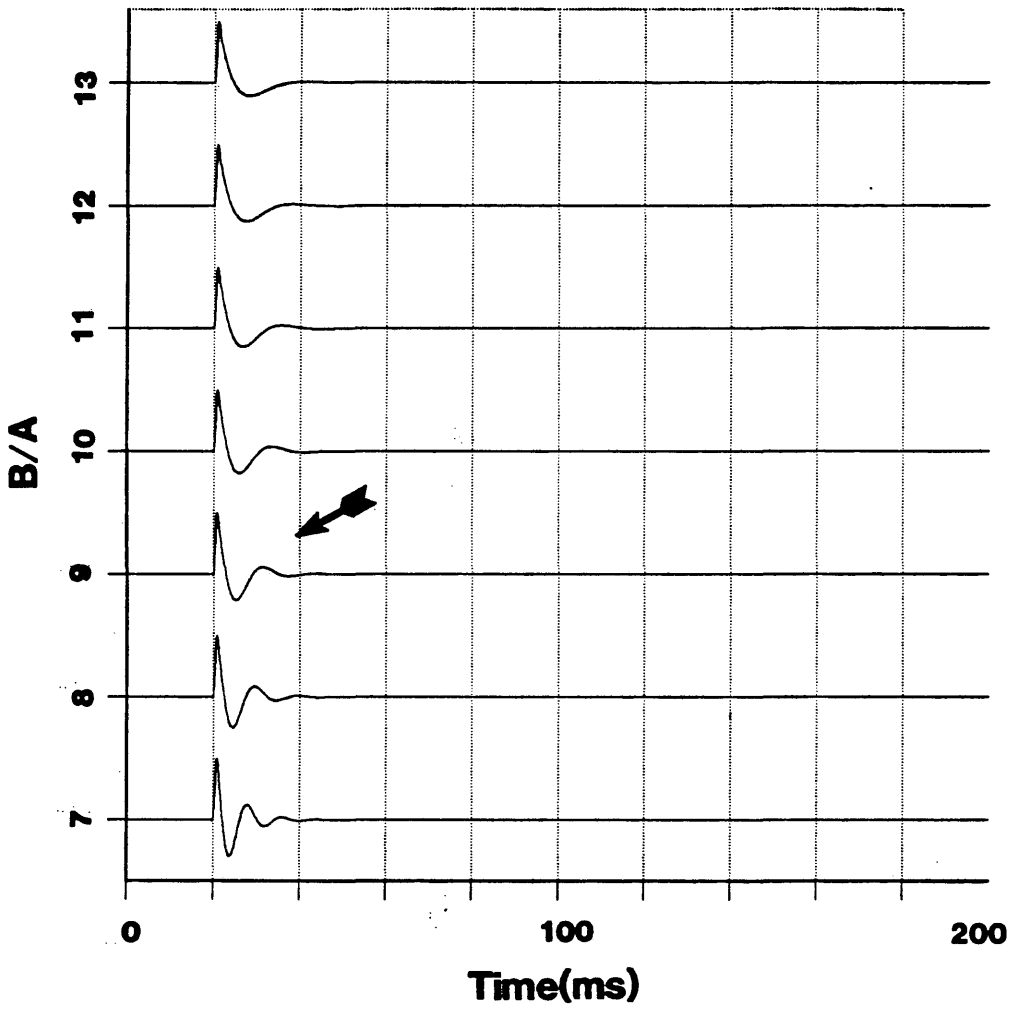

Figure 3-9 Particle velocity as a function of B/A ratio for a 20 lb charge in Taylor marl. (Viscosity = 30000 cP).

different initial values on the y-axis.

Peak amplitude values are noted on the right hand column only for the 5/8 lb case of Fig. 3.4 in order to observe the steady rise in amplitude with increasing B/A ratios. The basis for their calculations will be discussed in the latter part of section III.3.B.

The B/A ratios were then held constant in order to vary viscosity as to best select waveforms with sufficient amount of damping. An example for a 5 lb charge is exhibited in Figures 3.10 and 3.11. Note that as expected, viscosity changes do not alter peak frequency values of the amplitude spectrum but only result in velocity amplitude variations. Table 3.1 below indicates values for B/A ratio and viscosity that were selected as to best fit the field data:

Charge sizes (lb)	B/A	Viscosity($x10^3$) (cp)
5/8	6.7	22.0
1.25	7.8	22.0
2.5	9.1	23.0
5.0	9.1	24.0
10.0	9.7	30.0
20.0	9.6	30.0

Table 3.1- Values for viscosity and B/A that best fitted the field data. (α=10 sec^{-1})

Constants in Table 3.1 were used to construct selected waveforms for all charge weights. These are shown on Figure 3.12 and 3.13. As is evident, all waveforms indicate a rather encouraging similarity in shape and amplitude response with the field data of Figure 3.3.A. We furthermore observe the well known shift in peak amplitude responses towards lower frequencies with larger charge weights. Increasing charge weights should therefore give rise to a higher amplitude low-frequency ground motion.

We also observe in Figure 3.13 an abrupt cut-off of the frequency response at 1400 Hz which is solely due to the windowing. Note that each amplitude response is initially

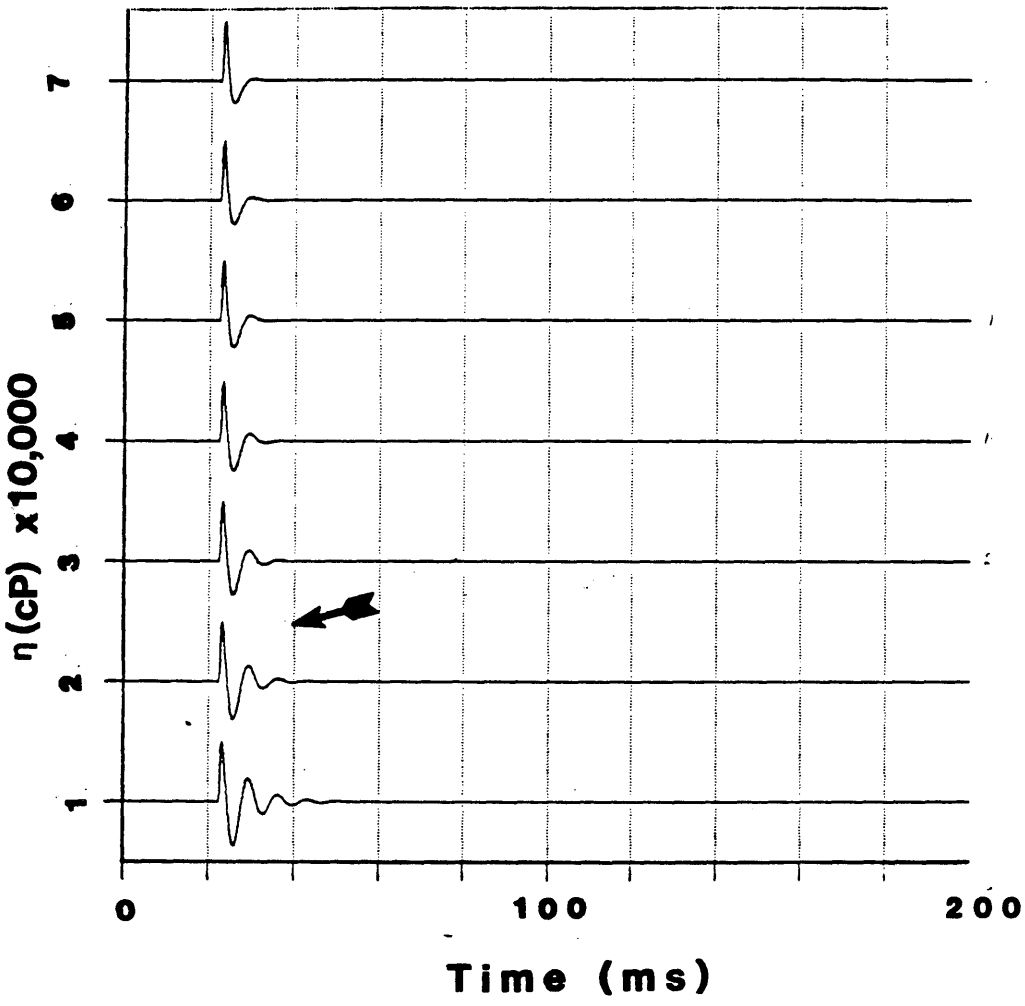

Figure 3-10 Particle velocity as a function of viscosity for a 5 lb charge in Taylor marl. (B/A = 7.2).

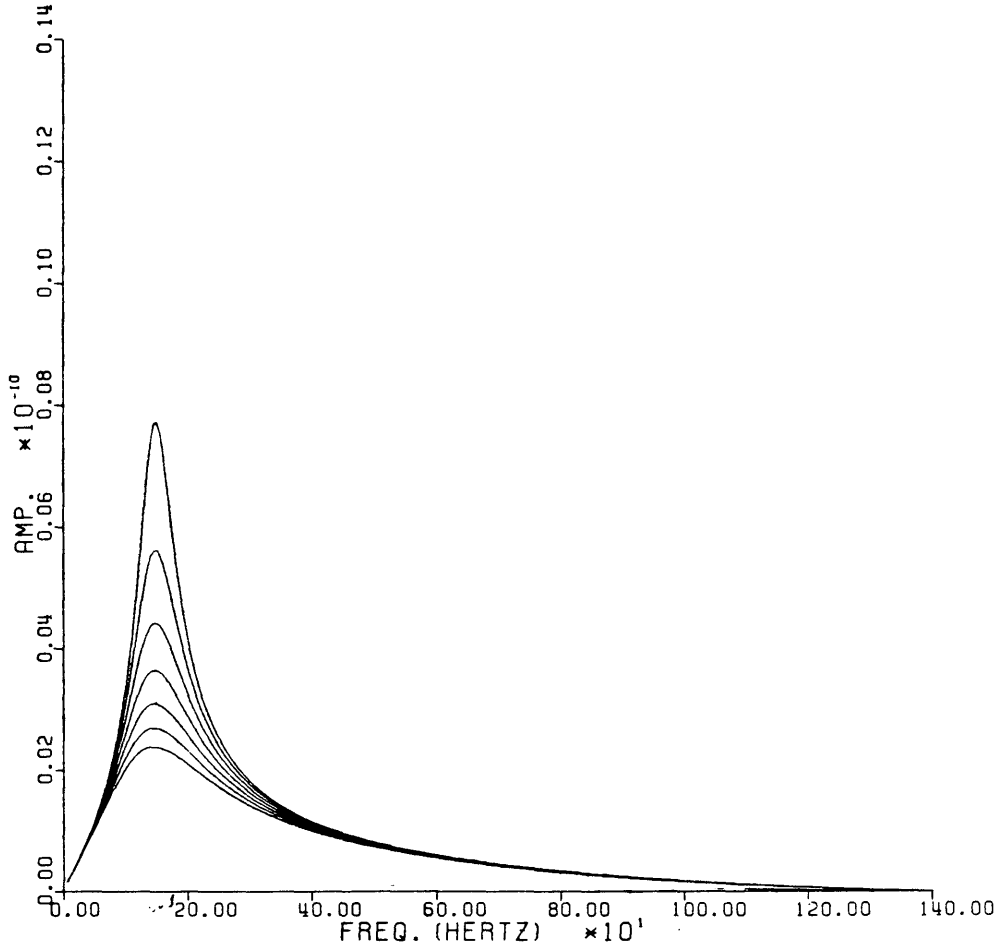

Figure 3-11 Amplitude spectra of waveforms in Fig. 3-10.

linear for some time which is essentially what we expect from a purely doublet type of waveform. It is also evident that a different functional relationship exists between charge weights and amplitude in differing regions of the amplitude spectrum. The amplitude increase is, for example, more pronounced at lower frequencies with an increase in charge weight. This phenomenon was also noted by Peet (1960) and by O'Brien (1960) on his data on marine and land dynamite shots.

Faster decaying source (α=600 sec^{-1}) results in, of course, faster oscillations which means that larger B/A are required for wavelet matchings. Same procedure for changing B/A and viscosity values gave rise to final waveforms in Fig. 3.14 and their associated frequency responses in Fig. 3.15. These selections are shown in Table 3.2 below

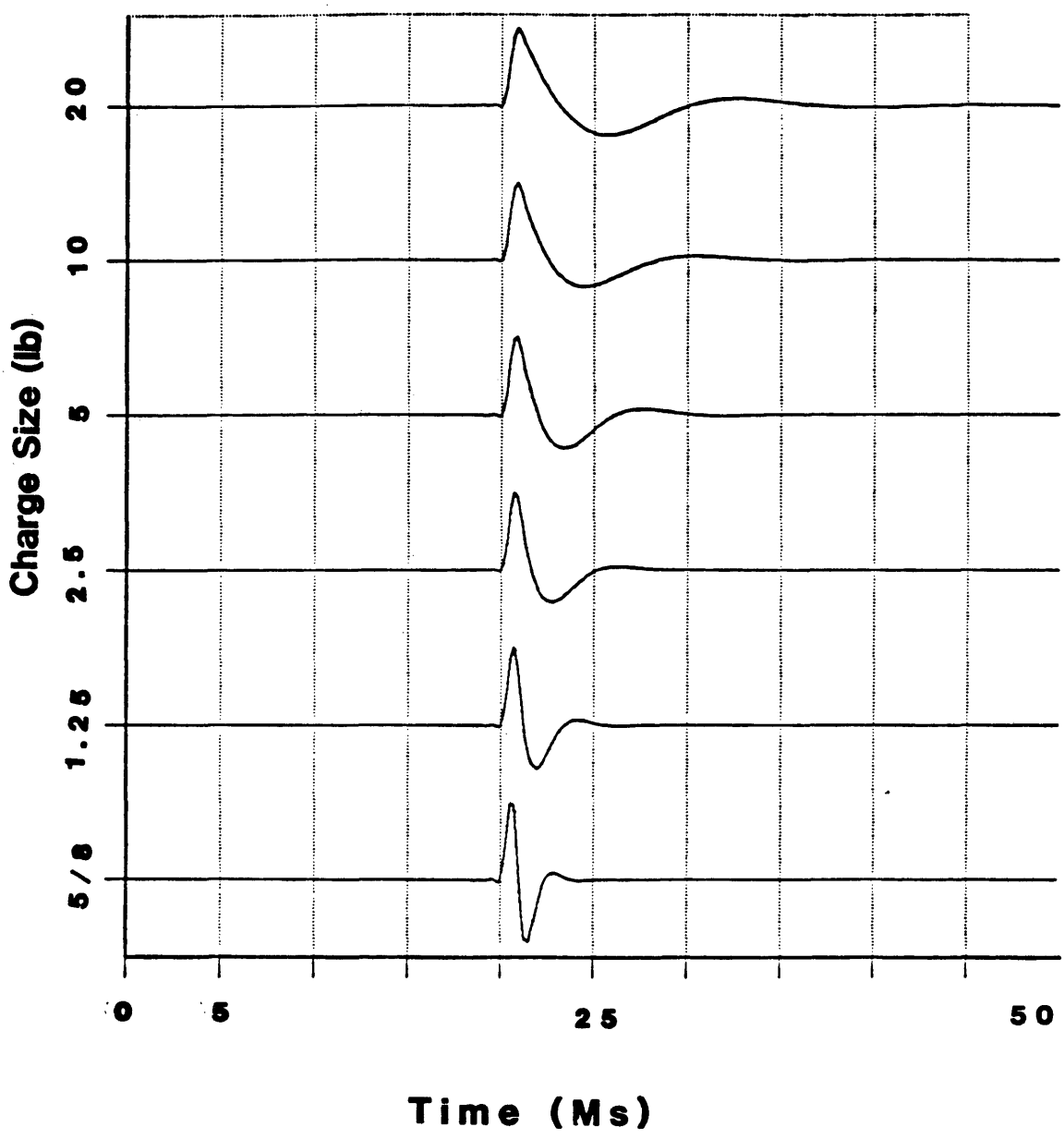

Figure 3-12 Particle velocity as a function of charge size in Taylor marl. (Slower decaying source, alfa = 10 sec^{-1}).

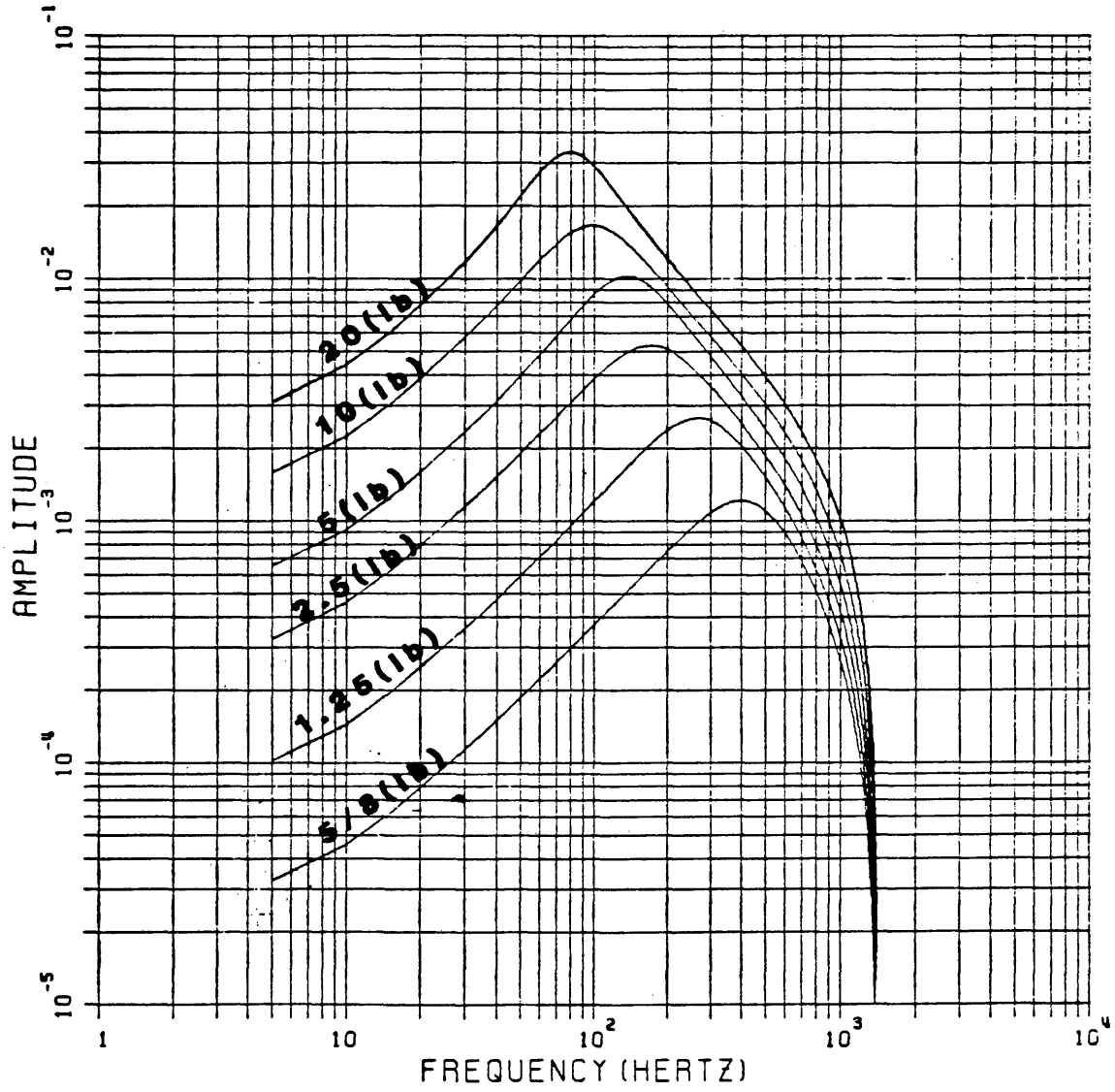

Figure 3-13 Amplitude spectra of waveforms in Fig. 3-12.

Charge Size (lb)	B/A	Viscosity($x10^3$) (cp)
5/8	7.18	26.8
1.25	9.2	20.4
2.5	10.9	16.8
5.0	10.5	18.9
10.0	12.6	27.5
20.0	12.5	27.5

Table 3.2- Best choices for B/A and viscosity values for the faster decaying source (α=600 sec^{-1}) in the Taylor marl.

As before, a general increase in B/A ratios and decrease in viscosity values are observed with increasing charge sizes. Time waveforms in Fig. 3.14 also seem to closely resemble the field data similar to the previous case of Fig 3.12. The frequency response, however, shows a faster rise and a much rounder peaking of amplitudes which more closely resemble the field data of Fig. 3.3.B. Note also that each peak is displaced by about same relative scale as a function of charge size when compared to the field data. Again differing amplitude relationships seems to be evident in different regions of the frequency spectrum as a function of charge size.

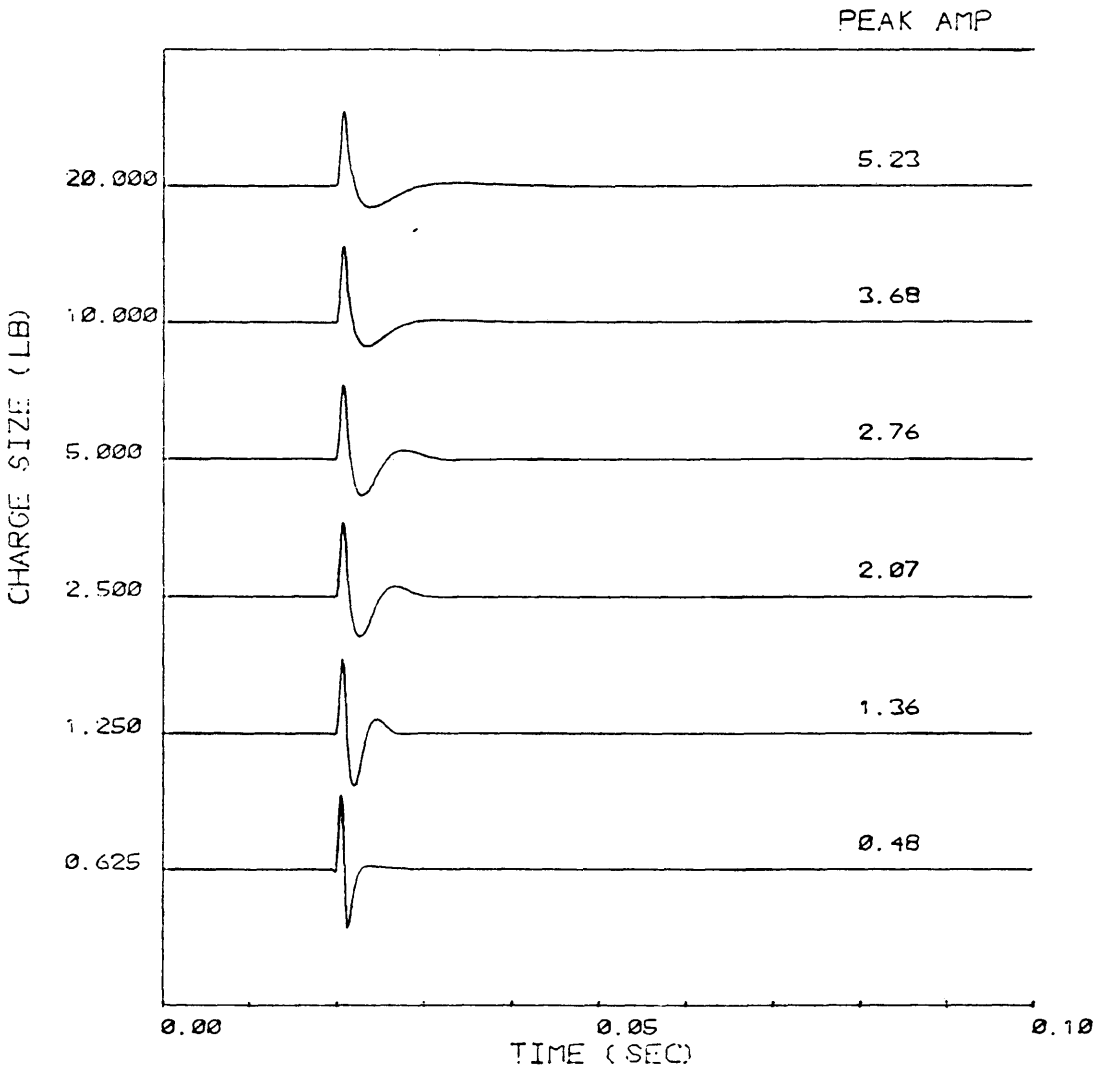

Figure 3-14 Particle velocity as a function of charge size in Taylor marl. (Faster decaying source, alfa = 600 sec^{-1}).

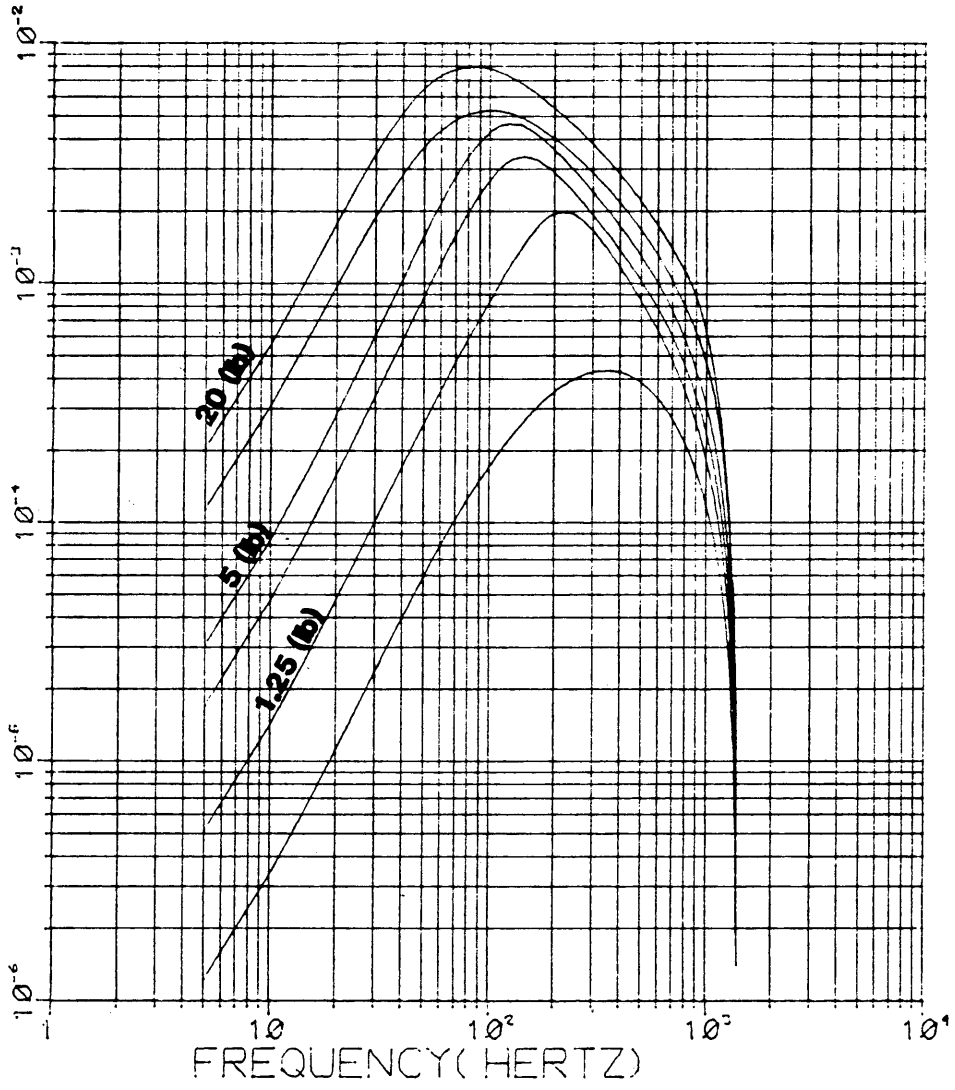

Figure 3-15 Amplitude spectra of waveforms in Fig. 3-14.

III.3.B Data obtained on the Pierre shale.

An unusually thick and homogeneous section of a Cretecious shale unit, known as the Pierre shale, has always provided an ideal site for the purpose of source studies conducted by various authors in the literarure. Sharpe (1942) investigated wave motion in Pierre shale and found it to be of some order of magnitude longer in duration than predicted by his theory. Ricker (1953) and later McDonal et al. (1958) observed both compressional and shear pulses in this formation which provided some of the early field data on the form and shape of the primary seismic pulse.

Recently, as a result of series of "source studies" experiments conducted by the then Exploration Research Laboratory (ERL) of the Geophysics Department of the Colorado School of Mines, Janak (1982) and Sixta (1982) published a comprehensive report on all the recordings obtained from the different seismic sources being tested. The test was conducted near the town of Brush in the Northeastern part of Colorado with the Pierre shale being reasonably homogeneous in its upper 1000 ft of the section.

Seven three-component clusters of 8-Hz geophones

were cemented in place in a borehole from 400 to 1000 ft with 100 ft intervals. Seismic sources were located on a circle, with the recording hole at its centre. A 50 ft radius between each source and the recording hole ensured a near vertical travelling signal, being transmitted approximately parallel to the borehole axis.

Figure 3.16 which was obtained from Sixta (1982, p. 16) displays recordings for a 5 lb charge at a depth of 177 feet. The term "All Corrections" refers to all the processing corrections that were done and will be described later. The recording hole was filled by slow-setting cement which exhibited excellent reproducibility and good coupling for pick up of higher frequency motion. Although one other gravel filled hole as well as a cased hole were also used, the cemented hole seemed to consistently give rise to the most dependable waveforms, which will be used here for the purpose of all theoretical comparisons.

Explosive charges ranging from 1 to 50 lb in weight were used as part of the sources being examined. These were located at depths from 10 to 200 ft down the borehole. Since an approximate 40 ft of eolian sand followed by another 40 ft of clay were present above the Pierre shale in the test site, only shots more than 100 ft deep were considered to be truly within the Pierre shale unit. We have accordingly

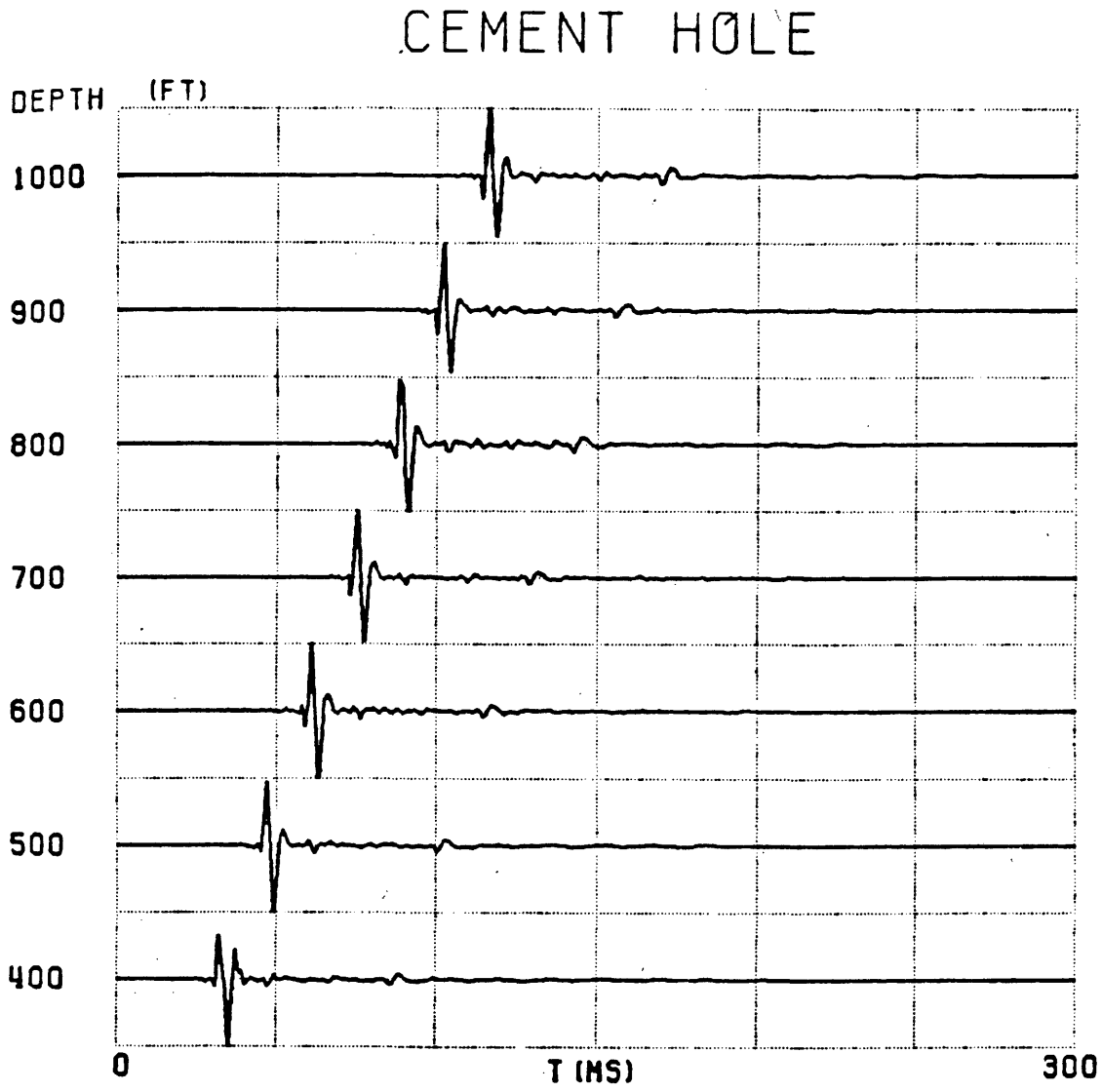

Figure 3-16 Field recordings of a 1 lb charge buried at 200 ft. (After Sixta, 1982).

selected shots fired at 200 ft depths and recorded by the 1000 ft depth geophones for all our comparisons.

Several steps in processing were applied to the raw field data. These included horizontal geophone orientation from shots on the 50-ft radius cement ring and construction of both inverse filters for the recording instruments and the geophone response. In addition to above corrections to the raw data, another set was displayed correcting for such factors as spherical spreading, transmission through the boundaries and attenuation losses. For our analysis, the wavelets that were chosen had been corrected for all the amplitude losses, so they were as if recorded 1 meter away from the shots.

Since the data were recorded using CSM's DFS V recording system, as mentioned above, an inverse filter to remove its effect had to be constructed. This meant that a net windowing similar to that of Figure 3.17 was done on the data and our previously truncating window of Figure 2.2 was no longer suitable. Both amplitude and phase responses on this figure were hand digitized and were used as our preconditioning window for computer calculations. The data file which contains this window specifications is called Tape 11. Notice that our digitally recorded data is severely band-limited and its amplitude is reduced up to 48 db above

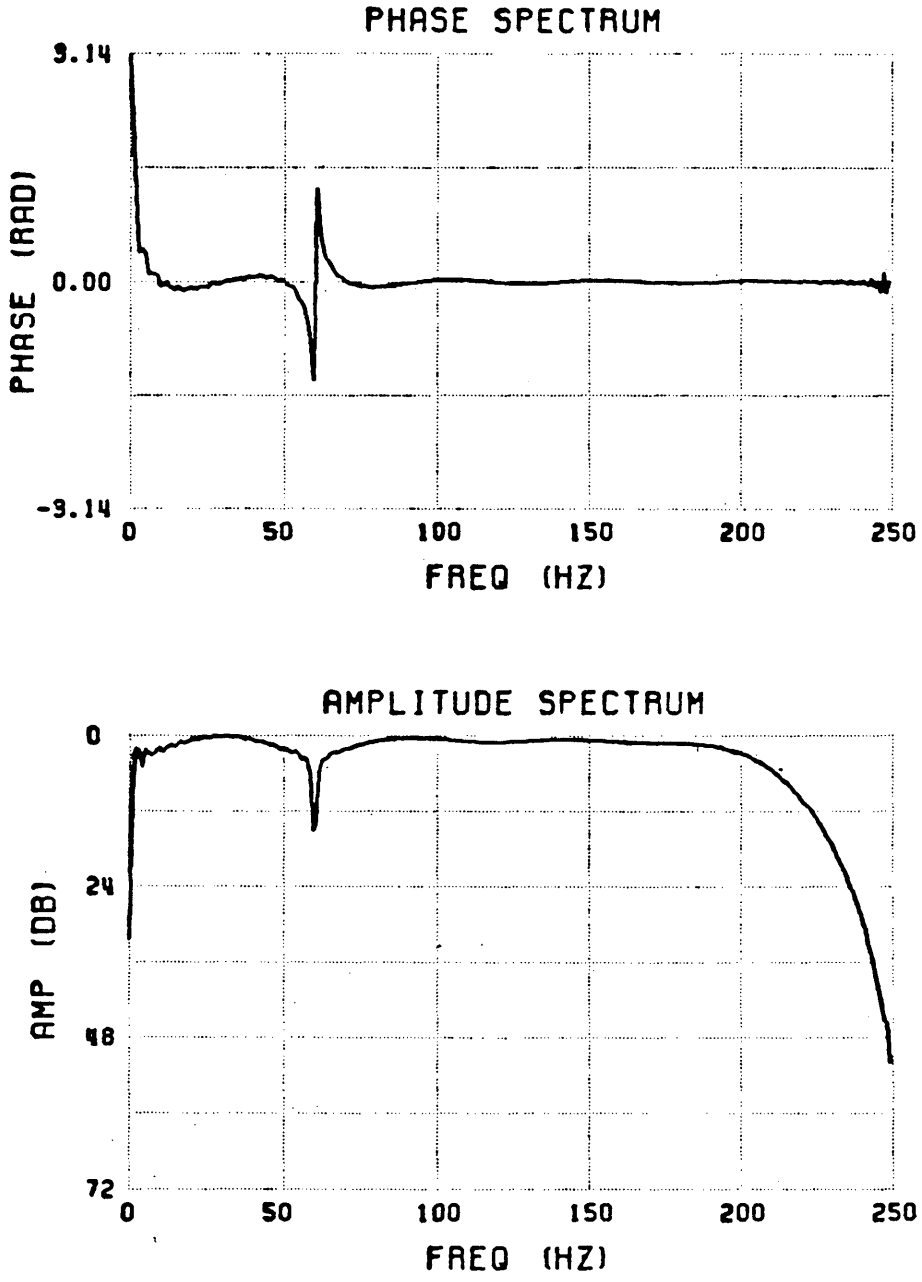

Figure 3-17 Amplitude and phase spectra of the DFS-V window.

250 Hz. It also contains a noticable 60 Hz notch filter and an associated phase at that frequency which was considered in Tape 11 so that all theoretical frequency responses should accordingly be affected by this cut-off. Frequencies greater than 250 Hz were zeroed out completely which meant that KFREQ variable in line 4 of Tape 1 is now equal to 50.

Both the geophone and DFS V inverse filtering had the net effect of removing the phase and were thus referred to as "Dephasing" of the data. Note that since both of these inverse filters were zero phase and non-causal, a back-loading of the energy results when aplied to causal waveforms. This effect is further accentuated with application of the attenuation correction, which is also a zero phase filter. The net effect on our waveforms is an artificial downwarp movement before the onset of our causal waveforms.

This artificial centering of energy is evident in all our data as in Figure 3.18, for example, which displays computed waveforms for a 10 lb charge using constants reported by Janak (1982). Also note that we do not observe any smooth waveforms but traces that are a bit ringy at the tail end. This is again attributed to an application of Gibb's phenomenon which means that for a 60 Hz notch type of cut-off, our time waveforms should oscillate at that

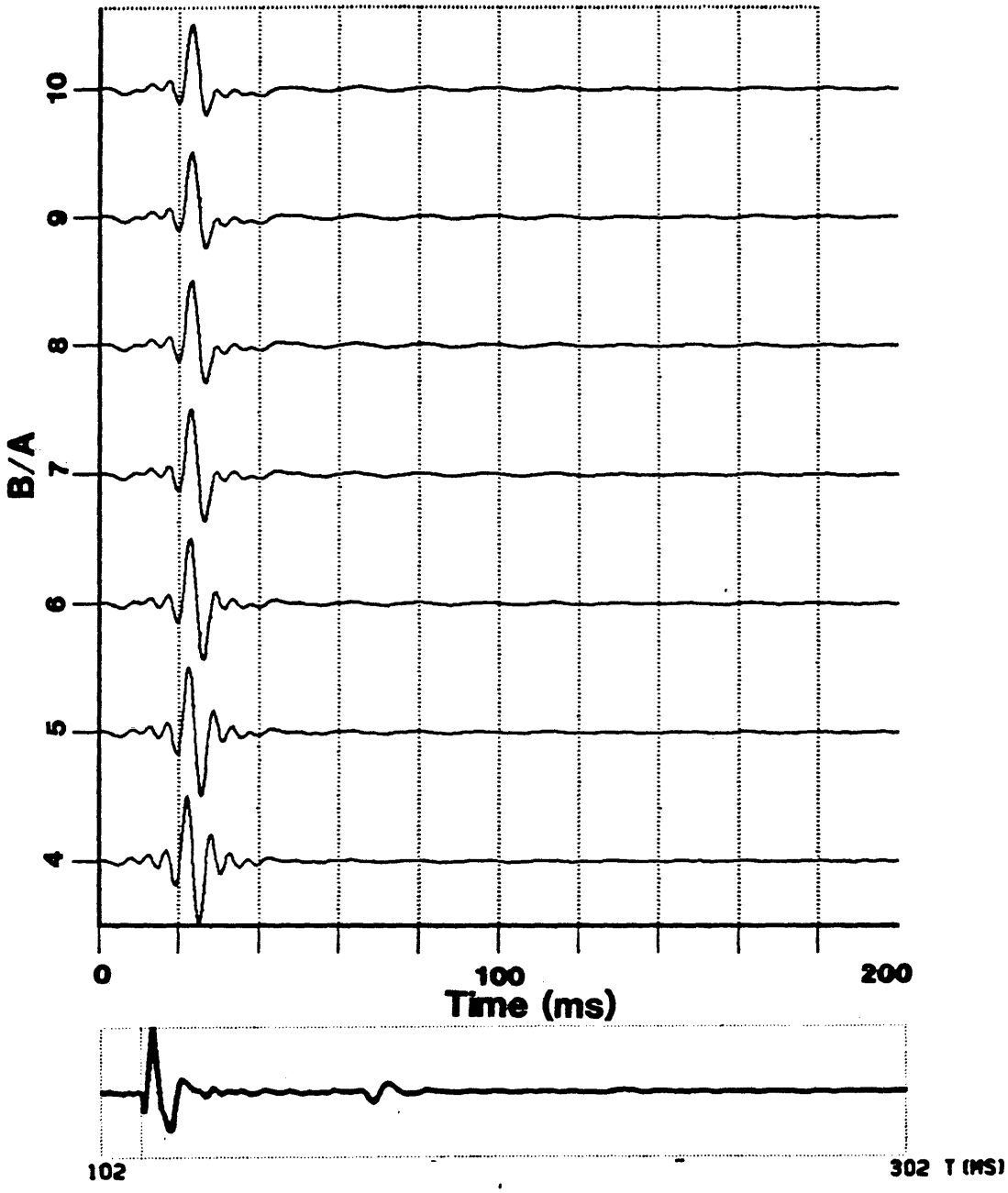

Figure 3-18 Particle velocity as a function of B/A ratio for a 10 lb charge in Pierre shale. (Viscosity = 90000 cP)

frequency (Papoulis, 1962). Shown at the bottom of this Figure are experimental data from Sixta (1982) for shots at 200 ft. Note that field data is also contaminated by a wavelet "ghost" which is a reflection off the bottom of the low velocity level. The degree of interference of the ghost wavelet with the primary seismic pulse gets, obviously, more severe at shallower shot points.

A mean compressional velocity value of 2.17 km/sec and shear velocity of 0.8 km/sec with rock densities of 2.11 gr/cm^3 were input in the computer as our data values. Dupont's 5 lb Tovex S charges with explosive density of 2.11 gr/cm^3 were used in constructing all the 5 to 50 lb charges in the field. The shot receiver distances for computer outputs were again 50 meters.

Using the following data, waveforms for all size charges were constructed. Here, the narrow band character of our preconditioning window placed severe constraints specially on waveforms obtained from smaller charges. Since it is known that amplitude response peaks at higher frequencies for smaller charges, our window was therefore, only suitable for large enough charges that contained most of their energy in the frequency band of our window. This is illustrated in Figure 3.19 for a 1 lb charge where we observe relatively no change in period with increasing B/A

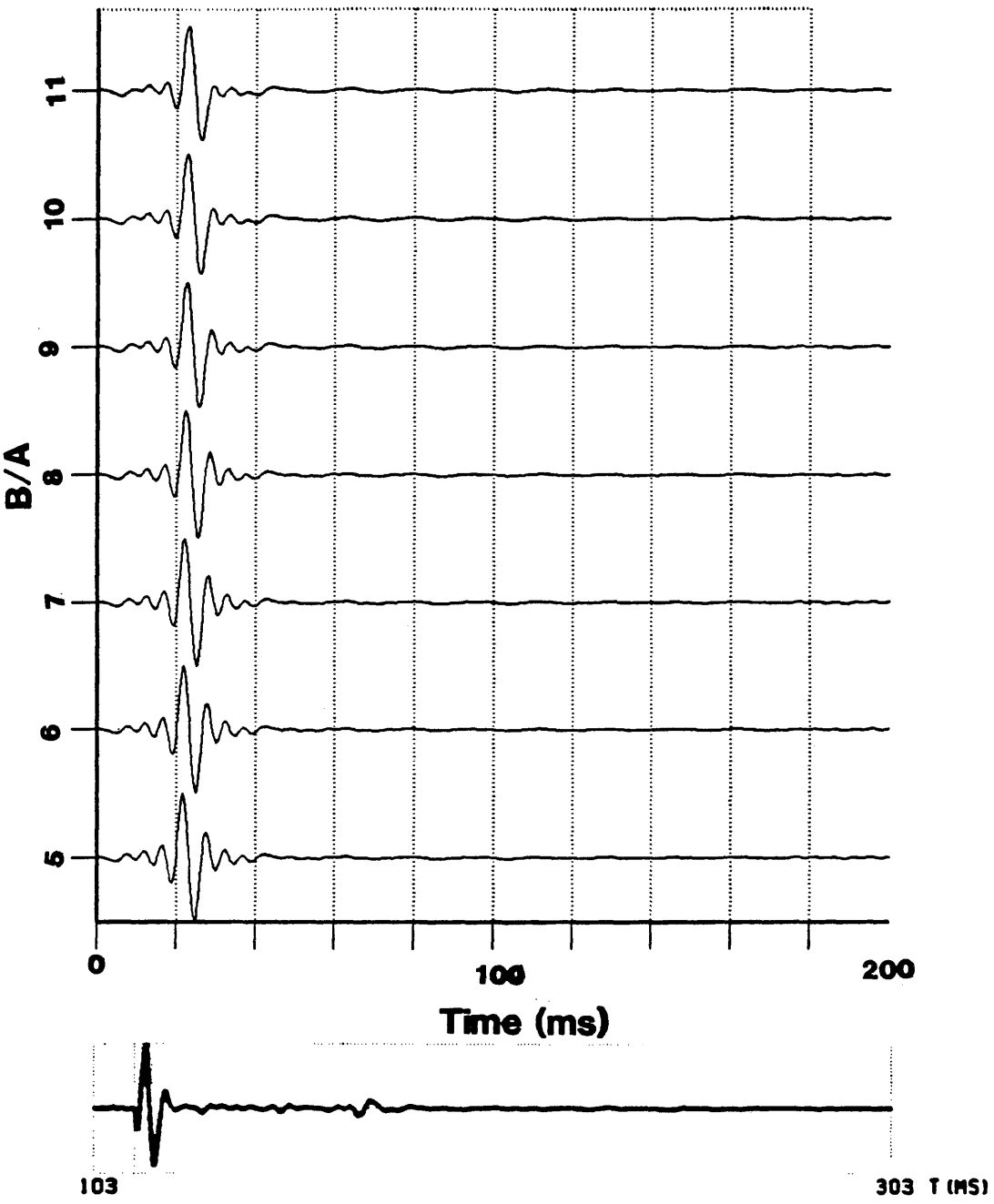

Figure 3-19 Particle velocity as a function of B/A ratio for a 1 lb charge in Pierre shale. (Viscosity = 20000 cP).

ratio. Displays for a 5 lb charge did also exhibit similar character and only outputs for 10 lb charges or higher were judged to be reliable for comparisons with the field data.

Considering the above, a viscosity menu for a 10 lb charge was made and is shown on Figure 3.20. Ounce again, a viscosity value of around 10^4 centipoises seems to be appropiate for our analysis. A ratio of almost 1:350 in amplitude variation is observed for viscosity changing from 10^7 to 10^4 cP in value. Higher than 10^4 viscosities exhibit waveforms that are essentially the time transformation of our frequency window as, similar to the previous case, most of the transmitted energy is outside the band-pass of our window.

Displays for 10, 25 and 50 lb charges were also constructed varying both B/A ratio and viscosity and best judged matches are shown in Figures 3.21 to 3.25. As before, we note a change in period with changing B/A ratio, and a change in degree of peak to trough oscillation, or amount of damping, with variations in viscosity. Closest matches with Sixta's waveforms were objectively judged-and perhaps not the "best" choices due to the inherent noisiness as a result of our narrow band notched filtering of the data-and are tabulated below for the reliable charge weights:

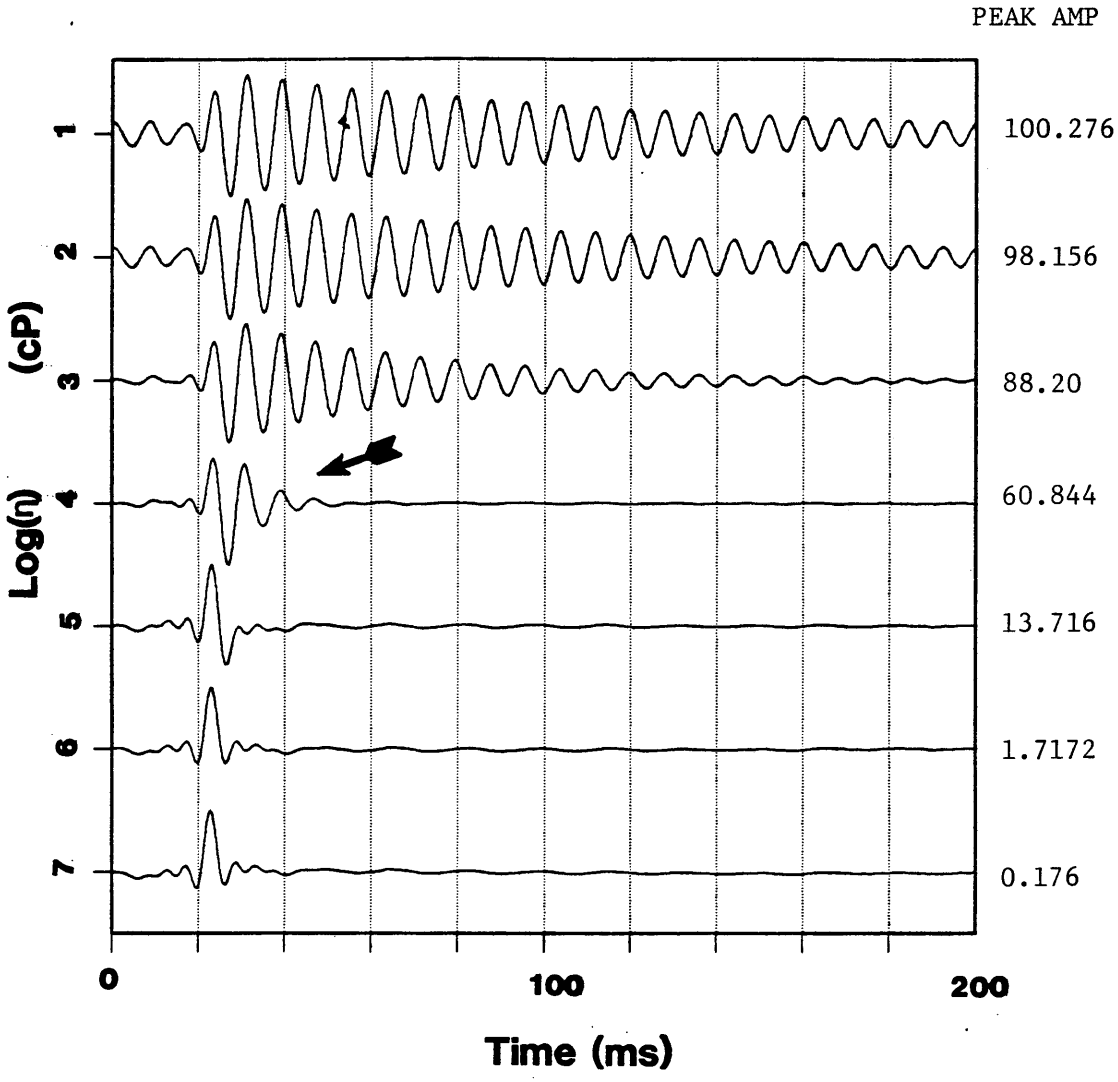

Figure 3-20 Particle velocity as a function of viscosity for a 10 lb charge in Pierre shale. (B/A = 7.5).

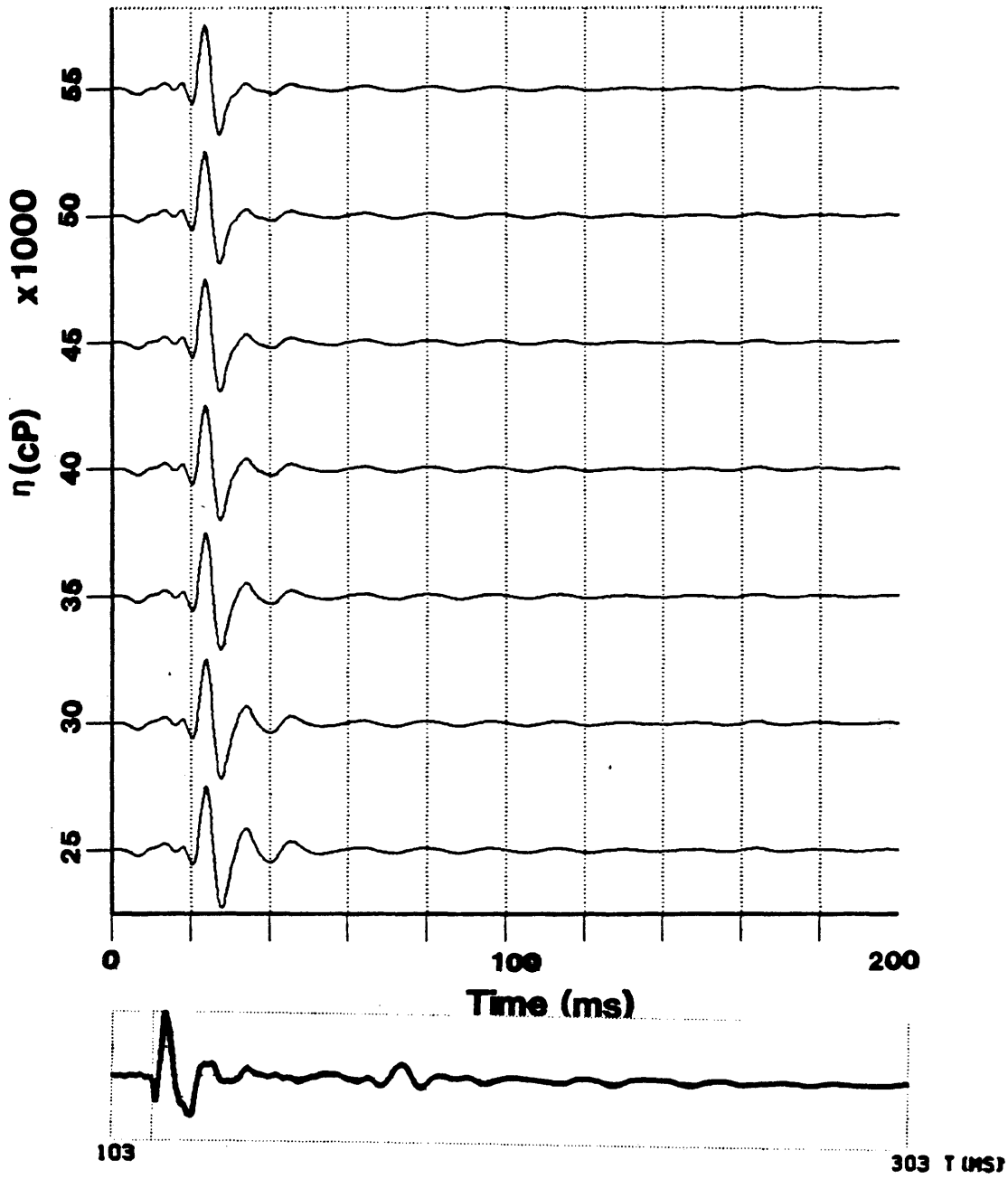

Figure 3-21 Particle velocity as a function of viscosity for a 10 lb charge in Pierre shale. (B/A = 7.5).

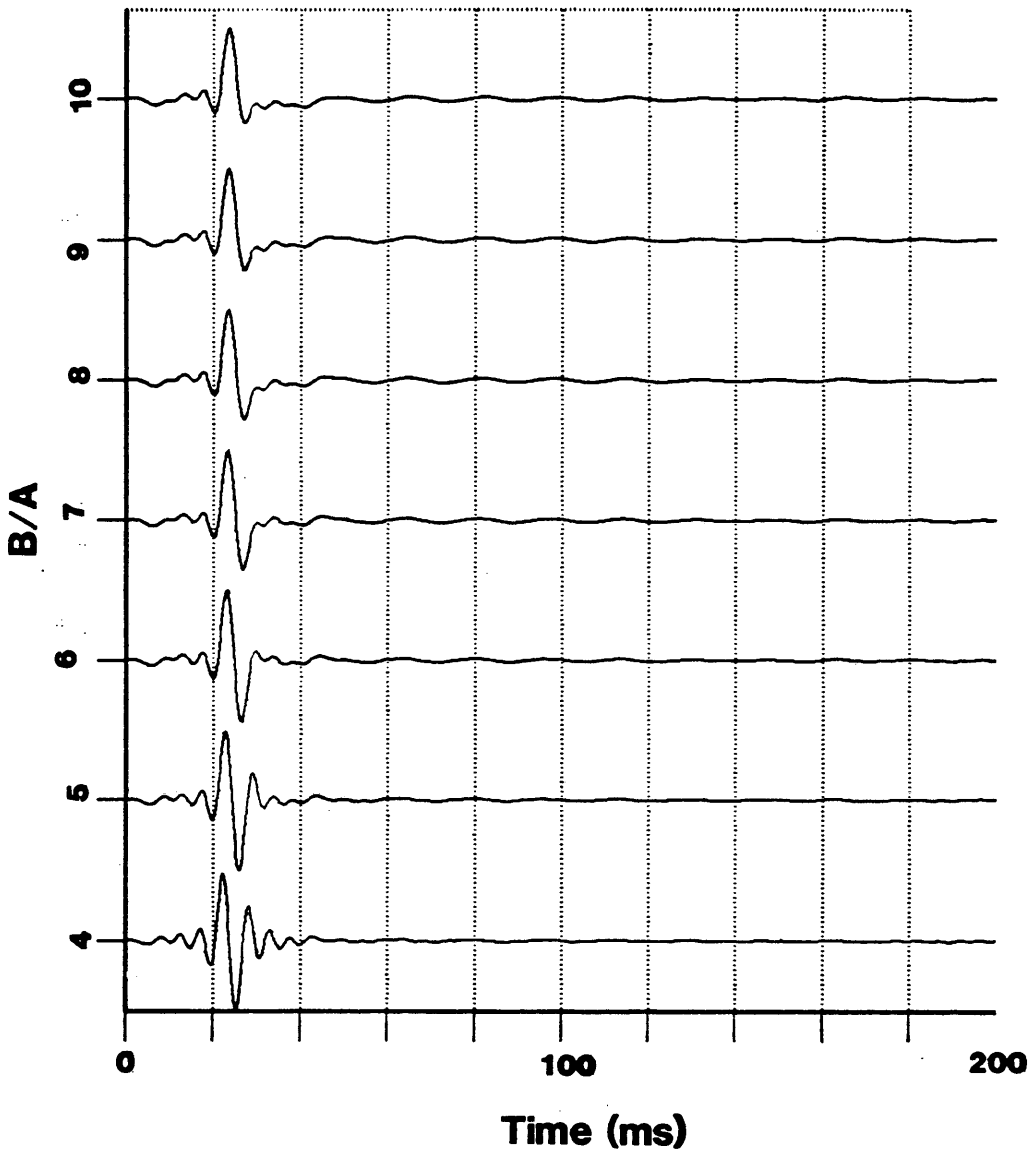

Figure 3-22 Particle velocity as a function of B/A ratio for a 25 lb charge in Pierre shale. (Viscosity = 90000 cP).

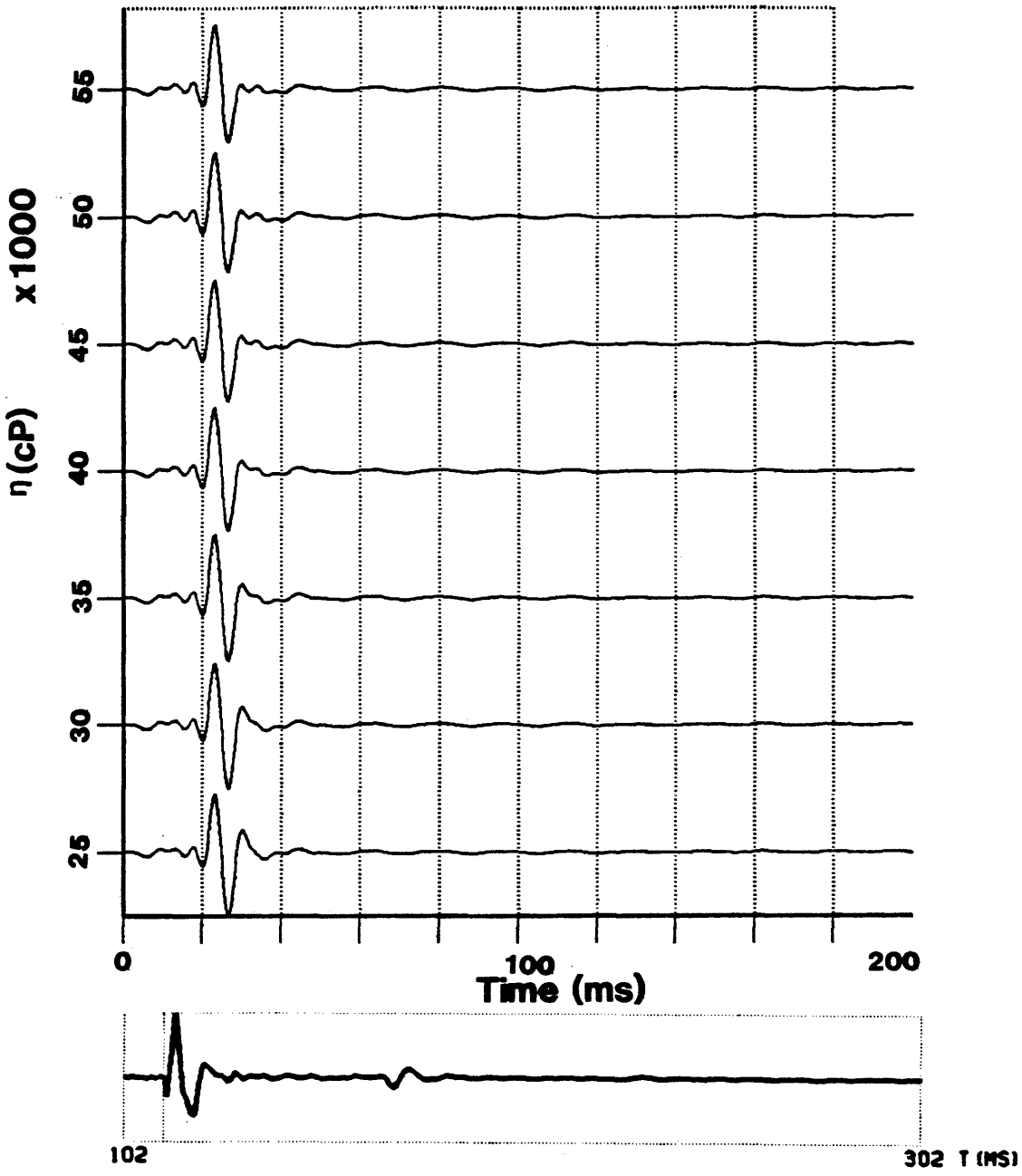

Figure 3-23 Particle velocity as a function of viscosity for a 25 lb charge in Pierre shale. (B/A = 7.75).

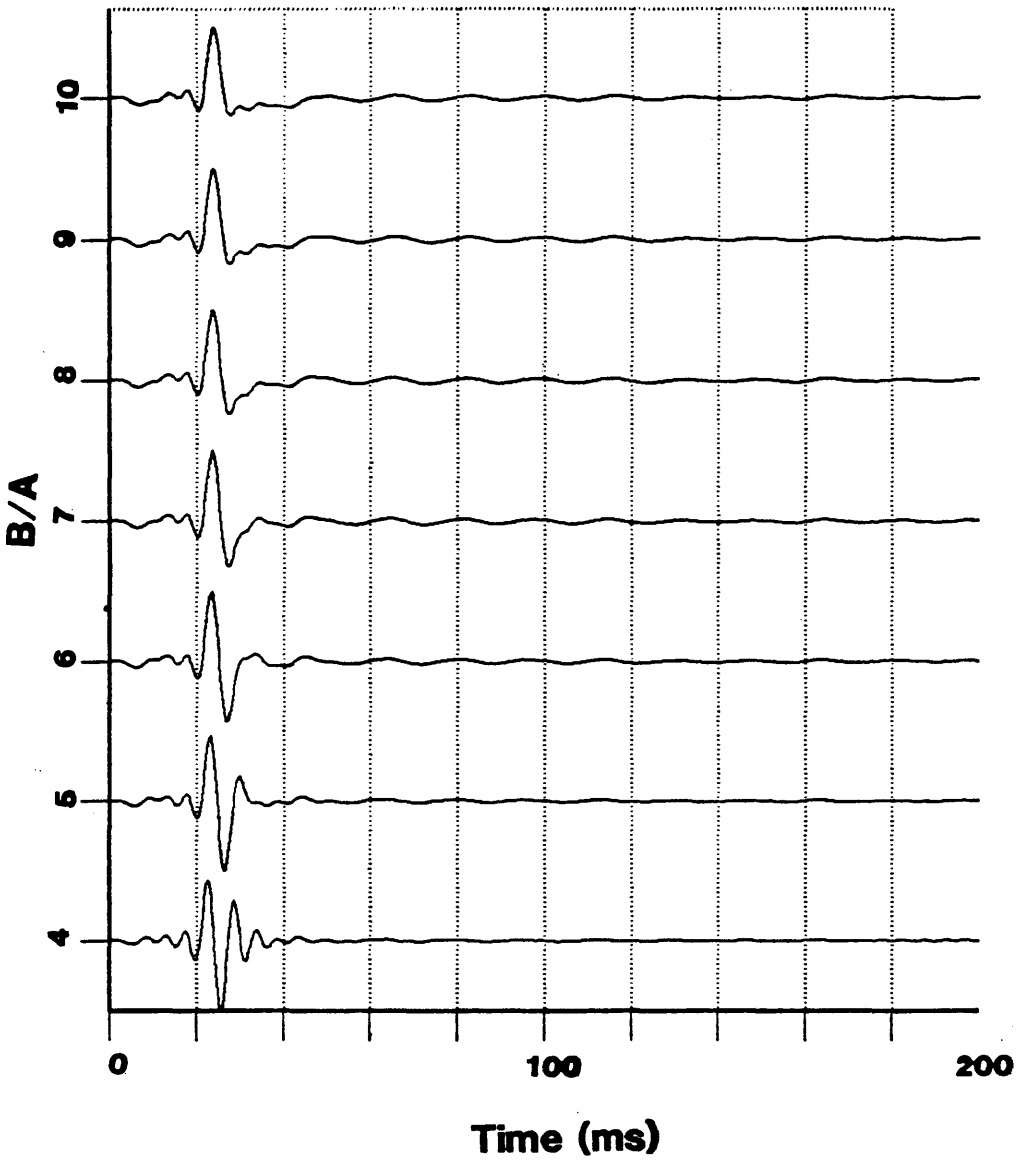

Figure 3-24 Particle velocity as a function of B/A ratio for a 50 lb charge in Pierre shale. (Viscosity = 90000 cP).

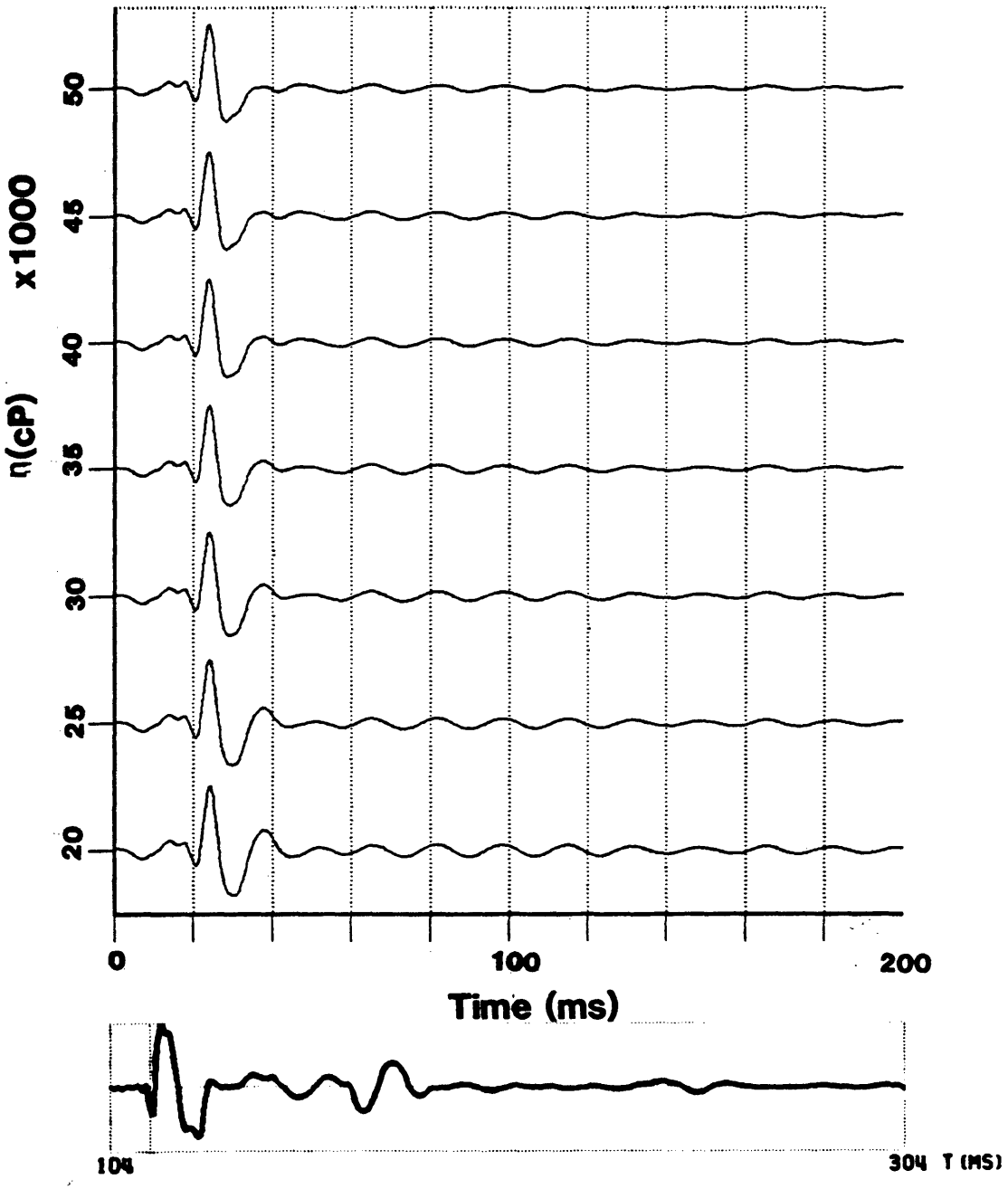

Figure 3-25 Particle velocity as a function of viscosity for a 50 lb charge in Pierre shale. (B/A = 8.25).

Charge size(lb)	B/A	Viscosity($x10^3$) (cP)
10	7.5	40.0
25	7.75	35.0
50	8.25	40.0

Table 3.3- Choices of B/A and viscosity for best match with field data in Pierre shale.

Here it should perhaps be noted that although the available information on the field parameters were far superior to the previous case, the variability in the shape of the waveforms put a constraint on the accuracy of all comparisons. Note for example, the rather ragged behavior of the second peak or even the first trough of the primary seismic wavelets for various charge weights.

Using constants stated in Table 3.3 and similar to the Taylor marl case, Figure 3.26 was made to display waveforms for the larger size charges. We again observe the same general trend of lower frequency motion for larger charges that are shot, of course, at the same depth. Illustrated in Figure 3.27 are the corresponding amplitude spectra. Notice the rather visible 60 Hz notch and, as

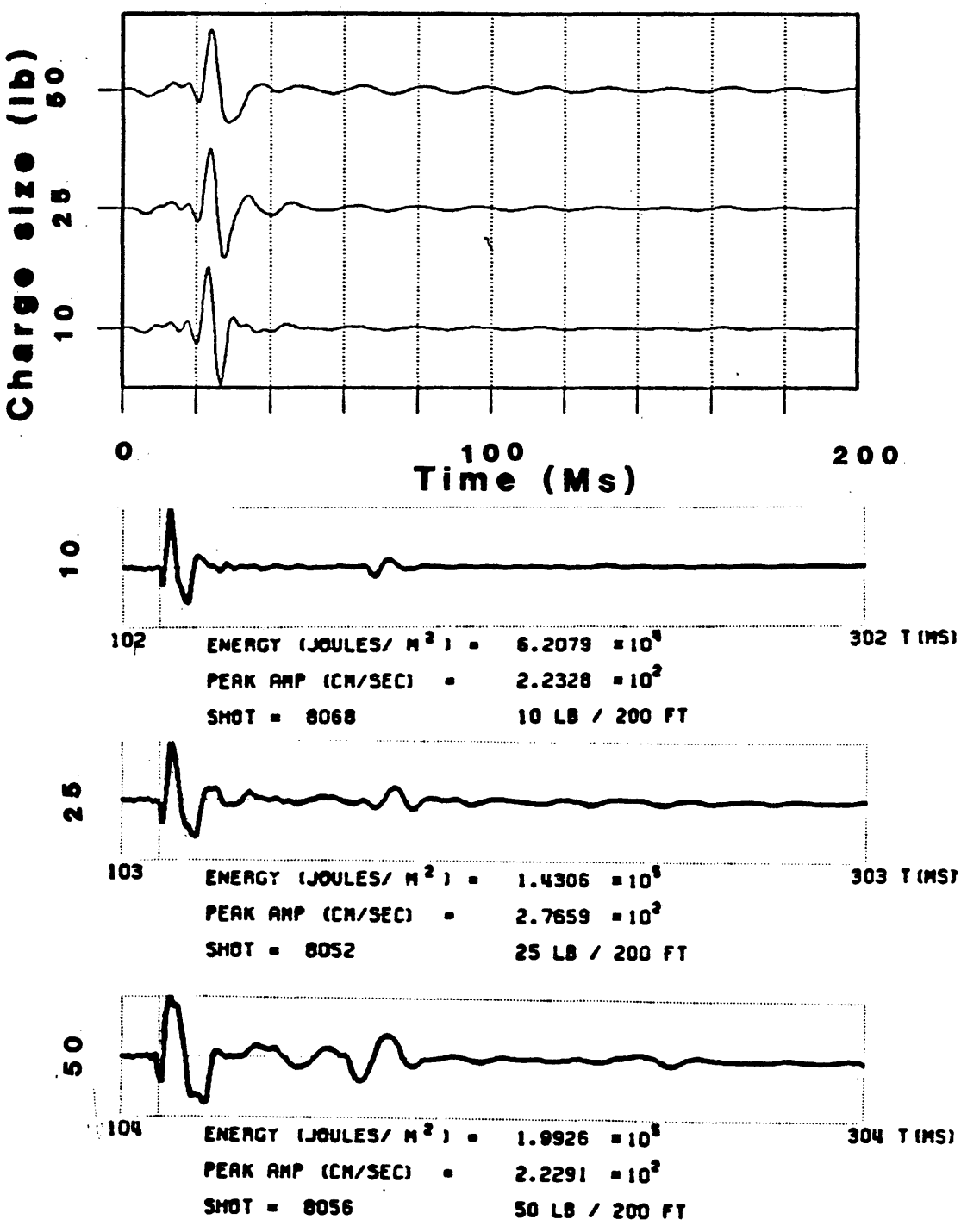

Figure 3-26 Particle velocity as a function of charge size in Pierre shale. (Slow decaying source, alfa = 10 sec^{-1})

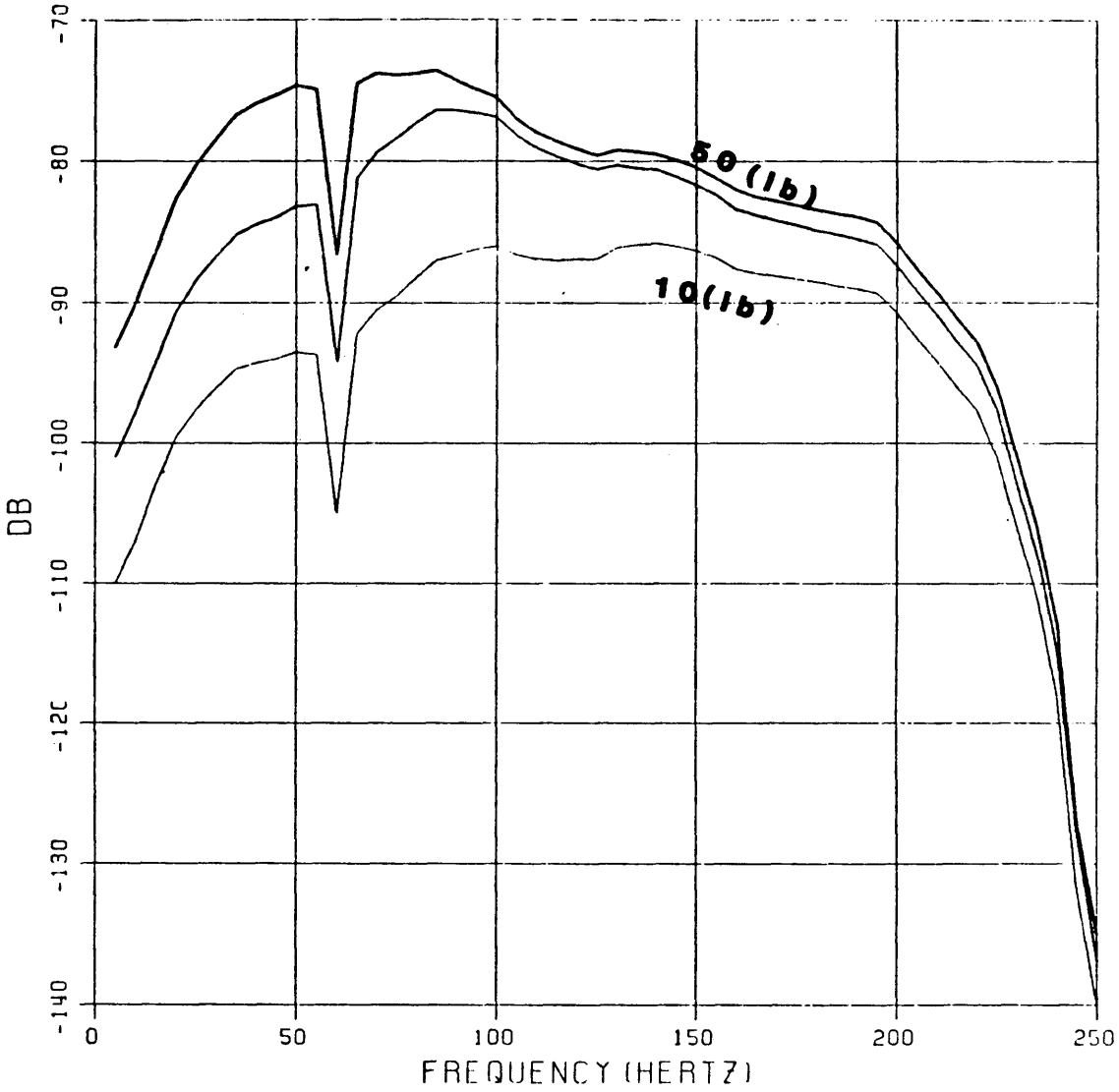

Figure 3-27 Amplitude Spectra of waveforms in Fig. 3-26.

before, larger amplitude/charge-weights dependance for lower parts of the frequency spectrum.

Larger B/A ratios and smaller viscosities were again observed for best fitted waveforms using faster decaying source (α=600 sec^{-1}) as shown in Table 3.4 below

Charge size (lb)	B/A	Viscos.($x10^3$) (cP)
10	9.3	38
25	9.2	28
50	10.4	25

Table 3.4- Selection of B/A and viscosity values for the faster decaying source (α=600 sec^{-1}) in the Pierre shale.

Values shown in Table 3.4 were used in making Figs. 3.28 and 3.29. Since no knowledge of dynamite's detonation pressure under borehole conditions were known, the amplitude corrected field data in the Pierre shale were used as a means of obtaining p_0 for the more reliable α=600 sec^{-1} source. This yielded to a value of $2.12x10^9$ dyn/cm^2. This scheme, therefore served as a means of calibration of our source for all the velocity waveforms in Pierre shale and other formations as well as the rock mechanics computations in Chapter IV.

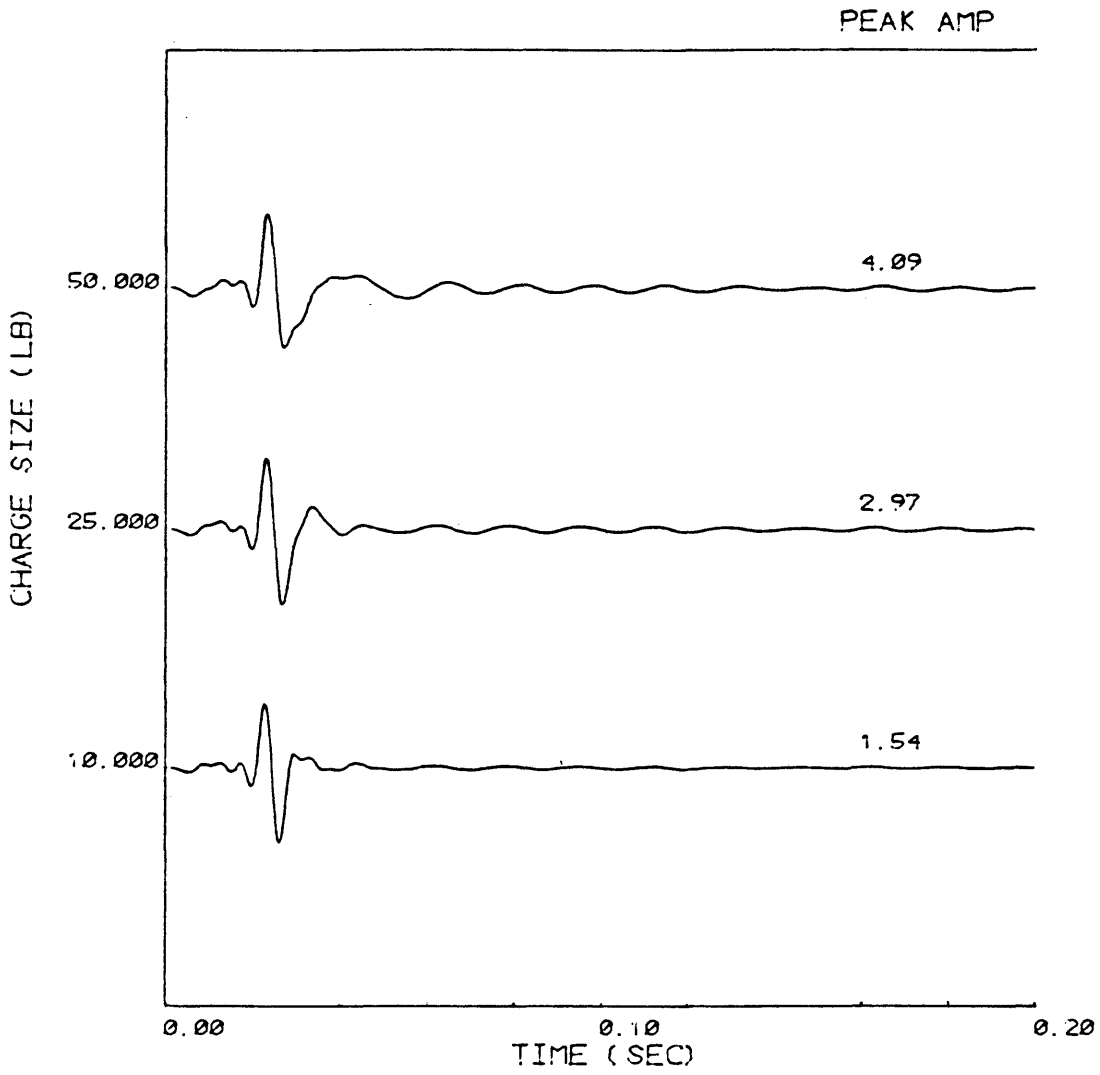

Figure 3-28 Particle velocity as a function of charge size in Pierre shale. (Faster decaying source, alfa = 600 xec^{-1})

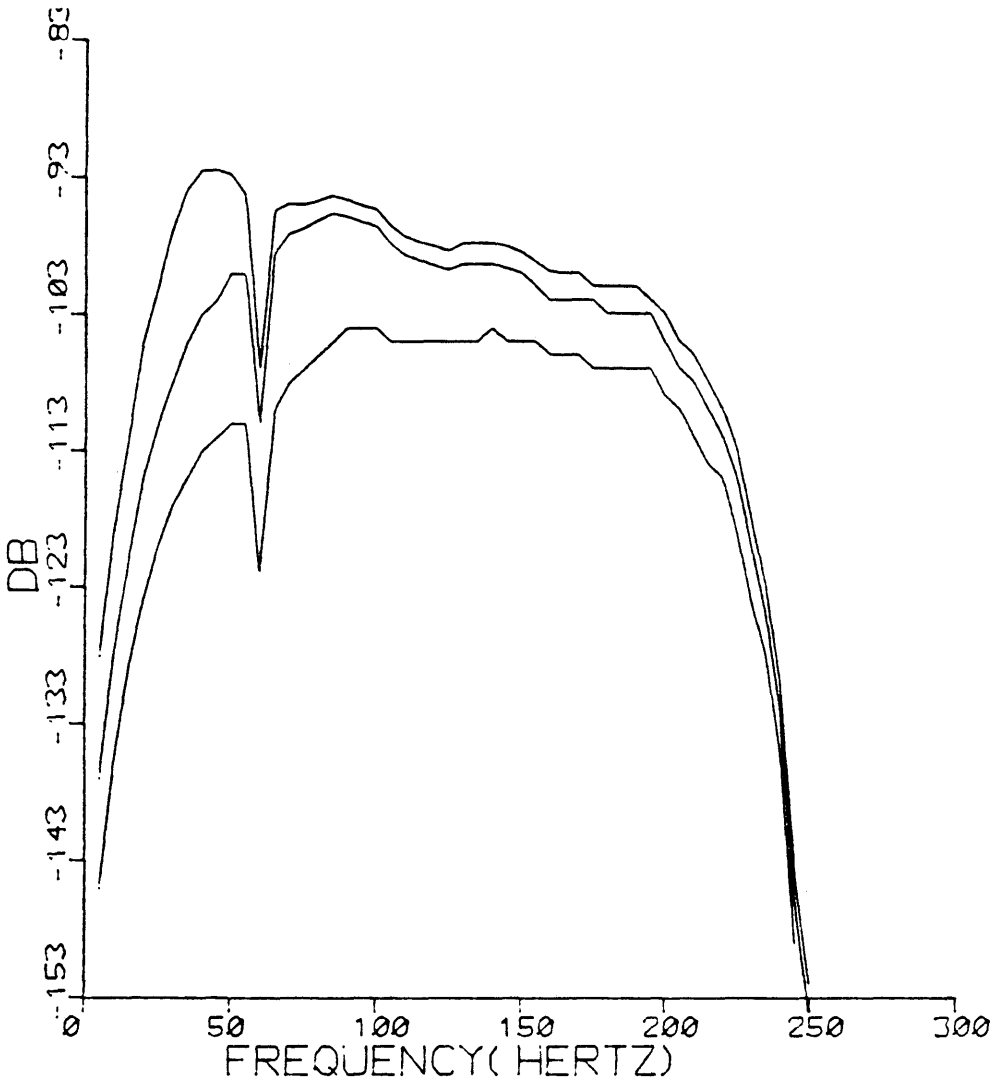

Figure 3-29 Amplitude spectra of waveforms in Fig. 3-28.

III.3.C Comparisons with Other Data in the Literature.

Perhaps, to reduce the problems associated with narrow-band filtering, we can consider other authors who also provided data on the same formation but using a more wide-band type of a filtering. Both McDonal et al. (1958) and Ricker (1953) obtained data on Pierre shale at locations near Limon in Eastern part of Colorado. Since the authors used rather flat response wide band recording systems, our previous 1/2 cycle sinc with 1400 Hz cut-off frequency was used for comparisons with this set of data for the slower decaying source only. An initial viscosity menu of Figure 3.30 exhibited the same acceptable 10^4 cP viscosity value, only now we note far less noisiness associated with zero phase back loading of energy and a much smoother behavior. A close look at expanded waveforms for a 10 lb charge using wide band filtering of Figure 3.31 does, however, show the slight artificial pre-onset non-zero lead.

Data for 1 lb charge can now be constructed rather reliably and is shown in Figure 3.32. This can in turn be used for comparisons with McDonal et al (Figure 3.33) for vertically travelling compressional wave and Ricker's

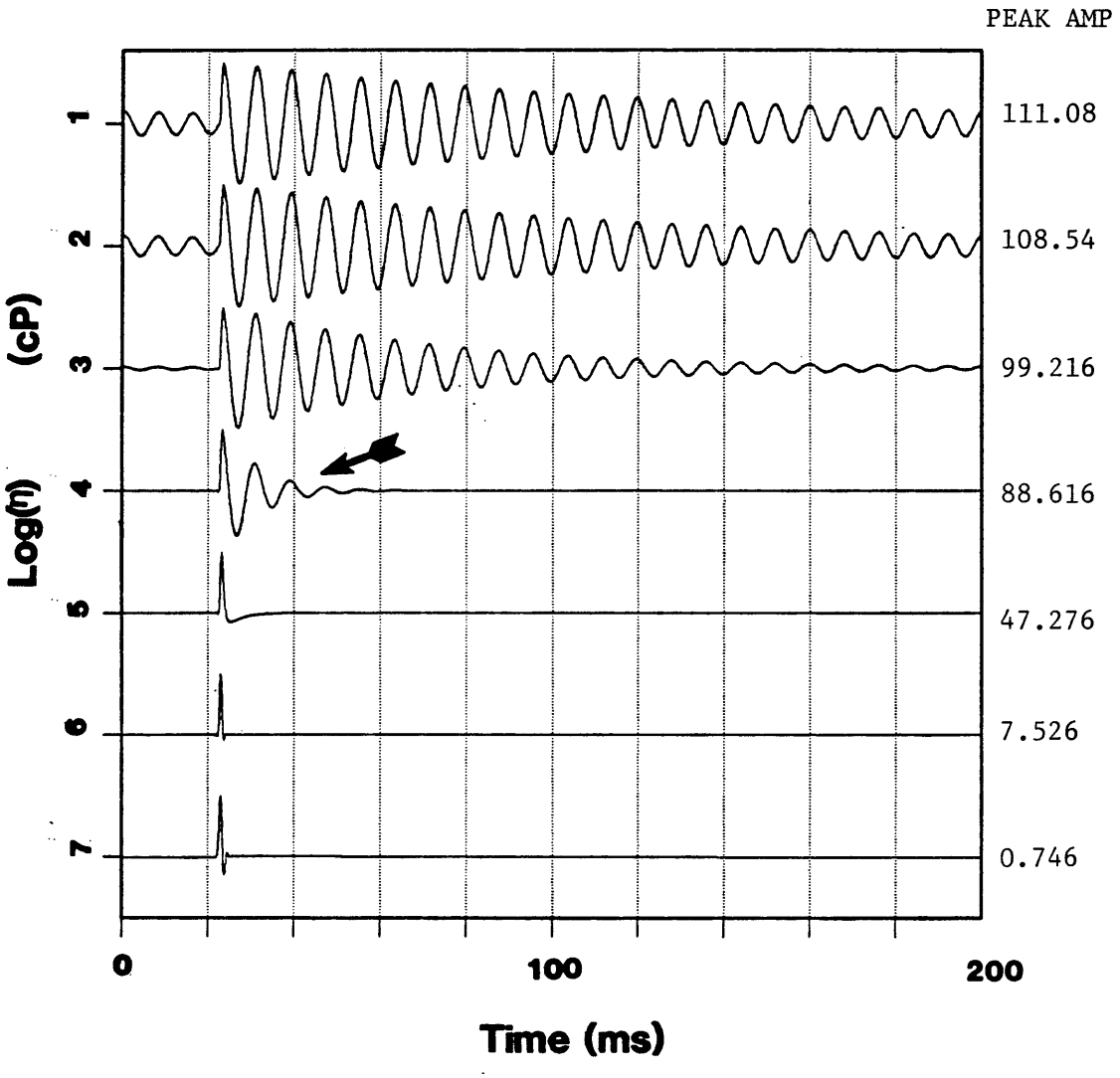

Figure 3-30 Particle velocity as a function of viscosity for a 10 lb charge in Pierre shale. (B/A = 7.5).

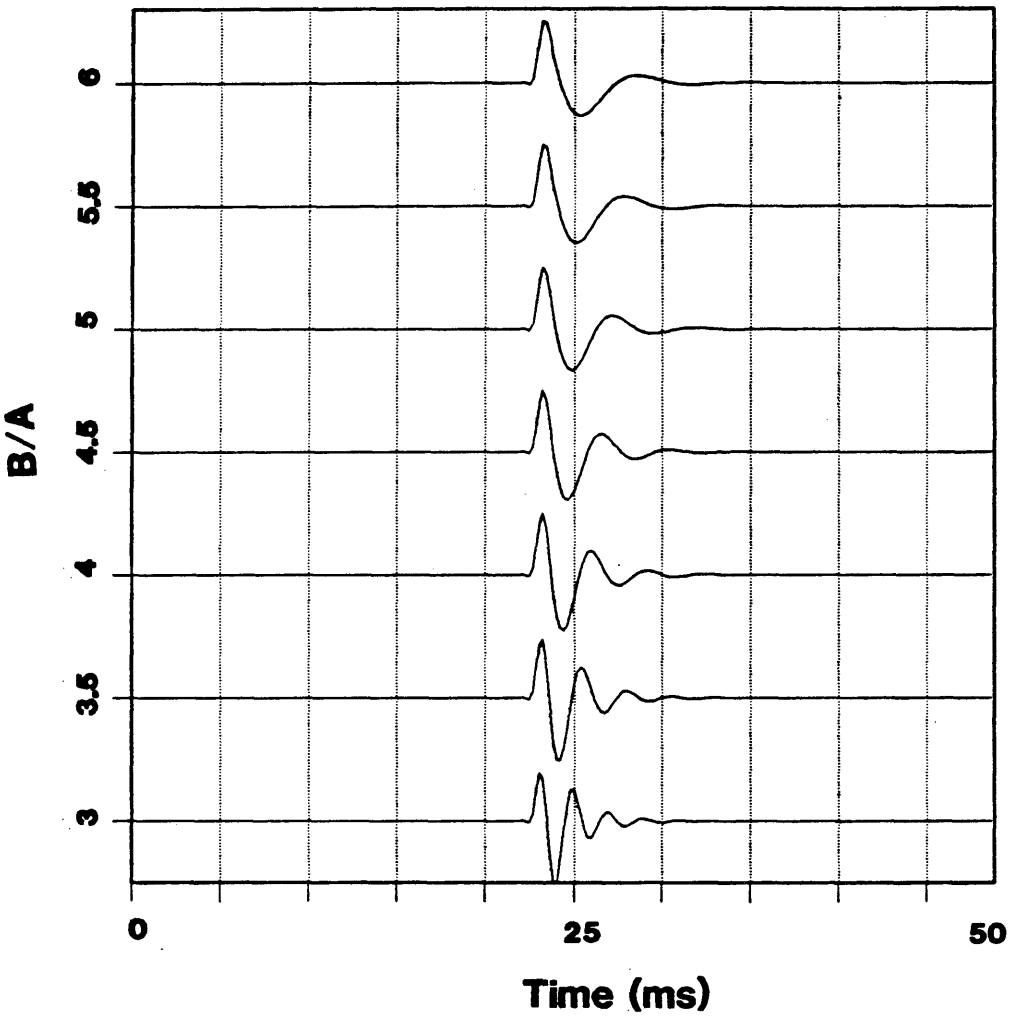

Figure 3-31 Particle velocity as a function of B/A ratio for a 10 lb charge in Pierre shale. (Viscosity = 40000 cP).

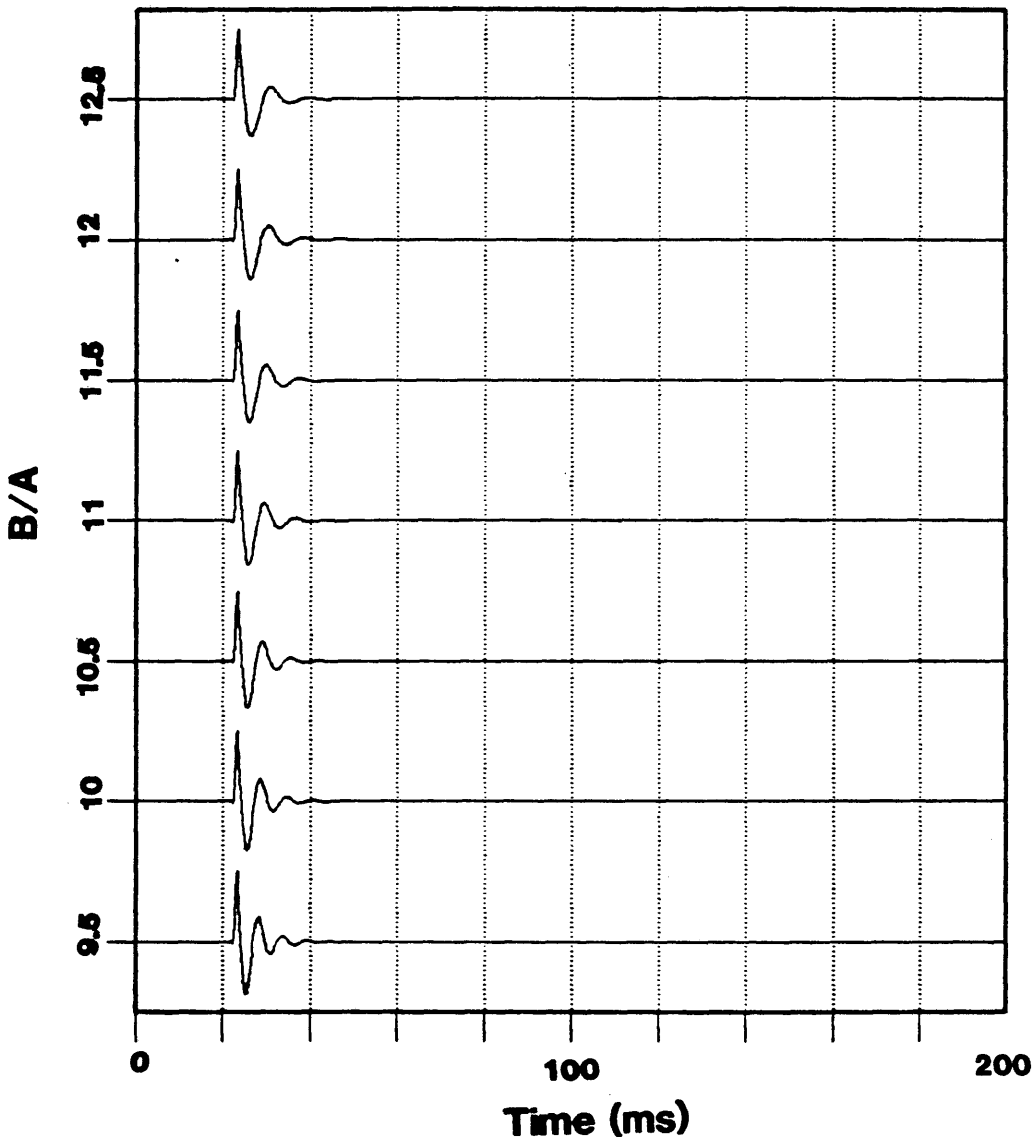

Figure 3-32 Particle velocity as a function of B/A ratio for a 1 lb charge in Pierre shale. (Viscosity = 50000 cP).

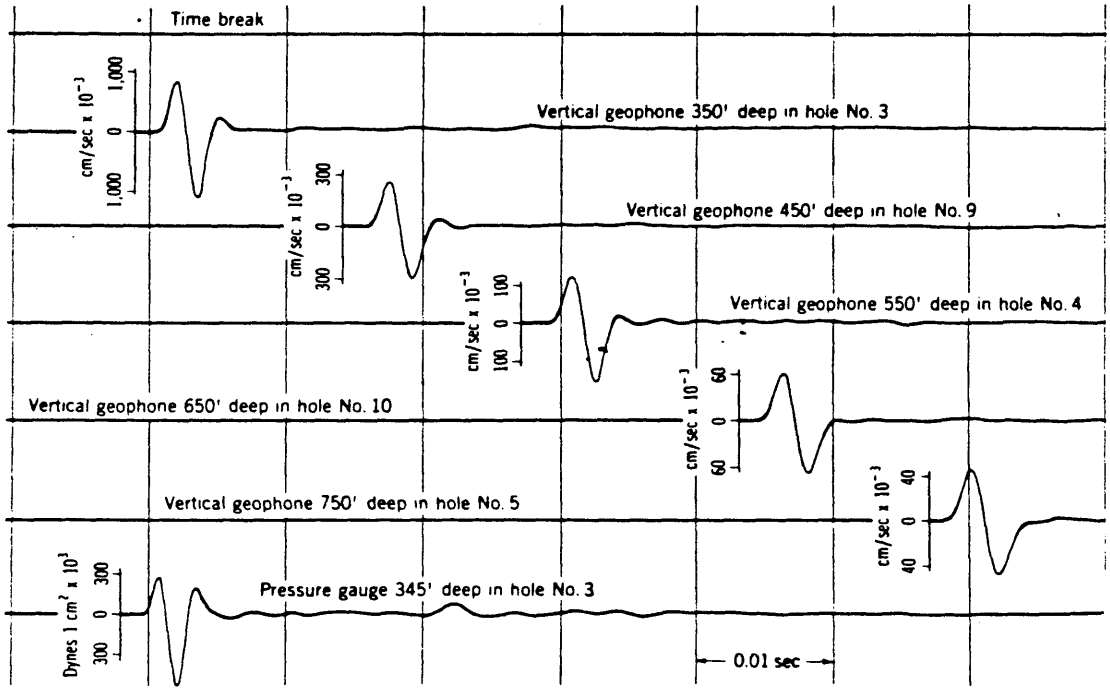

Figure 3-33 Compressional wave field recordings from a 1 lb charge at 260 ft. depth. (After McDonal et al., 1958).

(Figure 3.34) for shots at different depths. Slightly different velocity and density values were chosen in accordance to the logs reported in this paper. Compressional wave velocity are, in this case, around 2 km/sec for depths less than 400 ft and 2.134 km/sec for depths larger than 700 ft.

McDonal et al.'s data (1958, p. 427) were obtained by a Vertical Seismic Profile (VSP) type of survey for a 1 lb charge at a depth of 260 ft and recorded by 5 geophones placed at depths from 350 ft to 750 ft with 100 ft intervals. Although some degree of wave broadening as a function of travelled distance is apparent on the data, this attenuation effect is essentially negligible as far as our analysis is concerned. We thus took the same assumption for waveforms in the Taylor Marl where no attenuation corrections were performed on the data. A transient period of 4.5 ms roughly corresponding to a B/A of 10.5 in our theoretical data was found for this case. Comparisons with Ricker's data, on the other hand, gave rise to a B/A ratio of about 9.5

A glimpse at Table 3.3 we observe that comparisons with Sixta's data resulted in B/A values of around 8 which is slightly smaller than that of Ricker or McDonal et al.'s. This was explained by White (1962) where geophone clamping

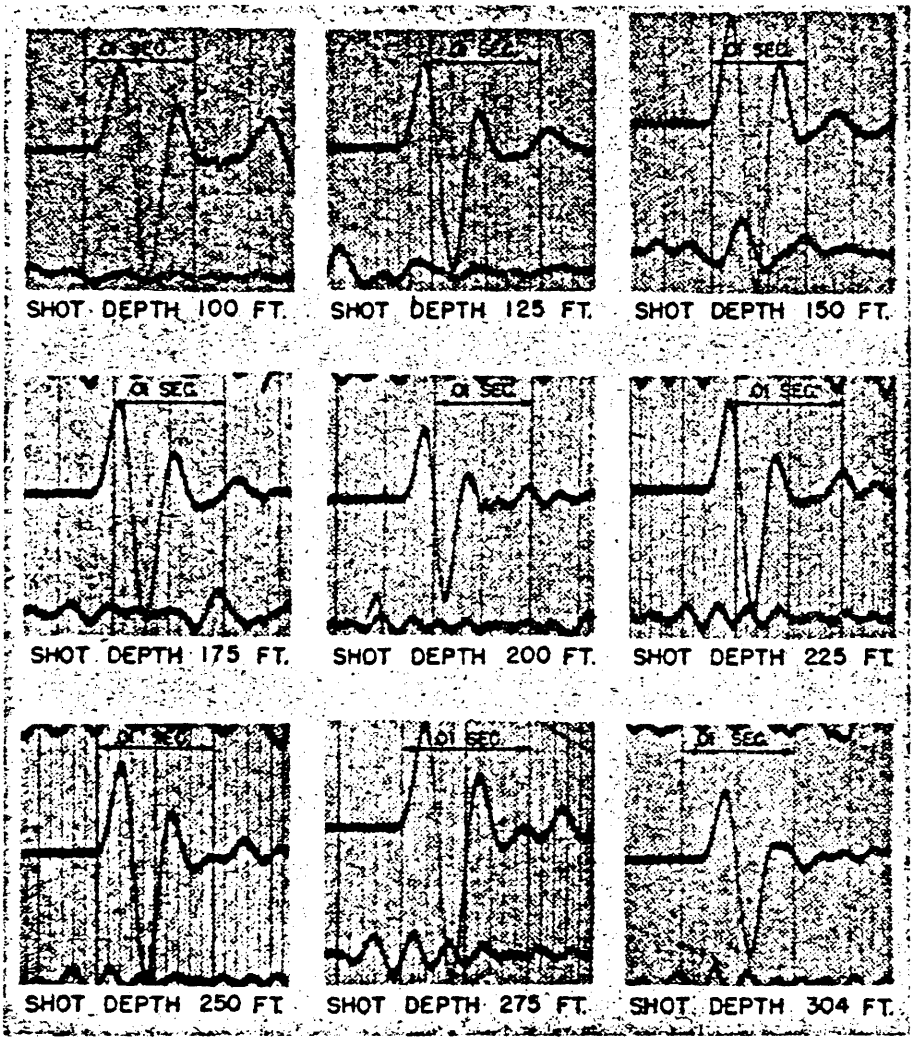

Figure 3-34 Compressional wave recordings as a function of geophone depth from a 1 lb charge. (After Ricker, 1951).

was explained not to follow the earth's motion as reliably as a hydrophone. Sixta (1982) and Janak (1982) made some improvement on this problem by filling the borehole with cement and thus creating a more homogeneous medium for wave-detection. This is also observed in Figure 3.32 where waveforms from a hydrophone pick up at 345 ft had a lower duration than a corresponding geophone at the same depth. The field data by Sixta (1982) and Sengbush (1978) are thus more suitable for theoretical comparisons. Extrapolation of periods to a lower value, brings the B/A obtained in Pierre shale in the same range. This viscosity value is, however, quite low and around 5000 cP.

Finally, outputs were obtained for comparisons with O'Brien's (1969) waveforms in a London clay formation. This formation had a net compressional velocity of 1.7 km/sec and a shear velocity of 0.6 km/sec and density of 2 gr/cm^3. A B/A ratio of about 10 was selected for both 0.31 kg and 1.55 kg charges as shown in Figs. 3.35 and 3.36 respectively. Each figure also displays a typical field wavelet as obtained by O'Brien for the charges being considered.

Our analysis therefore indicates that for the formations being considered, B/A ratios ranged from 6-12 in value for charge weights less than 50 lb. This suggests the size of the deformation boundary around a typical chemical

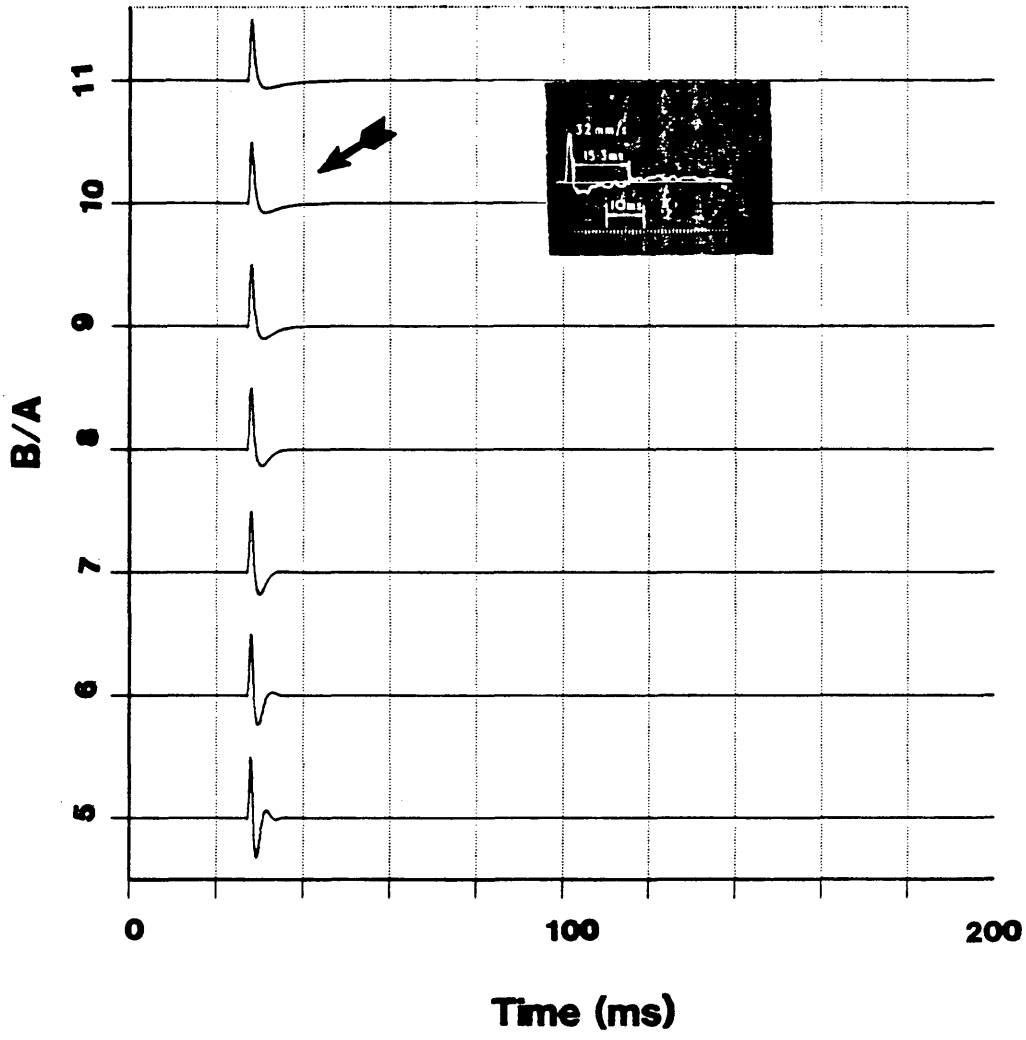

Figure 3-35 Compressional wave recordings from a 0.31 Kg charge at 23 m. depth in London clay. (After O'Brien, 1969).

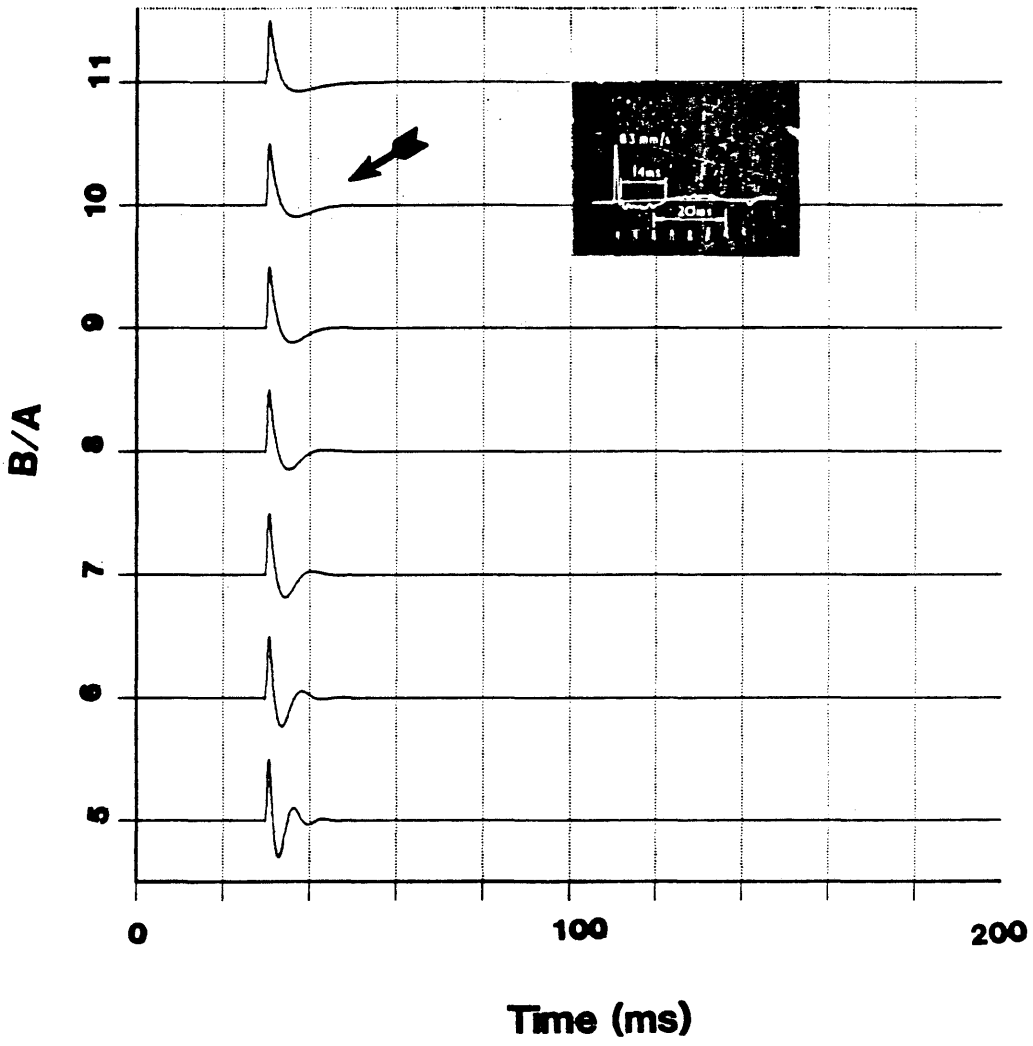

Figure 3-36 Compressional wave recordings from a 1.55 Kg charge at 24 m. depth in London clay. (After O'Brien, 1969).

explosive to be of relative small size, similar to many field observations.

CHAPTER IV. ROCK MECHANICS APPLICATIONS

IV.1 Calculation of dynamic stresses at the fracture boundary.

Besides the ability of the model to predict the far-field dynamical properties of the seismic wavelet, numerous other rock mechanics applications for the behavior of rocks at the limit of fracturing can be found as well. In particular, it is of interest to calculate the limiting stress value of rocks at the shattered boundary, B, where rock fracturing has ceased. Other interests include the size and extent of the deformation zone as well as the shape and properties of the transient stress wave that has been transmitted to the elastic region.

Results of calculation presented in chapter 3 in matching waveforms with the field data indicated that reasonable B/A ratios were obtained from the model, where A defined the physical radius of the charge. As mentioned previously in chapter 1, measurement of the shattered zone in granite, salt, limestone and marble by investigators from U.S Bureau of Mines indicated the extent of rock deformation around a commercial explosion to be of relatively small

size. B was generally found only about 5-12 times the charge radius, quite similar to the results obtained from the model. So the model can be held as approximately correct in predicting the extent of non-elastic deformation.

Before obtaining some numerical limiting stress values in rocks, however, two general parameters must be known in our model before theoretical calculations can be made. These are the time rate of decay of our source and its maximum amplitude P_0. P_0 was selected in chapter 3 by matching calculated peak velocity amplitudes to that of the amplitude-corrected field data as a means of calibration of our source. A value of 2×10^9 dyn/cm^2 was chosen that represented a considerable reduction in detonation pressure of dynamite in borehole environment as compared to ideal conditions. The source time constant α was chosen equal to 600 sec^{-1} corresponding to a moderately fast decaying source.

Since the wave motion in the elastic zone was assumed to be independant of all angular components, the only non-vanishing components of stress-possesssing a polar symmetry-are the radial normal stress

$$p_{rr} = (\lambda + 2\mu) \frac{\partial u}{\partial r} + 2\lambda \frac{u}{r} \qquad (4\text{-}1)$$

and perpendicular to r at any direction, the angular normal stress

$$p_{\theta\theta} = \lambda \frac{\partial u}{\partial r} + 2\ (\lambda + \mu)\ \frac{u}{r} \qquad (4\text{-}2)$$

where u denotes the radial displacement. Equations 4-1 and 4-2 can thus describe the set of stresses that are radiated outside the shattered boundary in to the elastic medium. The radial stress is found to be compressive and angular stress tensile.

Calculations were made to digitally obtain solutions to both stress equations 4-1 and 4-2 at the deformation boundary (R=B) using the same Fourier synthesis technique employed earlier in Chapter 2. The transient outputs then describe the stress waveforms that are emitted to the elastic zone as assumed by our model.

Figure 4.1 shows a typical diagram for both radial and angular stress superimposed on each other for a 5 lb charge and at the deformation boundary B. These waveforms represented transient responses due to our fast decaying source in Taylor marl and using best B/A ratio, viscosity and p_0 values obtained as a result of velocity matching in chapter 3.

Adopting a notation similar to material sciences

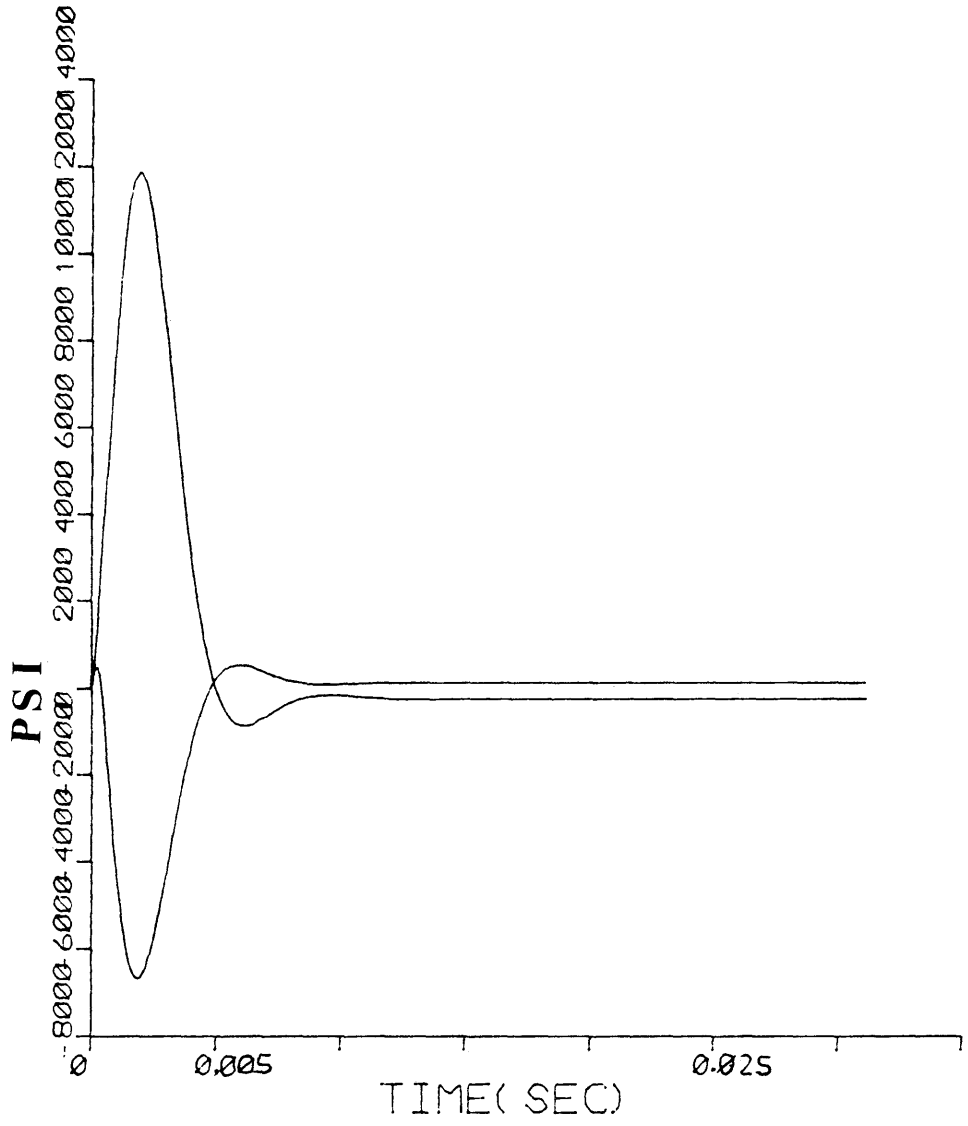

Figure 4-1 Radial and angular normal stress at R=B for a 5 lb charge in Taylor marl.

with negative denoting tension and positive as compression, we observe the radial stress to complete a positive compressive cycle with a small tensile undershoot before decaying to zero. The angular stress, on the other hand, undergoes a negative tensile cycle with a compressive undershoot. Both transients have a time duration of few milliseconds and when superimposed on each other, as in Fig. 4.1, they exhibit a similarity in shape with same zero crossing for both waveforms. This is readily evident from Eqs.4-1 and 4-2 where we observe that both stress relations show a similar functional dependance with displacement u but are only multiplied by different combinations of the elastic constants.

In calculation of the stress outputs we observe a slight frequency static component due to our source. As a reminder, this problem was accounted for in our calculations of particle velocity since the time differentiation of particle displacement resulted in a multiplication of an $i\omega$ factor in the frequency domain which zeroed out the static. In the case of stress calculation, however, we have to recognize this problem. Note also that Fig. 4.1 does not plot the full 0.2 second waveforms, so that each oscillation is not yet reduced to its full static value.

Using constants obtained in chapter 3, full radial

and angular waveforms for all size charges in Taylor marl are calculated and shown in Figs. 4.2 and 4.3 respectively. The time duration is 0.05 seconds so that each tic mark on the x-axis corresponds to 5 milliseconds. The peak values indicated on the right hand margins are in psi. Each transient behaves essentially as a half sinusoid with its time duration increasing and waveform shape becoming more oscillatory with larger size charges. The peak stress values show a decreasing trend with larger charges.

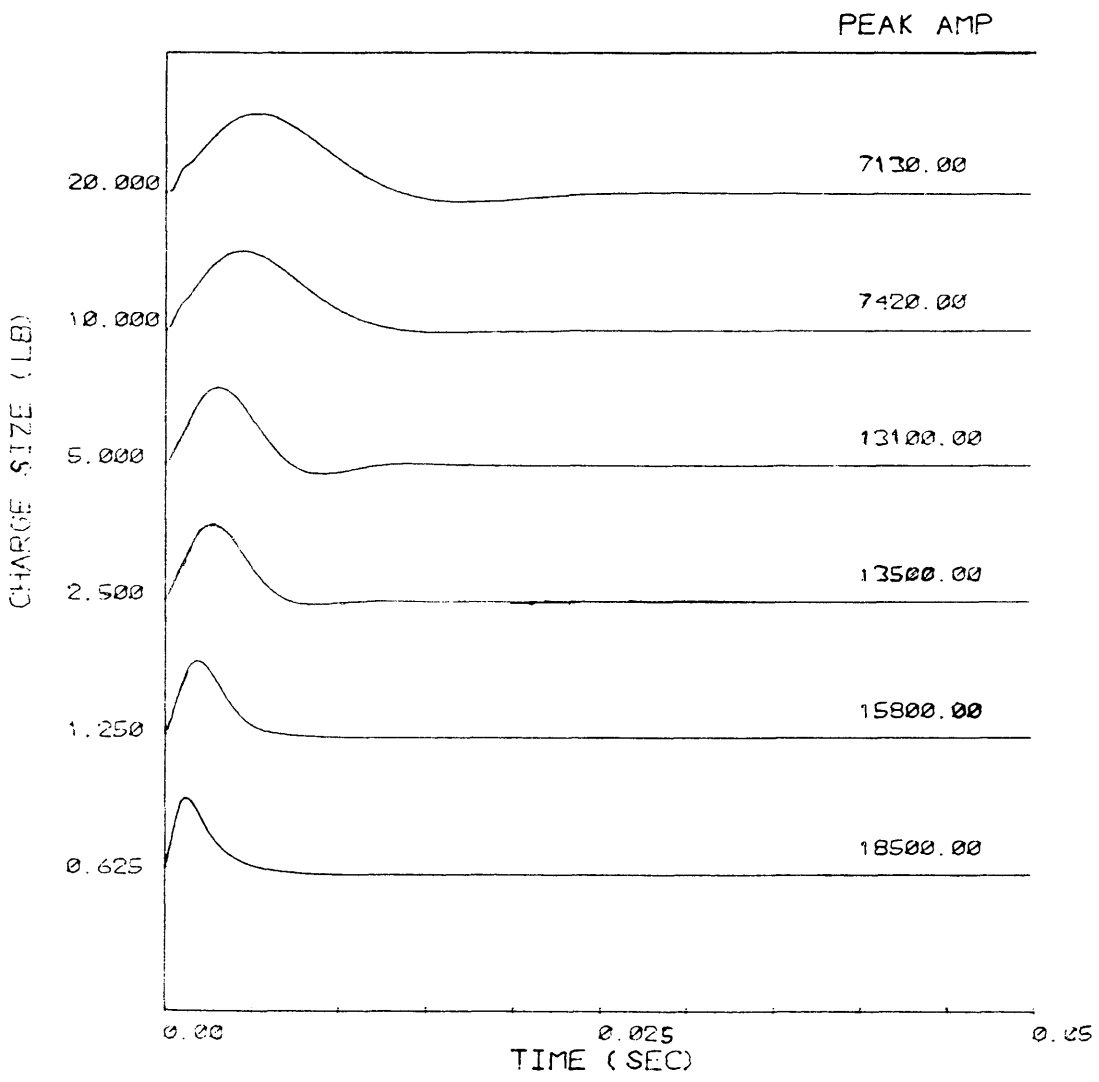

Figure 4-2 Radial normal stress as a function of charge size at R=B in Taylor marl.

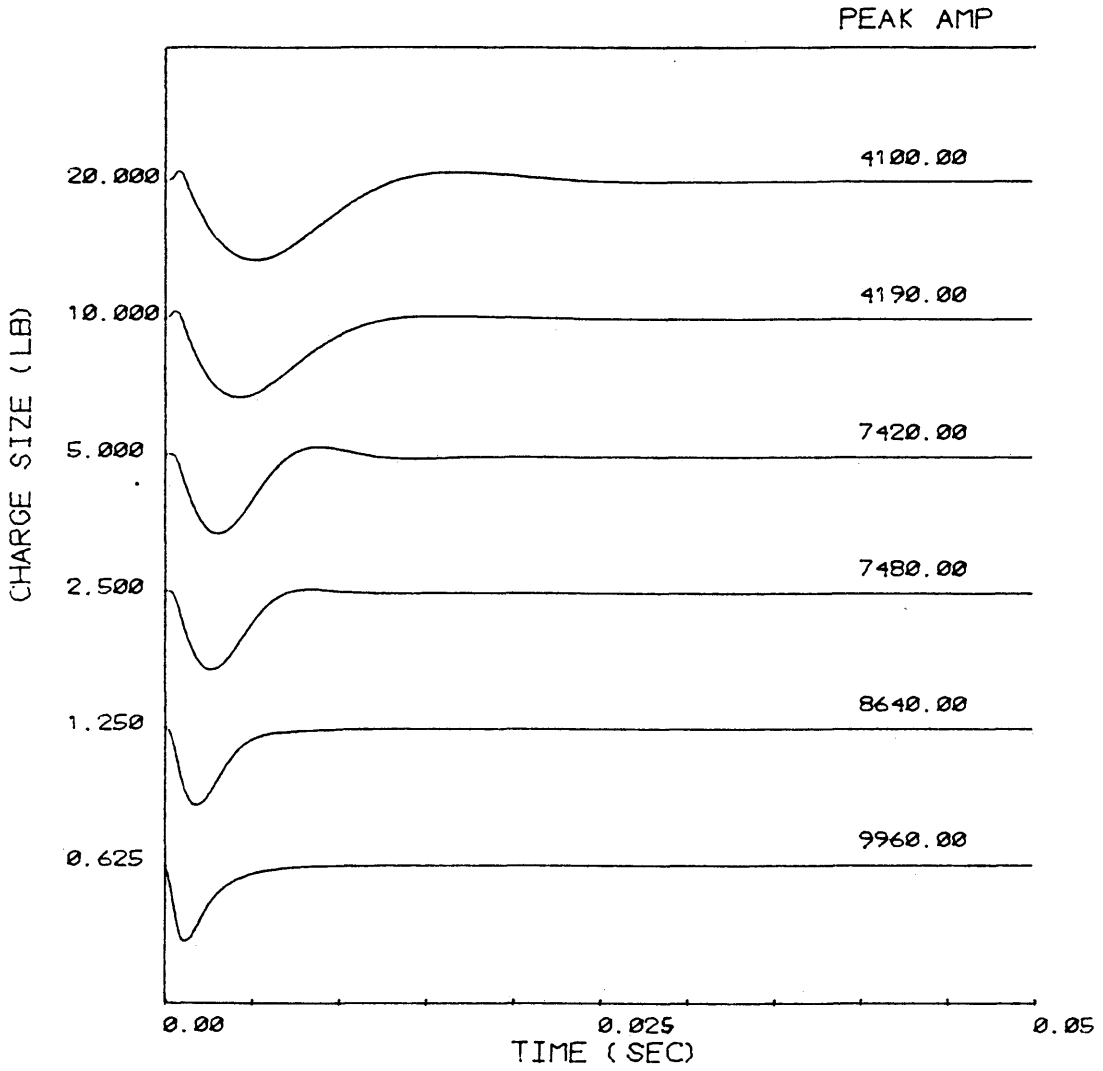

Figure 4-3 Angular normal stress as a function of charge size at R=B in Taylor marl.

IV.2 Failure Criteria.

Failure of rocks is generally explained as a functional relationship between "strength" of the rocks and the imposed stresses. The process of failure, however, is expected to differ considerably under dynamic loading rates of only a few milliseconds in duration, as compared with static loading of cylindrical samples of rocks. Moreover, the ratio between compressive and tensile strengths in rocks, known as the Blastability Coefficient, is generally very high suggesting that rocks fail much more easily under tension than compression.

If we consider the rock mass to contain a large number of flaws or pre-existing elliptically shaped cracks, Griffith's criteria can be adapted to explain crack propagation causing failure due to the radiated radial and angular stresses. Since in blasting operations the rate of the loading of the source is very fast, these Griffith cracks do not acquire suffficient time for closure. Orginal Griffith theory did not also account for crack closure associated with compressive applied forces and only effects of tensile forces at fracture were calculated. This can also imply that under dynamical situations, shear frictional stresses are probably not the contributing factors in

failure and only the normal stresses are involved.

The original Griffith theory, which was proposed to explain the low measured tensile strengths in glass, suggested that in two dimensions failure occurs when the tensile stress in a flat elliptical crack reaches a value characterictic of the material. Da Gama and Nelson (1970) extended the Griffith theory to dynamical situations in blasting to explain the hoop tensile stress to be the main cause of radial cracking in the cracked zone under the propagation of radiated waves over pre-existing "flaws". So the maximum tensile values of Fig. 4.3 can then be considered to correspond to the limiting dynamic tensile strengths that the hoop stress has attained at the limit of radial cracking. Due to the presumed geometry, moreover, the principal axis coincides with the polar system which means the the radial stress P_{rr} is the maximun normal stress σ_1 and the angular stress $P_{\theta\theta}$ is the minimum normal stress σ_3. In the Mohr space these define a circle which intersects the failure envelope at σ_3 as shown in Fig. 4.4. According to Griffith's hypothesis, σ_3 defines the limiting tensile strength of rocks in the formation of radially extending cracks at failure.

Da Gama and Nelson (1970) adapted fracture mechanics from Griffith's crack concept to explain the formation of

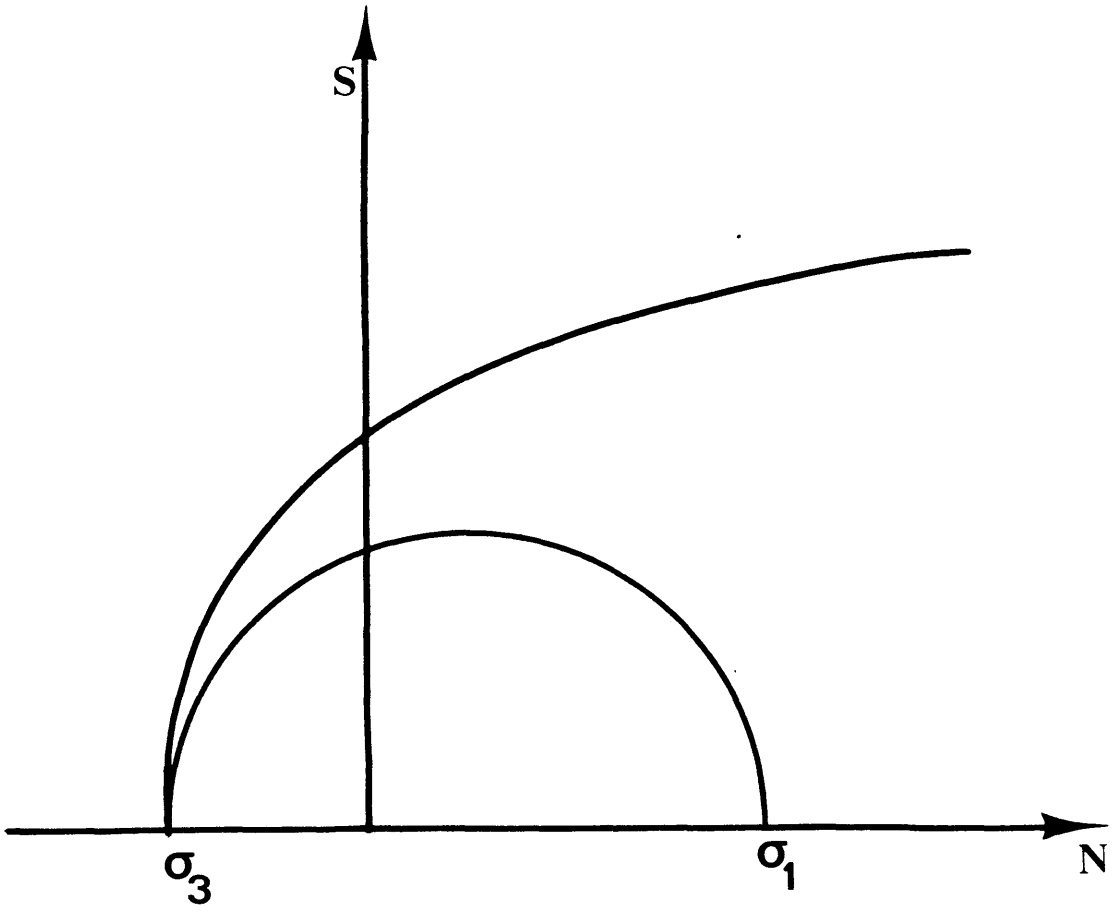

Figure 4-4 State of stress at failure according to Griffith criteria.

these radial cracks outside the crushed zone. Implication of this theory suggested that radial cracks occur even though the radial compressive stress has an amplitude less than the compressive strength of the rock. The net effect of the compressive stress P_{rr}, they concluded, was not in rock failure but only allignment of flaws and their small extension in a radial direction which coincides with the direction of the maximum principal stress.

The tangential tensile wave would then reinitiate these radial cracks causing them to propagate until the tensile wave "outruns" the slower moving crack tips. The radial direction of failure, therefore, may not coincide with the original direction of the crack. The extent of radial cracks is, of course, dependant on many factors including explosive parameters, charge parameters and rock parameters as was discussed in chapter 1.

Assuming that the peak values in Fig. (4.3) represent the characteristic dynamic tensile strength in Taylor marl we here proceed to tabulate them along with the radial stress values as a function of charge size. The values presented in the table are corrected for the source static which was found equal to +128 for the angular and -256 for the radial stresses. These, therefore, represent the values by which both stresses need to be adjusted by in

order to shift the stress curves correctly to the zero line.

Charge size(lb)	P_{rr}(psi)	$-P_{\theta\theta}$ (psi)	$\lvert P_{rr}/P_{\theta\theta} \rvert$
5/8	18756	9832	1.91
1.25	16056	8512	1.89
2.5	13756	7352	1.87
5.0	13356	7292	1.83
10.0	7676	4062	1.89
20.0	7386	3972	1.86
			Ave.=1.87

Table 4-1. Dynamic peak tensile and radial values at the deformation boundary after static correction have been made.

Curves for radial and angular normal stress for B/A and viscosity values obtained in Pierre shale also show the same trend of an increase in oscillatory behaviour with charge size as shown in Figs. 4.5 and 4.6. However, no expected decrease of peak amplitude between 10 to 25 lb charges has occurred, but none-the-less a general decreasing trend is evident. This is probably due to the distortions introduced by the narrow band windowing of the data which has made the correct wavelet selection not as reliable as the Taylor marl case. These are shown in the Table 4-2 below:

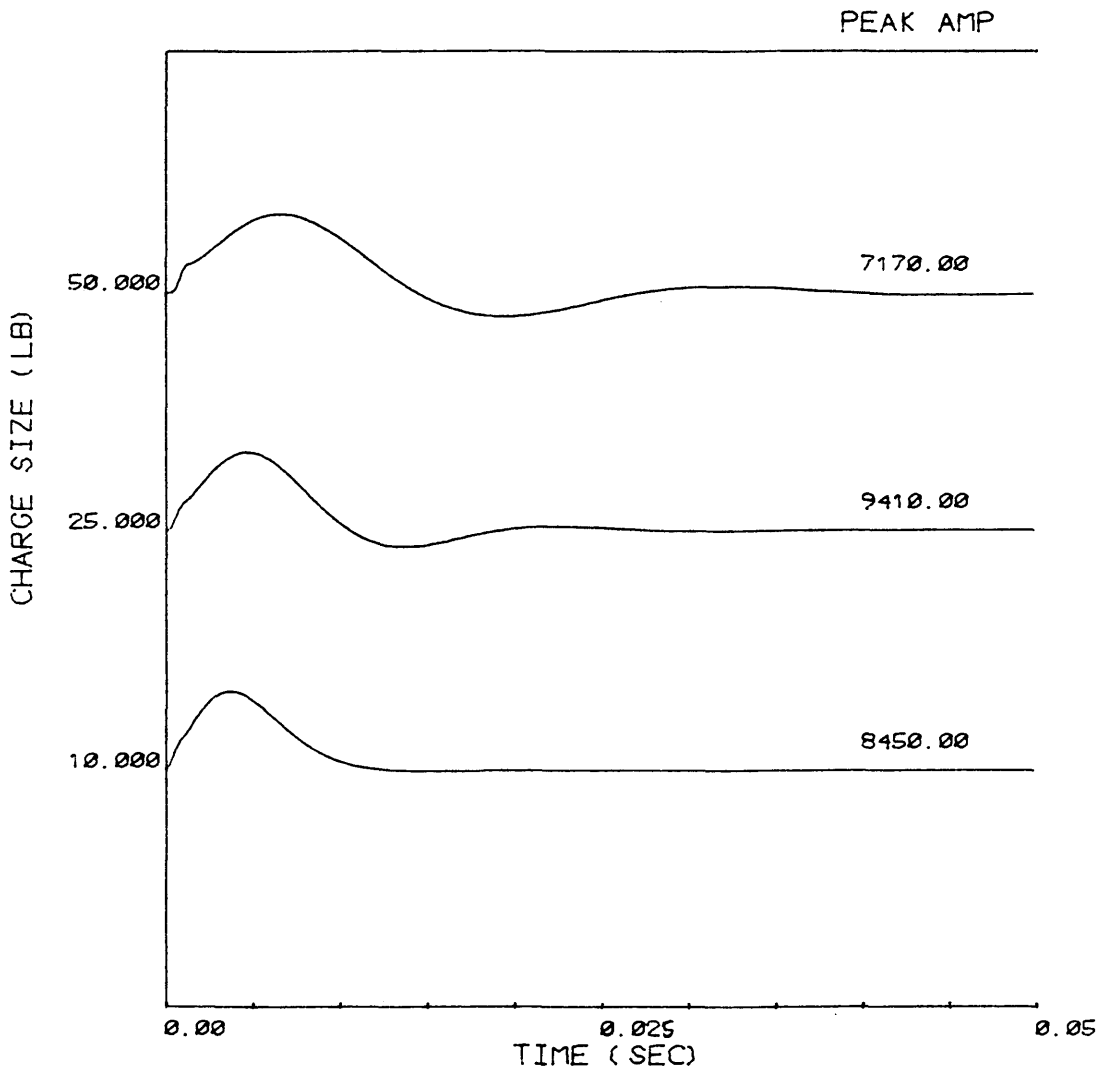

Figure 4-5 Radial normal stress as a function of charge size at R=B in Pierre shale.

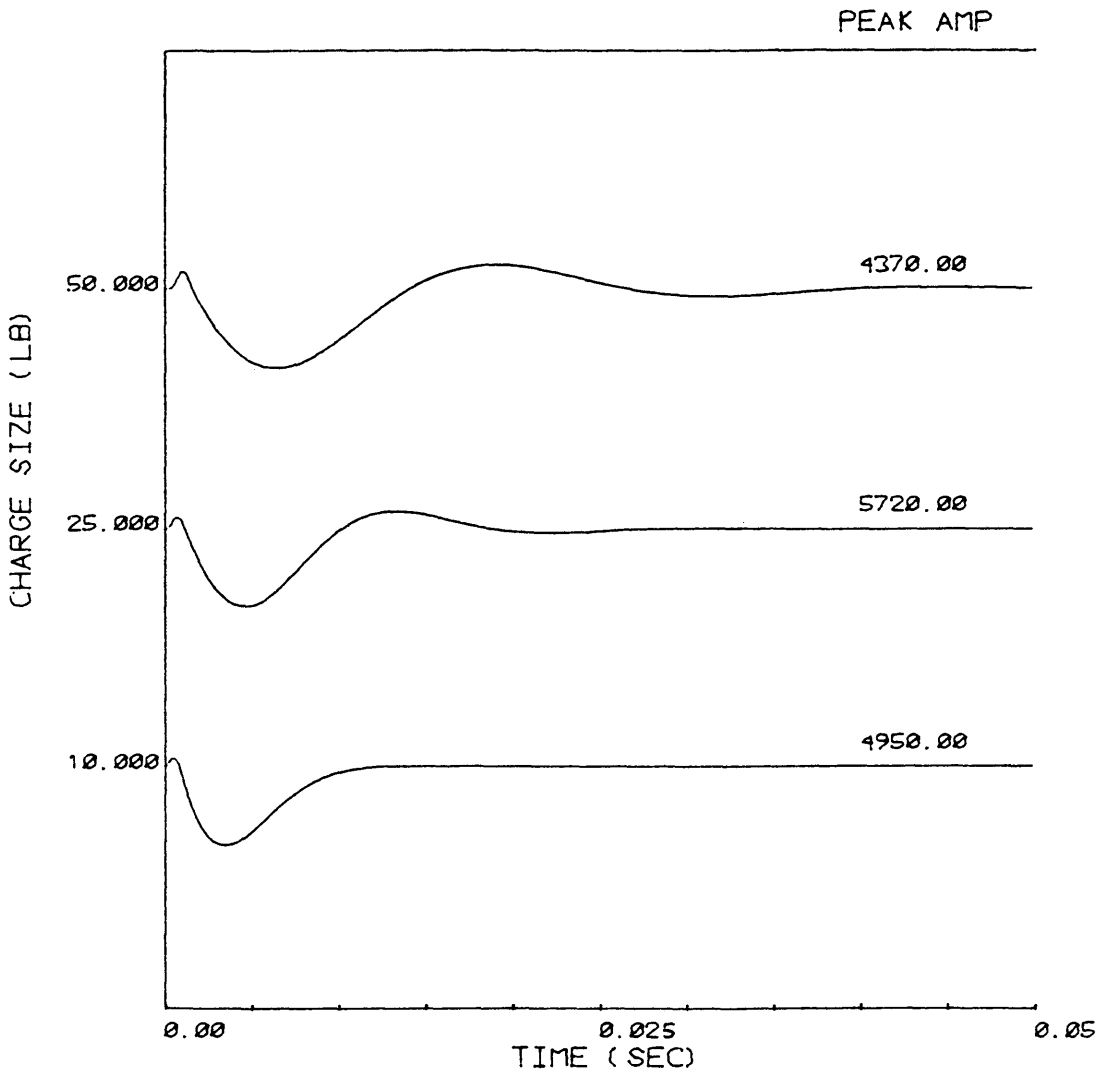

Figure 4-6 Angular normal stress as a function of charge size at R=B in Pierre shale.

Charge size(lb)	P_{rr}(psi)	$-P_{\theta\theta}$(psi)	$\lvert P_{rr}/P_{\theta\theta} \rvert$
10.0	8706	4855	1.80
25.0	9666	5592	1.73
50.0	7462	4242	1.75
			Ave.=1.76

Table 4-2. Corrected radial and angular normal stress in Pierre shale.

From the data in tables 4-1 and 4-2 above we observe dynamically calculated tensile strengths that range from 4000 to 10000 psi in value. These might at first appear as rather large when compared to laboratory obtained "static" tensile strengths. Many experimental techniques designed to calculate dynamic tensile stresses do, however, indicate that these large differences in fact exist. In calculation of Young's modulus, for example, a ratio ranging from 0.85 to 2.9 between dynamically and statically calculated values were measured by the U.S. Bureau of Reclamation (1953) on 20 different rock samples. This was also observed for Poisson's ratio which likewise varied with rate of applied stress. With respect to "strength" of rock in failure, Hawkes (1959) has measured tensile waves due to explosion in a rock core with peak amplitudes three times the static tensile strength without fracturing.

A variety of experimental techniques has been employed to calculate tensile strength of rocks under dynamical stresses. Birkimer (1970) used an "air fired projectile impact loader" to induce high compressive pulses in the specimen and a surface strain gage type system to detect the strain pulse near fracture locations. For cylindrical bars being struck at one end, he presented a "critical normal fracture strain energy" theory which explained the fracture strength of brittle rocks to increase with strain rate of loading to the one third. His experimental data also agreed with this power law relation, as rocks are then expected to be stronger in tension under faster loadings of rock bodies.

In a separate experiment, Clark and Candle (1961) investigated brittle fracture of small beams of rocks under the action of central transverse impact loads. The sources were introduced by either dropping steel balls or firing a no.6 blasting cap on a 1 inch and 2 inch thick supported beams. In order to record the correct times of fracture, strain measurements were taken at the midspan, where strain was at a theoretical maximum. His results indicated a ten-fold increase in dynamic fracture strain for the blasting cap type loadings in hydrostone. This experiment, as was the case previously, therefore suggested that the dynamically

obtained tensile breaking strains to increase with increasing straining rates.

Generally speaking though, calculations for dynamic compressive and tensile strengths are very hard to make in the laboratory. Birkimer (1970), none-the-less, surveyed the literature on comparative static and dynamic strengths of the rocks and his data are shown below:

	Static	Dynamic	
Rock	psi	psi	Ratio
Bedford limestone	600	3900	6.5
Yule Marble (parallel to the bedding)	300	2700	9.0
Yule Marble(perpendicular to the bedding)	900	7000	7.8
Granite	1000	5700	5.7
Taconite	700-1000	13200	13.0

Table 4-3 Comparative tensile strength of rocks (after Birkimer, 1970)

Considering the data presented in table 4-3 a ratio of 6-10 approximately can be assumed for the dynamic to static strengths in sedimentary rocks. In addition, these high values of dynamic tensile strength were not found to be constant and they noticeably depended on the strain rate. So

our calculated values for tensile strengths in Table 4-1 can be assumed to be of reasonable magnitude.

It must be noted that under the obtained high dynamic tensile stresses, earth's vertical lithostatic pressure can be expected to exert minimal effects in rock failure under dynamite loading. The lithostatic or hydrostatic pressure is the pressure exerted at a depth from the weight of overburden of the confining rocks and is simply equal to ρgh where g is the acceleration due to gravity, ρ density, and h the height to the surface. This means that for shallow shots of equal weight, there should not be a great difference in fragmentation and wave propagation for small variations in shot depths.

IV.3 Seismic Scaling Laws

Oftentimes it has been of interest to the geophysicist to obtain various power law relationships between two or more variables as a result of an explosion. Many have investigated the scaling laws between elastic wave parameters such as stress vs. time or distance in both theory and experiment. Here, however, our interest is more confined in the performance parameters of explosives such as scaling between a charge parameter and a wave parameter such as "Amplitude". Three types of scaling relationships have been recognized: 1)energy scaling 2)weight scaling and 3)volume scaling. Each finds its proper application depending on how explosives are used. Volume scaling is, for example, used when one wants to compare the effectiveness of two different explosive types of the same size in a given borehole. Energy scaling is mostly used for large boreholes for lower density explosives.

In our analysis, however, we make the assumption that all rock and explosive parameters are constant. This means that for an energy density of an explosive, energy is proportional to its weight which is directly proportional to its volume. So, as is often the case in seismology, we

choose to investigate various scaling relationships as a function of charge weight.

In most such investigations laws of similtude, or scaling theory, is normally employed to examine the effect of charge weight Q on various parameters of interest. A simple such scaling relationship as was developed by Lampson (1946) for selected quantities of interest is shown in Table 4-4 below. Note that each scaled quantity shown will remain constant at the same scaled time and distance.

Quantity	Symbol	Scaled Quantity
Length	L	$L/Q^{1/3}$
Time	T	$T/Q^{1/3}$
Mass	M	M/Q
Volume	V	V/Q
Energy	E	E/Q
Stress	σ	σ
Strain	ε	ε
Displacement	U	$U/Q^{1/3}$
Velocity	V	V

Table 4-4 Scaling relationships between charge weight and other quantities of interest.

In the scaling relationships above, the effect of

gravity which is only noticeable for "apparent cratering" type of phenomenon is considered to be negligible so that the cube root relationship holds.

As an example of the scaling theory above; in the same rock with constant properties, a 1000 lb charge would give same peak stress at 10 ft from the source as a 1 lb charge at 1 ft. Since linearity is not required, the volume of deformation zone can then be assumed to be proportional to the charge weight Q so that the shattered radius B, should scale as the cube root of charge size. As radius of charge A also varies as the cube root of charge weight, application of the laws of similtude would require that B/A ratio obtained in both theory and experiment to be constant.

Constancy of the B/A ratios under the application of the scaling theory can only be true if the limiting stress at the boundary of rock deformation would be expected to retain a constant value independant of all charges being used. As mentioned before, experiments on rock failure under dynamical conditions indicated that the dynamical tensile breaking strength of rocks shows a noticeable variation with charge size or straining rate of the explosive source. This was well demonstrated in Tables 4-1 and 4-2 and are plotted as a function of charge size in Fig. 4.7 for the former case. As evident from this Figure, the tensile values vary

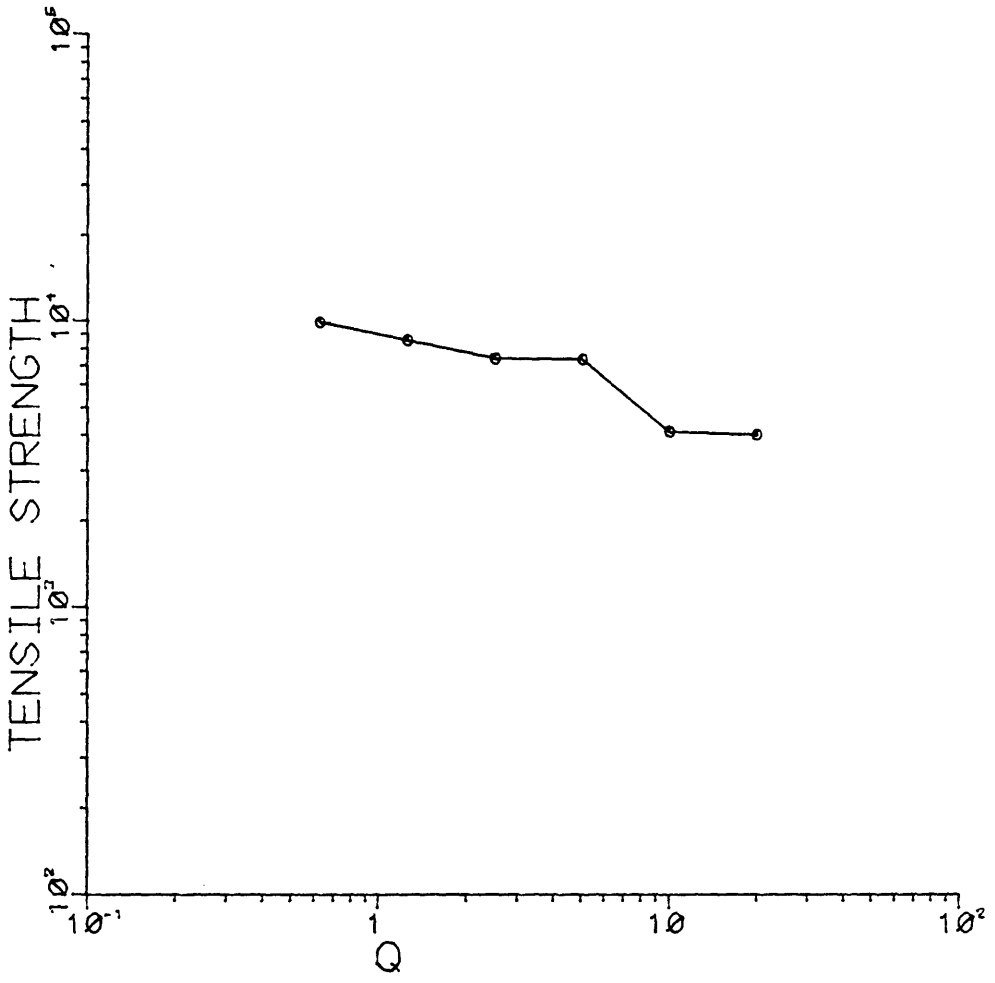

Figure 4-7 Tensile strength as a function of charge size Q in lb. in Taylor marl.

slightly with increasing charge size.

As tensile strengths decreases slightly with larger charges, the deformation radius B is then expected to vary at a larger ratio than a third with charge weight. This was demonstrated in Fig 4.8 where a log-log plot of B vs. Q indicates B to change nearly as $Q^{1/2}$ so that the B/A ratios are expected not to reach a constant value and increase with charge size. We can therefore conclude that a cube root normalization of linear dimensions-as often held necessary due to the laws of similtude-is strictly speaking not correct.

Apparent deviations from the cube root scaling relationships have been observed for gram size charges by D'Andrea et al (1968) and at kiloton ranges by Vortman (1963). It must be noted that defining the limits of the deformation boundary after an explosion is a difficult task since the transition from inelastic to elastic behavior is probably not sharp. But none-the-less the cube root law has been assumed by various authors in the literature.

Another scaling relation of interest has been between peak velocity "amplitude" and charge weight, or finding the exponent n in the relation $A=cQ^n$. Here we define amplitude as the maximum value reached in the velocity waveforms above the zero onset line.

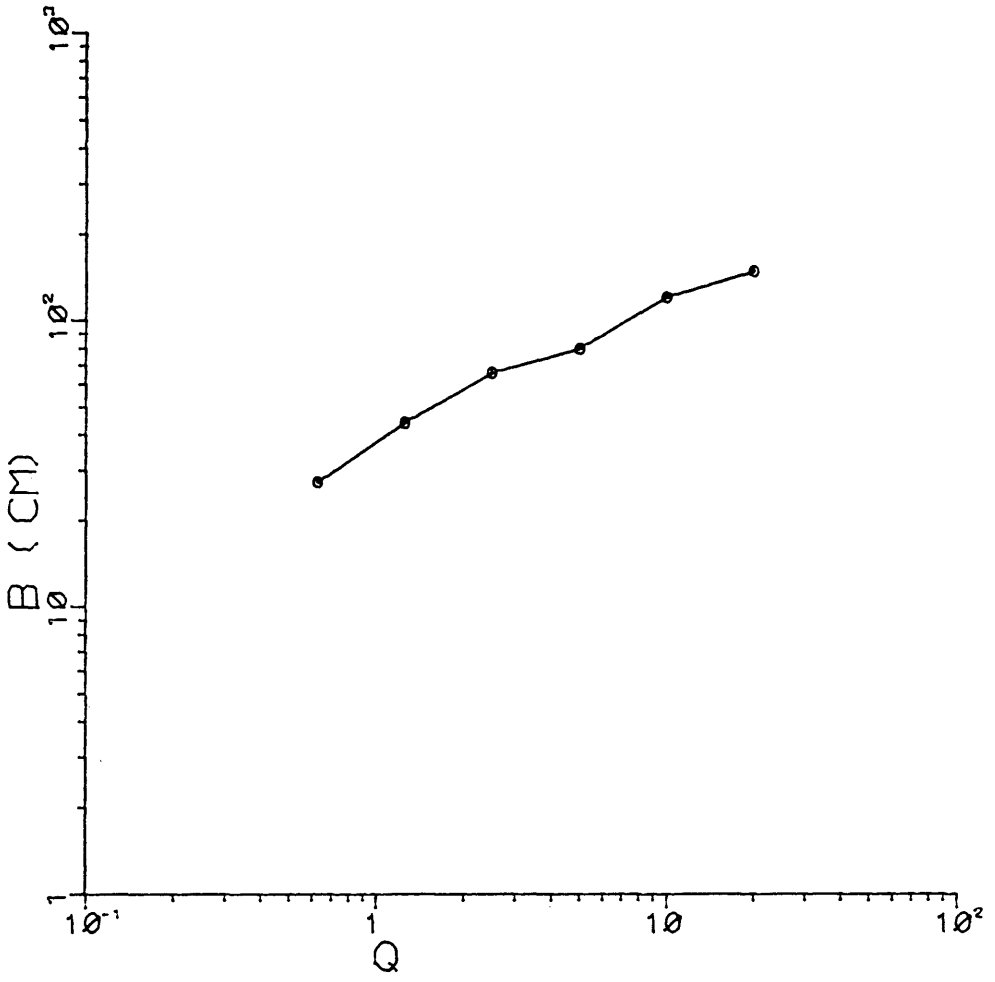

Figure 4-8 Radius of deformation vs. charge size Q (lb) in Taylor marl.

The value for the exponent n has been known to vary considerably from one experiment to another. Where distances of measurement from the source have been relatively large, n generally equals or is slightly larger than 1. This is demonstrated by Gaskell (1956) where he found n in Bunter sandstone to equal 1.18 for refracted velocity waveforms some 20,000 ft from the shots of up to 200 lbs in weight. Latter et al (1959) also observed an almost linear relationship for nucleur charges in kiloton range over a distance of about 180 Km.

Observations closer to the source have yielded different results depending on the size of the charges being used. For shots of up to 100 lbs at 20 ft depth, Blair and Duvall (1954) found n to equal 0.730 ± 0.07 for distances between 25 to 1000 ft. O'Brien (1960) obtained a value closer to 1 or slightly larger for dynamites ranging between 2.5 to 300 lb in weight. Habberjam and Whetton (1952) also found n equal to 0.88 for 4-198 lb charges. Only Peet (1960) reasoned the exponent n to change depending on charge weight which, in his data, was reduced from 4/3-for larger charges- to about 1/3 in the smaller charge end.

Despite of the wide range in the value of n, energy considerations would at first suggest a simple square root relationship between amplitude and Q. If one equates the

square of amplitude of ground velocity with intensity, laws of similtude of Table 4-4 would then require energy to be proportional to charge weight or amplitude to vary as a square root of Q. But this can only be permissible for a pure sinusoidal type wave and not a pulse type wavelet where a frequency spectrum is observed.

A closer look at the theoretical curves for velocity in Taylor marl strongly suggested a larger change in amplitude response at lower portions of the frequency spectrum with peak amplitudes shifting to lower frequencies for larger charges. Since the attenuation characteristics of earth and our recording system can be considered as a low pass filter, most of the high frequencies emitted by smaller charges are expected to be cut by the action of earth filtering. The lower portions of the spectrum of these small charges can therefore show a comparatively larger relation with charge weight with n higher than 1. Larger charges, on the other hand, produce a spectrum which more fully falls within the band pass of our equivalent "earth filter" (Peet, 1960) and the exponent n is therefore expected to generally be reduced to a value less than 1. This hypothesis is well observed for the theoretcal peak amplitudes in Fig.4-9, where the initial n of 1.5 is reduced to about 0.5 for larger charges.

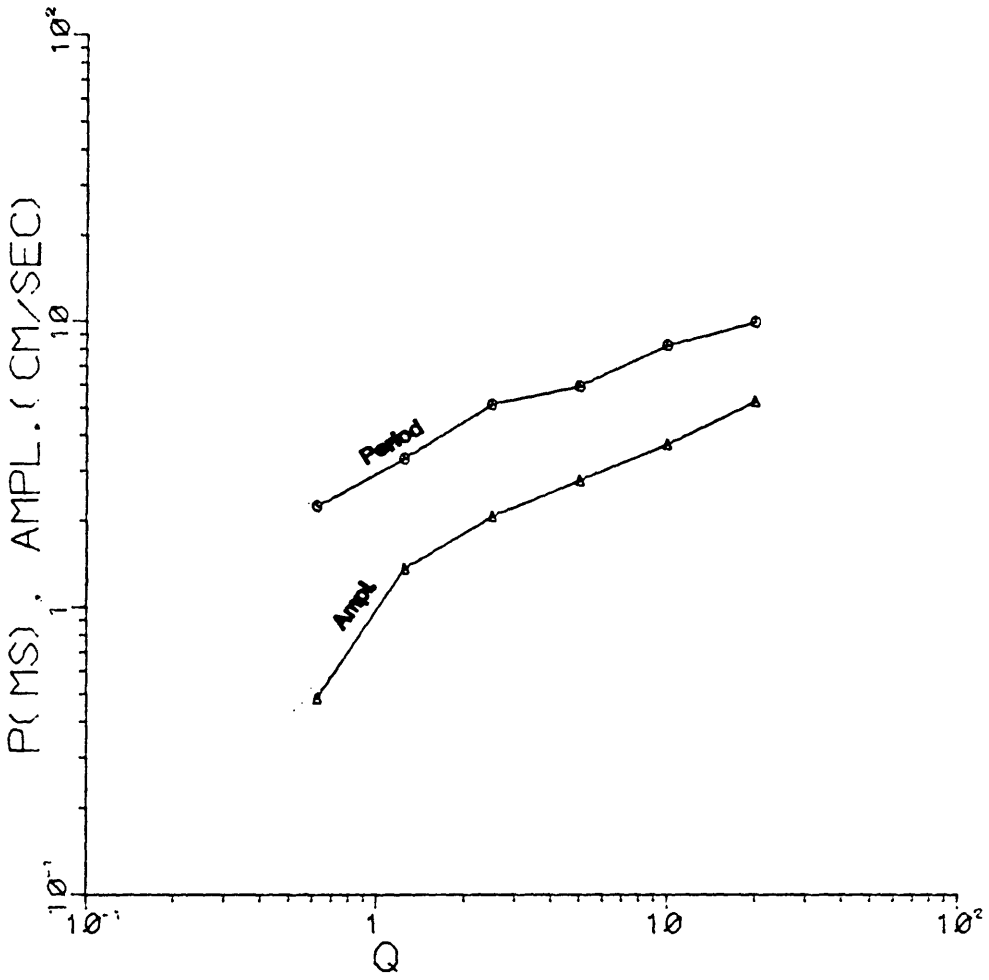

Figure 4-9 Amplitude vs. charge size Q (lb) in the Taylor marl for the faster decaying source.

In the time domain, the measured field waveforms can be considered as a convolution of the initial seismic wavelet with the time domain equivalent window of the combined earth and recording instrument filter responses. For smaller charges, with the time duration of the pulse being less than or about the same as the window, the pulse is usually contaminated by the earth filtering and total period of the pulse is slightly increased from its real value. If we define "Period" as the length in time between the initial onset and the second zero crossing from it, we expect a power relationship between period and Q with the exponent n being reduced to a limiting 1/3 value for the ideal case in the scaling theory. Fig. 4-9 shows this relationship between period P in MS and Q as a change in slope from 0.6 to 0.4 is observed with increasing charge sizes.

As a reminder, the presented scaling relationship were obtained from application of the faster decaying source in Taylor Marl. Amplitude scaling relationships for the slow decaying source shown in Fig. 4-10, however, indicates a more linear relationship between amplitude and charge size with again the exponent n decreasing with larger charges.

Finally, it must perhaps be noted that the scaling relationships (if they exist) in themselves can not be used

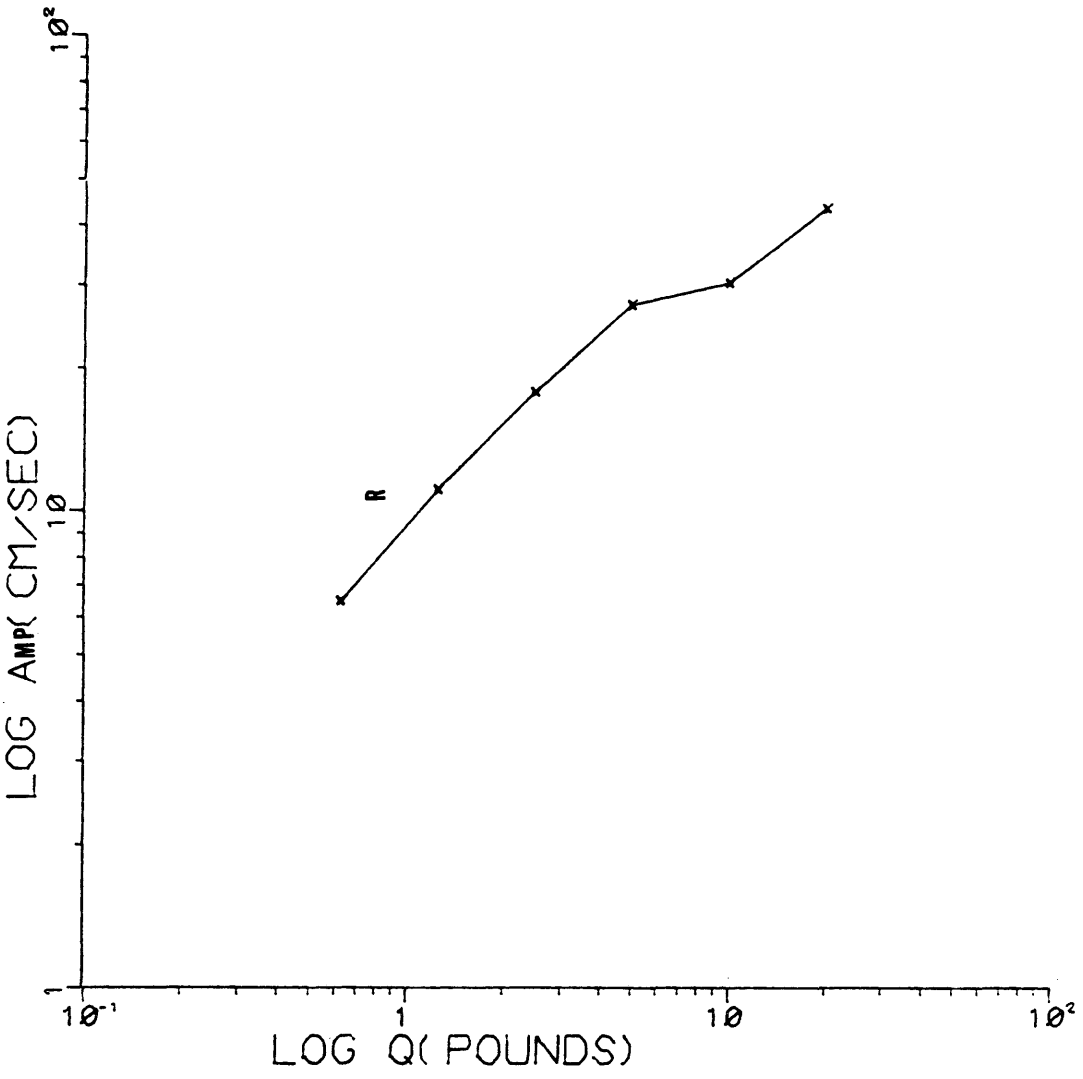

Figure 4-10 Amplitude vs. charge size Q (lb) in the Taylor marl for the slow decaying source.

to predict functional relationship between the variables, such as variations of stress with time or distance, and only can be used to predict the value of a scaled quantity at a scaled distance or time, independant of the charge size.

V. CONCLUSIONS

Based on the analysis thus presented, a few conclusions regarding the model and its applications can be drawn, which are as follows:

1-A better model is presented in predicting the shape and form of the primary seismic wavelet from a dynamite charge than that previously proposed in the literature. Theoretical differences in shape and properties of the seismic pulse in changing geological environments confirmed field observations.

2-The model incorporates a visco-elastic liquid in the problem as the damping mechanism for the loss of energy that occurs as a result of rock fracturing around an explosive source. The physical size of this boundary, as predicted from the theory and obtained from wavelet matching, is found to be reasonable.

3-The shape of the frequency response more closely follow the field data than a Sharpe (1942) type of model, with a shift of maximum peak amplitude to lower frequencies as a result of increasing charge size. A more pronounced functional relationship between amplitude and charge size is evident in the lower part of the frequency spectrum than

high.

4-The model can find various applications in rock mechanics, including a prediction of shape and properties of the emitted stress wave at the boundary of rock deformation. The limiting tensile breaking strength values thus obtained reasonably agreed with the experimental data.

5-In agreement with recent experimental findings, the model predicts the dynamic tensile strength of rocks to vary with size of the charge or the duration of the tensile stress. This is contrary to the assumption made in obtaining various scaling laws in the literature in which a simple cube root relationship between the radius of the "shattered" zone B and charge size is implied. Theoretically obtained scaling relationships are in agreement with the hypothesis forwarded above, and in the case of "amplitude" scaling to that of the latter part of conclusion 3.

REFERENCES

Atchison, T.C., 1968, Fragmentation principles: In Surface Mining, E P. Pfleider Ed., Mudd Series, AIME, pp.355-372.

Atchison, T.C., Duvall, W.I. and Pugliese, J.M., 1964, Effects of decoupling on explosion-generated Strain pulses in rocks: Bureau of Mines Report of Investigation 6333:49.

Birkimer, D.L., 1970, A possible criterion for the dynamic tensile strength of rocks: in Dynamic Rock Mechanics, Proceedings, AIME, Twelfth Symposium on rock mechanics, George B. Clark editor, University of Missouri, pp. 573-590.

Blair, B.E. and Duvall, W.I., 1954, Evaluation of gauges for measuring displacement, velocity and acceleration of seismic pulses: U.S. Bureau of Mines Report of Investigation, 5073. (Washington U.S.A.)

Blake, F.G., 1952, Spherical wave propagation in solid medium: J. Acoustical Society of America, v. 24, pp. 211-215.

Born, W.T., 1941, The attenuation constant of the earth materials: Geophysics, v. 6, pp. 137-148.

Brigham, O.E., 1974, The Fast Fourier Transform: Prentice-Hall, Inc., New Jersey, 252 pp.

Cherry, J.T., 1967, Computer calculations of explosion produced craters: International Journal of Rock Mechanics and Mining Sciences, v. 4, no. 1, pp. 1-22.

Claerbout, J.F., 1976, Fundamentals of Geophysical Data Processing with Applications to Petroleum Prospecting: McGraw-Hill, New York.

Clark, G.B., 1952, Propagation of small shock waves from a spherical cavity in an infinitely isotropic elastic medium: Ph.D Thesis, University of Illinois.

Clark, G.B., 1966, Blasting and dynamic rock mechanics,

Proceedings, AIME, 8 Symposium on Rock Mechanics, University of Minnesota, Minneapolis, Minnesota, pp.463-499.

Clark, G.B., 1968, Explosions: In Surface Mining, E.P. Pfleider Ed., Mudd Series, AIME, pp. 341-354.

Clark, G.B. and Caudle, R.D., 1961, Brittle fracture of small short rock beams under central transverse impact loading: Mining Engineering Series, Proceedings, Fourth Symposium on Rock Mechanics, The Pennsylvania State University, pp. 137-141.

Cole, R.H., 1948, Underwater Explosions: Princeton University Press, Princeton, New Jersey.

Collins, F., 1960, Plane compressional Voigt waves: Geophysics, v. 25, pp. 483-492.

Cook, M.A., 1974, The Science of Industrial Explosives: R.E. Krieger Publishing Company, Huntington, New York, 11743

D'Andrea, D.V., Fischer, R.L. and Fogelson, D.E., 1968, An investigation of crator scaling for small charges: Bureau of Mines RI,

da Gamma, C.D., Nelson, C.R., 1970, The formation of radial cracks in rock blasting analyzed in terms of modified Griffith's theory: Dynamic Rock Mechanics, Proceedings, AIME, Twelfth Symposium on rock mechanics, University of Missouri, Rolla, Missouri, pp. 517-528.

Duvall, W.I., 1953, Strain wave shapes in rocks near explosions: Geophysics, v. 18, pp. 310-323.

Duvall, W.I. and Atchison, T.C., 1957, Rock breakage by explosives: U.S. Bureau of Mines, Report of Investigation 5356, Government printing office, Washington, U.S.A.

Ewing, W.M., Jardetzky, W.S. and Press, F., 1957, Elastic Waves in Layered Media: McGraw-Hill, New York, N.Y., 380 pp.

Habberjam, G.H. and Whetton, J.T., 1952, On the relationship

between seismic amplitude and charge of explosive fired in routine blasting operations: Geophysics, 17 (1), pp. 116-128.

Hadsell, F.A., 1982, Class notes for CSM course GP 501: Golden, Colorado School of Mines, unpublished manuscript.

Hawkes, I.,1959, Stress Waves in Rocks: Colliery Engineering, v. 36, no. 423, p. 186.

Heelan, P.A.. 1953, Radiation from a cylindrical source of finite length: Geophysics, 18, pp. 685-696.

Hino, K., 1959, Theory and Practice in Blasting: Nippon Kayaha Co., Asa, Yama Guchi-Ken, Japan.

Janak, P.M., 1982, A comparison and analysis of seismic land source energy relationships and radiation patterns: Colorado School of Mines, M.Sc. Thesis #T-2588.

Knopoff, L., 1956, The seismic pulse in materials possessing solid friction, I. Plane Waves: Bulletin of Geol. Soc. of Am., v. 46, pp. 175-183.

Lampson, C.W., 1946, Final report on effects of underground explosions: Division 2, National Defense Research Committee of the Office of Scientific Research and Development of U.S.A., N.R.D.C. Report A-479.

Latter, A.L., Martinelli, E.A. and Teller, E., 1959, Seismic scaling laws for underground explosions: Physics of Fluids, v. 2, no. 3, pp. 280-282.

Lee, T.M., 1964, Spherical waves in visco-elastic media: J. Acoustic society of America, v. 36, no. 12, pp.2402-2407.

McDonal, F.J., Angona, F.A., Mills, R.L., Sengbush, R.L., Van Nostrand, R.G. and White, J.E., 1958, Attenuation of shear and compressional waves in Pierre shale: Geophysics, v. 23, pp. 421-439.

McReady, H.J., 1940, Shothole characteristics in reflection seismology: Geophysics, v. 5, pp. 374, 379-381.

Nash, H.E., Martin, J.M., 1936, Significance of some

fundamental properties of explosives, with special reference to geophysical prospectings, Geophysics, V. 1, no. 2, pp. 239-251.

O'Brien, P.N.S., 1960, Seismic energy from explosions: Geophysics, v. 3, pp. 29-44.

O'Brien, P.N.S., 1969, Some experiments concerning the primary seismic pulse: Geophysical Prospecting, v. 17, pp. 511-547.

Oppenheim A.V., Schafer, R.W., 1975, Digital Signal Processing: Prentice-Hall, New Jersey, 585 pp.

Otuonye, F.O., Skidmore, D.R., Konya, C.J., 1983, Measurements and predictions of borehole pressure variations in model blasting systems: First International Symposium on Rock Fragmentaion by Blasting, v. 1, Lulea, Sweden, pp.7-20.

Papoulis, A., 1962, The Fourier Integral and its Applications: McGraw-Hill, New York, 318 pp.

Peet, W.E., 1960, A shock wave theory for the generation of the seismic signal around a spherical shothole: Geophysical Prospecting, v. 17, pp. 509-533.

Ricker, N., 1940, The form and nature of seismic waves and the structure of seismograms: Geophysics, v. 5, pp. 348-366.

Ricker, N., 1951, The form and laws of propagation of seismic wavelets: Proc. 3rd World Petroleum Congress, Section I, pp. 514-536.

Sengbush, R.L., 1978, Modern Seismic Exploration: Pexcon International, Houston, Texas, 318 pp.

Sharpe, J.A., 1942, The production of elastic waves by explosion pressures, parts I and II: Geophysics, v. 7, pp. 144-154, 311-321.

Sheriff, R.E., 1975, Factors affecting seismic amplitudes: Geophysical Prospecting, v. 23, pp. 125-138.

Short, N.M., 1961, Fracturing of rock salt by a contained high explosive: Proceedings of the Tenth Annual

Drilling and Blasting Symposium, Colorado School of Mines Quarterly, v. 56, no. 1, pp. 221-257.

Sixta, D.P., 1982, Comparison and analysis of downgoing waveforms from land seismic sources: M.Sc. thesis, Geophysics Department, Colorado Scool of Mines, Golden, Colorado.

Sokolnikoff, I.S., 1983, Mathematical Theory of Elasticity: R.E. Krieger Publishing Company, Inc., Malabar, Florida, Reprint Edition, 476 pp.

Stokes, G.G., 1845, Transactions Cambridge Phil. Soc., V. 8, Part III, PP. 287, 319.

U.S. Bureau of Reclamation, 1953, Physical properties of some typical foundation rocks: U.S. Bur. of Reclamation Concrete Lab. Report., No. SP-39, 50 pp.

White, J.E., 1982, Personal communication.

White, J.E., 1983, Underground Sound: Application of Seismic Waves: Elsevier, New York, NY, 253 pp.

APPENDIX A

INTRODUCTION TO VISCO-ELASTICITY

Since the zone of deformation around the spherical cavity is hypothesized as a visco-elastic liquid, here we proceed with a brief introduction to visco-elastic behavior.

A visco-elastic or Voigt solid is a medium where stress is both proportional to strain (as a linear Hookean solid) and strain rate

$$\tau_{ij} = C_{ijk\ell}\, \varepsilon_{k\ell} + C'_{ijk\ell}\, \dot{\varepsilon}_{k\ell} \tag{A-1}$$

where τ_{ij} is the stress tensor, C's represent proportionality-constants and $\varepsilon_{k\ell}$ and $\dot{\varepsilon}_{k\ell}$ are strain and strain rate tensors respectively. Since not all the 81 components of the C matrices are independent here we adopt the compacted version of (A-1) (Sokolnikoff, 1983), as

$$\tau_{\alpha} = C_{\alpha\beta}\varepsilon_{\beta} + C'_{\alpha\beta}\, \dot{\varepsilon}_{\beta} \tag{A-2}$$

where $C_{\alpha\beta}$ contains 36 independent components. In writing (A-2) we make use of the following notation below

$$\tau_{11} = \tau_1 \quad \tau_{22} = \tau_2 \quad \tau_{33} = \tau_3 \quad \tau_{23} = \tau_4 \quad \tau_{31} = \tau_5 \quad \tau_{12} = \tau_6 \tag{A-3}$$

$$\varepsilon_{11} = \varepsilon_1 \quad \varepsilon_{22} = \varepsilon_2 \quad \varepsilon_{33} = \varepsilon_3 \quad 2\varepsilon_{23} = \varepsilon_4 \quad 2\varepsilon_{31} = \varepsilon_5 \quad 2\varepsilon_{12} = \varepsilon_6$$

For a homogeneous isotropic medium, we only have two independent constants commonly known as Lame's coefficients λ and μ. Matrix $C_{\alpha\beta}$ then takes the form

$$C_{\alpha\beta} = \begin{pmatrix} \lambda+2\mu & \lambda & \lambda & 0 & 0 & 0 \\ \lambda & \lambda+2\mu & \lambda & 0 & 0 & 0 \\ \lambda & \lambda & \lambda+2\mu & 0 & 0 & 0 \\ 0 & 0 & 0 & \mu & 0 & 0 \\ 0 & 0 & 0 & 0 & \mu & 0 \\ 0 & 0 & 0 & 0 & 0 & \mu \end{pmatrix} \tag{A-4}$$

Sinilarly $C'_{\alpha\beta}$ in (A-2) is the primed matrix version of (A-4). Hooke's law for a homogeneous isotropic visco-elastic medium thus becomes

$$\tau_{ij} = (\lambda\theta\delta_{ij} + 2\mu\varepsilon_{ij}) + (\lambda' \dot{\theta} \delta_{ij} + 2\mu' \dot{\varepsilon}_{ij}) \tag{A-5}$$

where θ is dilatation given by

$$\theta = \varepsilon_{11} + \varepsilon_{22} + \varepsilon_{33} \tag{A-6}$$

With the assumption of radial symmetry, we write (A-5) as

$$\tau_{11} = \theta(\lambda + \frac{2}{3}\mu) + \dot{\theta}(\lambda' + \frac{2}{3}\mu') \tag{A-7}$$

Due to the assumed radial symmetry, tangential straius become zero so that

$$\tau_{12} = 2\mu\varepsilon_{12} + 2\mu' \dot{\varepsilon}_{12} = 0 \tag{A-8}$$

In general, four constant λ, λ', μ and μ' are required to completely specify a Voigt solid, but many authors take some simplifying assumptions. Recognizing bulk modulus k in (A-7) as

$$\lambda + \frac{2}{3}\mu = k$$

$$\lambda' + \frac{2}{3}\mu' = k' \tag{A-9}$$

we can associate the compressibility k with k' in (A-7) and μ with μ' in (A-8). For a liquid with no rigidity (μ=0) (A-8) becomes

$$\tau_{12} = 2\mu' \dot{\varepsilon}_{12} = 0 \tag{A-10}$$

It is known from fluid mechanics that for a moving fluid, the general equation involving shear stress S_{ij} can be written as

$$S_{ij} = \eta(v_{i,j} + v_{j,i}) \tag{A-11}$$

where v is the velocity of flow, η is viscosity and comma implies covarient differentiation. Comparing (A-10) and (A-11) and recognizing definition of strain in terms of displacements u_i

$$\varepsilon_{ij} = \frac{1}{2}(u_{i,j} + u_{j,i}) \tag{A-12}$$

We see that μ' represents nothing but ordinary viscosity in shear for a viscous liquid. In our case, however, we have assumed no shear strains so that value of viscosity in shear does not contribute to any losses.

It has been recognized for some time that in addition to the viscous flow in shear, another type of flow also occurs when the volume changes upon compression or decompression. This is deformation involving dilatation as opposed to shear and is known as dilatational viscosity $k' (=\lambda' + \frac{2}{3}\mu')$ (Kolsky, 1963). This dilatation or bulk viscosity is a measure of the time lag, associated with fitting the constituent atoms of a compressible liquid structure closer together and thus filling the free column under compression. Occasionally, it is referred to as the second coefficient of viscosity.

Some workers took this dilatational viscosity to be zero (Skokes, 1845; Ewing, Jardetsky and Press, 1957) and thus

$$\lambda' = -\frac{2}{3}\mu'$$

leaving only the single constant μ' to account for shear viscosity. The assumption that dilatational viscosity is negligible compared to shear viscosity is only justifiable for rubber-like materials, as argued by Kolsky (1963) and not true in general.

In this thesis, we took a different simplifying assumption, that $\lambda' = 0$; so here the dilatational viscosity becomes 2/3 of the shear viscosity and it solely accounts for the loss of energy in our model.

The Stokes Wave Equation (Ricker, 1977)

In deriving the wave equation for a Voigt medium, we start with the classical wave equation

$$(k + \frac{4}{3}\mu)\ \nabla^2\phi = \rho\ \frac{\partial^2\phi}{\partial t^2} \tag{A-13}$$

and, for dilatational waves, perform the following replacements in (A-13)

$$k \text{ by } k+k'\ \frac{\partial}{\partial t}\ ,\ \mu \text{ by } \mu + \eta\frac{\partial}{\partial t} \tag{A-14}$$

we then have

$$(k + \frac{4}{3}\mu)\ \nabla^2\phi + (k' + \frac{4}{3}\eta)\ \ \frac{\partial}{\partial t}\ \nabla^2\phi = \rho\ \frac{\partial^2\phi}{\partial t^2} \tag{A-15}$$

or

$$\nabla^2(\phi + \frac{k' + 4/3\eta}{\rho c^2}\ \frac{\partial\phi}{\partial t}) = \frac{1}{c^2}\ \frac{\partial^2\phi}{\partial t^2} \tag{A-16}$$

where c is the compressional wave velocity given by

$$c^2 = \frac{k + 4/3\mu}{\rho}\ . \tag{A-17}$$

If we now define ω_o as

$$\frac{1}{\omega_o} = \frac{k' + 4/3\eta}{\rho c^2} = \frac{\lambda' + 2\eta}{\lambda + 2\mu} \tag{A-18}$$

The wave equation (A-16) becomes

$$\nabla^2(\phi + \frac{1}{\omega_o}\ \frac{\partial\phi}{\partial t}) = \frac{1}{c^2}\ \frac{\partial^2\phi}{\partial t^2} \tag{A-19}$$

where for spherical waves we have:

$$\frac{\partial^2}{\partial r^2}\left[r\phi + \frac{1}{\omega_o}\frac{\partial(r\phi)}{\partial t}\right] = \frac{1}{c^2}\frac{\partial^2}{\partial t^2}(r\phi) \qquad \text{(A-20)}$$

as is used in the text.

Appendix B. User's Manual for the computer programs.

The computer program CONSTANT as used in this thesis is listed in Appendix C. The program is written in the FORTRAN code to initially run on the CDC Cyber computer model 720 of the Geophysics department of the Colorado School of Mines. It was later modified to also accomodate CSM'S Digital Equipment Corporation DEC-10 computer. The program listing in Appendix C runs on the DEC-10.

To execute the main program, the user needs to create an input file called FOR01.DAT on the DEC-10 (or TAPE1 on Cyber). The data on the FOR01.DAT is in free format and in the following order:

Line 1: DENSE

Line 2: XC2, XC2S, RHO

Line 3: ALFA

Line 4: DELTAF, KFREQ

Line 5: WGHT, FACTOR, XMU1P

where all these data are real except KFREQ which is an integer as described below:

DENSE : The dynamite charge density in grm/cm^3

XC2 : The compressional wave velocity of the outside medium in cm/sec.

XC2S The shear wave velocity of the outside medium in cm/sec.

RHO The density of the outside medium in gr/cm^3.

ALFA : The source'a time constant in sec^{-1}.

DELTAF : Sampling interval in the Frequency domain

KFREQ : Number of points in the frequency domain up to window's cut-off frequency.

WGHT : The weight of the charge in lb.

FACTOR : The B/A factor being used.

XMU1P : The visco-elastic fluid viscosity in cP.

The program is designed to calculate particle velocity (in cm/sec) at a specified distance from the source as used in the program. The plots in this thesis were obtained from a distance of 50 meters (R=5000). The program can also compute the radial and angular normal components of stress (in dyn/cm^2) at the deformation boundary B. In this case, therefore, R must be put equal to B. The computed transient waveforms will be written on FOR02.DAT and the amplitude spectra will be on files FOR16.DAT up to FOR21.DAT

if 6 transient waveform are, for example, desired. The transient waveforms were ploted by the program DPLOT.EXT modified from Shiao and the frequency spectra were plotted using available softwsre program on DEC-10 called GRAPH. As described in this thesis, a half cycle sinc function is used for the truncation of our digitized data except for the case of the Pierre shale where a digitized form of the DFS-V type of windowing was entered in the program by a file called FOR11.DAT.

The computer program consisted of a main program and two subroutines as follows:

Program	Description
CONST	Main program to compute transient waveforms (particle velocity or two components of stress) and asoociated amplitude spectra in an homogeneous, infinitely extended isotropic elastic medium.
FOURIER	Subroutine to fill a matrix with the Fourier coefficient and then call FORK to do the FFT.
FORK	Subroutine to perform the FFT.

```
EXAMPLE INPUT DATA
FOR THE CALCULATION
OF PARTICLE VELOCITY
IN TAYLOR MARL.
1.25
2.44E05,1.0E05,2.16
600.
5.,280
0.625,7.18,26800.
1.25,9.2,20400.
2.5,10.9,16800.
5.0,10.5,18900.
10.0,12.6,27500.
20.0,12.5,27500.
```

```
C       MAIN PROGRAM TO COMPUTE THE COMPLEX COEFFICIENT
C       (C) OF AN OUTGOING SPHERICAL WAVE FROM A RADIALLY
C       OSCILLATING SPHERICAL CAVITY IN AN INFINITELY
C       EXTENDED SOLID MEDIUM. THIS COEFFICIENT ENABLE
C       US TO CALCULATE PARTICLE VELOCITY OR RADIAL OR
C       ANGULAR NORMAL COMPONENTS OF STRESS AT A
C       SPECFIED DISTANCE FROM THE SOURCE FOR EACH
C       VALUE OF FREQUENCY. THE FOURIER COEFFICIENTS
C       WERE THEN TRANSFORMED INTO THE TIME DOMAIN IN
C       IN ORDER TO OBTAIN THE TRANSIENT WAVEFORMS BY
C       USING A MODIFIED FAST FOURIER TRANSFORM (FFT)
C       ALGORITHM DEVELOPED BY CLAERBOUT (1976).
C
C
C       PROGRAM IS WRITTEN BY FARROKH JALINOOS.
C       JANUARY, 1983; MODIFIED MARCH 1984.
C
C          THE MODEL USED IN THE PROGRAM CONSISTS OF A
C          SPHERICAL CAVITY BOUNDED BY A VISCOUS LIQUID
C          OF VISCO-ELASTIC RHEOLOGY EMBEDDED IN AN
C          INFINITELY EXTENDED ELASTIC MEDIUM.
C
C              INPUT IS WRTTEN ON TAPE1 IF CYBER COMPUTER
C              IS IN USE OR FOR01.DAT IN CASE OF DEC-10.
C
C              TRANSIENT WAVE OUPUTS WILL BE WRITTEN ON
C              FOR02.DAT AND AMPLITUDE RESPONSE DATA ON
C              FOR16.DAT UP TO FOR21.DAT.
C
C       CGS SYSTEM OF UNITS IS USED IN ALL CALCULATIONS.
C
C
              IMPLICIT COMPLEX(C)
              COMPLEX XX,YY,ZZ,AA,BB,QQ
              COMPLEX BETA,ZTETA,XM,GAMMA
              COMPLEX PW,CEXP
           IMPLICIT COMPLEX(C)
           COMPLEX XX,YY,ZZ,AA,BB,QQ      AM2P,GAM3P
           COMPLEX BETA,ZTETA,XM,GAMMA(7,280),BMC1(7,280)
           COMPLEX PW,CEXP
              DIMENSION AC2(1024),AMC2(7,280),BMC2(7,280)
              DIMENSION AC3(1024),AMC3(7,280),BMC3(7,280)
              DIMENSION X(1024),AMP1(280),XAX(280)
              COMMON/CONST/PI,DELW,DELTAT
   22   FORMAT(2E14.3)
33       FORMAT(E14.3)
*
*          READ THE INPUT PARAMETERS FROM FILE TAPE1
*
C
C       READ IN THE CHARGE MIXTURE DENSITY IN
C       GRM/CM**3
C
        READ(1,*) DENSE
C
C       READ COMPRESSIONAL WAVE VELOCITY XC2, SHEAR
C       WAVE VELOCITY XC2S IN CM/SEC AND DENSITY
C       RHO IN GR/CM**3
C
        READ(1,*) XC2,XC2S,RHO
```

```
C
CC       CALCULATE LAME'S COEFFICIENTS LANDA
C      (COEFFICIENT OF DILEIATION) AND MU (SHEAR
C      MODULUS) FOR VARIOUS MODELS WHERE X (AS IN XLAN1,
C
C      FOR EXAMPLE) ENSURES A REAL VALUE FOR THE
C       COEFFICIENTS. P REFERS TO PRIME
C       AS IS DEFINED IN THE MODEL.
C
C       NOTE THAT XLAN1P AND XMU1 ARE ZERO.
C
        XMU2=(XC2S**2)*RHO
        XLAN2=(XC2**2)*RHO-2*XMU2
        XC1=(XLAN2/RHO)**0.5
        XLAN1=XLAN2
C
CC       CALCULATE PLANE WAVE MODULUS. SAME
C        CONVENTION AS ABOVE IS USED.
C
        XM2=XLAN2+2.*XMU2
C
CC          READ THE SOURCING FUNCTION'S DECAY CONSTANT,
C           ALFA.
C
        READ(1,*) ALFA
C
CC       READ DELTAF, THE SAMPLING INTERVAL IN FREQUENCY
C        DOMAIN AND KFREQ, THE CORRESPONDING NUMBER OF
C        POINTS UP TO WINDOW'S CUT-OFF FREQUENCY.
C
        READ(1,*) DELTAF,KFREQ
        DELTAT=1./(1024.*DELTAF)
        PI=ATAN(1.)*4.
        DELW=2*PI*DELTAF
C
CC      CALCULATE CONSTANTS USED IN THE ATTENUATION
C       EQUATIONS BELOW.
C
        TETAP=0.031
        OMEO=16000.*PI
C
CC       START A LOOP FOR CALCULATION OF
C        N TRANSIENT WAVEFORMS AS A FUNCTION
C        OF THE VARIABLE OF INTEREST.
C
        NN=1
        DO  700  N=1,6
C
CC         READ IN CHARGE WEIGHT IN LB, B/A FACTOR
C          AND VISCOSITY IN CP. NOTE THAT
C          FEW VARIABLES ARE TO PRINTED OUT ON
C          THE TERMINAL TO SERVE AS A MEANS OF
C          CHECKING THE PROGRAM.
C
        READ(1,*) WGHT,FACTOR,XMU1P
C
        WRITE (4,*) WGHT
        WGHT=WGHT*4.448505
```

```
      POWER=1./3.
      A=(3*WGHT/(4*PI*DENSE*980.))**(POWER)
       WRITE (4,*) A,FACTOR,XMU1P,ALFA
      B=A*FACTOR
C
CCC    R DENOTES THE RADIAL DISTANCE FROM
CCC    THE SOURCE. NOTE THAT FOR NORMAL STRESS
CCC    CALCULATIONS R=B
C
      R=5000.
       WRITE (4,*) FACTOR
      WZERO=XLAN1/(2*XMU1P)
C
CCC   START A LOOP FOR CALCULATING FREQUENCY VALUES
CCC   UP TO KFREQ. DELW IS THE FREQUENCY INCREMENT
CCC   THAT IS TO BE CALCULATED.
C
   66 DO 500   I=1,KFREQ
      W=I*DELW
C
CCC    CALCULATE THE VISCOUS LIQUID'S ATTENUATION
CCC    VALUE A1 AS USED IN THE CALCULATIONS.
C
      A1=W**2/(WZERO*2*XC1)
C
CCC       CALCULATE THE FORCING FUNCTION P(W). NOTE
CCC       THAT IF RADIAL OR ANGULAR STRESS IS THE
CCC       OUTPUT A DIFFERENT FORCING FUNCTION OF
CCC       THE FORM:
CCC            PW=1./CMPLX(ALFA,W)
CCC        MUST BE USED.
C
      CPW=CMPLX(0.,W)
      CCPW=CMPLX(ALFA,W)
      PW=CPW/CCPW
C
CCC    MULTIPLY P(W) BY P0, THE DYNAMITE'S
C      DETONATION PRESSURE (IN DYNES/CM**2)
C
      PW=PW*(2.12E09)
C
CCC       CALCULATE THE VALUES OF HALF CYCLE SINC
C         FUNCTION USED AS OUR TRUNCATING WINDOW.
C
      WM=2*PI*1400.
      FF=(PI*W)/WM
      WINDOW=SIN(FF)/FF
C
CCC       CALCULATE THE COMPLEX VALUES K1,K2,BETTA
CCC       AND GAMMA WHICH WERE THE DEFINED VALUES
C         USED FOR SOLVING THE BOUNDARY CON-
C
C         DITION IN THE PROBLEM.
C
      D=W**2*XMU1P
      E=W*XMU1P
      F=W/XC2
      G=W/XC1
```

```
*-----------ANGULAR NORMAL STRESS
*
38       CCU1=-C1*(-2*XMU2/R**3-2*CK2*XMU2/R**2
     *+XLAM2*CK2**2/R)*CEXP(-CK2*R)
         CCU1=CCU1*PW

69       AMC1(N,I)=REAL(CCU1)
         BMC1(N,I)=AIMAG(CCU1)
         AMP1(I)=(AMC1(N,I)**2+BMC1(N,I)**2)**0.5
79       XAX(I)=W/(2.*PI)
C              IF ANY OTHER FORM OF TRUNCATION
C              OTHER THAN THE HALF CYCLE SINC
C              FUNCTION IS DESIRED, DO THE FOOLWING:
C    1- TURN THE WINDOW=SIN(FF)/FF INTO A COMMENT
C              STATEMENT
C    2- TURN THE C1=C1*WINDOW INTO A COMMENT STATEMENT.
C    3- REMOVE THE NEXT GO TO 529 STATEMENT.
C
C      NOTE THAT DATA IS ENTERED FROM FOR32.DAT.
         GO TO 529
         IF (I.LE.50) GO TO 39
         IF (I.GT.50) GO TO 49
39       READ (32,*) XWIND,YWIND
         CWIND=CMPLX(XWIND,YWIND)
         GO TO 59
49       CWIND=CMPLX(0.0,0.0)
59       CCU1=CCU1*CWIND
       AMC1(N,I)=REAL(CCU1)
       BMC1(N,I)=AIMAG(CCU1)
         A0=1000.
C
C        THIS CALCULATED AMPLITUDE IN THE
C        DECIBELLS SCALE.
C
       AMP1(I)=20.*ALOG10(((AMC1(N,I)**2+BMC1(N,I)**2)
     ***0.5)/A0)
         XAX(I)=W/(2.*PI)
529      IDLE=1
  500    CONTINUE
         CALL FOURIE (AC1,AMC1,BMC1,N,0,KFREQ)
C
C           START A LOOP FOR CALCULATING THE VALUES
C           OF X-AXIS.
C
       DO 600   J=1,1024
       X(J)=DELTAT*(J-1)
C
C        FOR NORMAL STRESS CALCULATIONS,
C        THE NEXT CARD PERFORMS THE UNIT
C        CONVERSIONS TO PSI
C
C        AC1(J)=AC1(J)*14.5/1E06
  600  CONTINUE
         WRITE (2,33) (AC1(M), M=1,512)
       NN=N+15

       WRITE (NN,22) (XAX(L),AMP1(L), L=1,KFREQ)

 700  CONTINUE
```

```
      STOP
      END
C       SUBROUTINE TO PERFORM FFT
C       TAKEN FROM TONGTAOW (1932)
C       WITH SOME MODIFICATIONS.
C
      SUBROUTINE FORK(LX,CX,SIGNI)
      COMPLEX CX(LX),CARG,CEXP,CW,CTEMP
      COMMON/CONST/PI,DELW,DELTAT
      J=1
C--MULTIPLY BY THE PHYSICAL UNITS OF DELTA T
C--AND DELTA OMEGA TO OBTAIN REAL UNITS.
      IF(SIGNI.EQ.-1.) SC=DELTAT
      IF(SIGNI.EQ. 1.) SC=0.5*DELW/PI
      DO 30 I=1,LX
      IF(I.GT.J)GO TO 10
      CTEMP=CX(J)*SC
      CX(J)=CX(I)*SC
      CX(I)=CTEMP
   10 M=LX/2
   20 IF(J.LE.M)GO TO 30
      J=J-M
      M=M/2
      IF (M.GE.1)GO TO 20
   30 J=J+M
      L=1
   40 ISTEP=2*L
      DO 50 M=1,L
      CARG=CMPLX(0.0,1.0)*(PI*SIGNI*(M-1))/L
      CW=CEXP(CARG)
      DO 50 I=M,LX,ISTEP
      CTEMP=CW*CX(I+L)
      CX(I+L)=CX(I)-CTEMP
   50 CX(I)=CX(I)+CTEMP
      L=ISTEP
      IF(L.LT.LX)GO TO 40
      RETURN
      END
C
C         SUBROUTINE TO FILL FOURIE COEFFICIENTS IN
C         ARRAY OF 1024 POINTS AND CALL ANOTHER
C         SUBROUTINE TO DO THE FFT.

      SUBROUTINE FOURIE(AC,AMC,BMC,N,KLOW,KFREQ)
      COMPLEX CAA
      DIMENSION AC(1024),CAA(1024),AMC(7,KFREQ)
      DIMENSION BMC(7,KFREQ)
      DO 1 I=1,1024
      AC(I)=0.0
      CAA(I)=CMPLX(0.0,0.0)
    1 CONTINUE
C--FILLING THE FFT ARRAY, STARTING AT PROPER
C--FREQUENCY AND USING BOTH REAL AND IMAGINARY PARTS.
      DO 2 J=1,KFREQ
      CAA(J+KLOW+1)=CMPLX(AMC(N,J),BMC(N,J))
      CAA(1024-KLOW-J+1)=CMPLX(+AMC(N,J),-BMC(N,J))
    2 CONTINUE
      CALL FORK(1024,CAA,1.0)
C--CALL FORK TO PERFORM FFT COMPUTATIONS.
      DO 4 L=1,1024
```

```
      AC(L)=REAL(CAA(L))
    4 CONTINUE
      RETURN
      END
```